1997

# Unimolecular dissociation of polyatomic ions by molecular beam photoionization mass spectrometry and collision-induced dissociation

Yu-Ju Chen
*Iowa State University*

# INFORMATION TO USERS

This manuscript has been reproduced from the microfilm master. UMI films the text directly from the original or copy submitted. Thus, some thesis and dissertation copies are in typewriter face, while others may be from any type of computer printer.

**The quality of this reproduction is dependent upon the quality of the copy submitted.** Broken or indistinct print, colored or poor quality illustrations and photographs, print bleedthrough, substandard margins, and improper alignment can adversely affect reproduction.

In the unlikely event that the author did not send UMI a complete manuscript and there are missing pages, these will be noted. Also, if unauthorized copyright material had to be removed, a note will indicate the deletion.

Oversize materials (e.g., maps, drawings, charts) are reproduced by sectioning the original, beginning at the upper left-hand corner and continuing from left to right in equal sections with small overlaps. Each original is also photographed in one exposure and is included in reduced form at the back of the book.

Photographs included in the original manuscript have been reproduced xerographically in this copy. Higher quality 6" x 9" black and white photographic prints are available for any photographs or illustrations appearing in this copy for an additional charge. Contact UMI directly to order.

**UMI**

A Bell & Howell Information Company
300 North Zeeb Road, Ann Arbor MI 48106-1346 USA
313/761-4700 800/521-0600

# Unimolecular dissociation of polyatomic ions by molecular beam photoionization mass spectrometry and collision-induced dissociation

by

Yu-Ju Chen

A dissertation submitted to the graduate faculty

in partial fulfillment of the requirements for the degree of

DOCTOR OF PHILOSOPHY

Major: Physical Chemistry

Major Professor: Cheuk-Yiu Ng

Iowa State University

Ames, Iowa

1997

Graduate College

Iowa State university

This is to certify that the doctoral dissertation of

Yu-Ju Chen

has met the thesis requirement of Iowa State University

Signature was redacted for privacy.

Major Professor

Signature was redacted for privacy.

For the Major Program

Signature was redacted for privacy.

For the Graduate College

TABLE OF CONTENTS

# GENERAL INTRODUCTION

Reliable thermochemical data for chemical species are among the most fundamental and useful information for the prediction of the chemical reactivity. Knowledge of the structures and energetics of those chemical species formed in a photochemical process or a bimolecular reaction is very important for revealing the complex process involved in combustion, plasma, and atmospheric chemical cycles.[1] Owing to the great progress in experimental techniques in the past decade, detailed photoionization and dissociation studies on numerous small molecules and their ions have been made. Despite the existence of much information about the energetics and dissociation dynamics of small molecular neutrals and ions, similar information on more complex polyatomic species and their ions is quite limited. The purpose of this thesis research is to perform detailed photoionization and dissociation studies on relatively complex polyatomic neutral and ionic species using vacuum ultraviolet (VUV) photoionization (PI) mass spectrometry and collision-induced dissociation (CID).

The first part of the dissertation consist of two chapters concerning the photoionization studies of Group IV transition metal carbonyls and sulfur hexafluoride using the molecular beam photoionization mass spectrometric apparatus. These studies have provided reliable information about the dissociative photoionization channels, ionization energies (IEs), and the bond dissociation energies of these systems. These studies have also provided valuable insight into the bonding of these molecular systems. When possible, high level *ab initio* calculations have also been made to compare with experimental findings.

The second part of the dissertation focuses on the unimolecular dissociation process of selected organosulfur ions induced by collisional activation. The comparison between the results of this collisional activation study and those obtained in photoionization and charge transfer studies suggests that the low energy CID of $CH_3SH^+$, $CH_3CH_2SH^+$, and $CH_3SCH_3^+$ are non-statistical. *Ab initio* calculations have also been performed to rationalize the observed CID channels.

**Dissertation Organization**

This dissertation is separated into two parts. A general introduction to each part is presented. Part I consists of two independent papers on molecular beam photoionization mass spectrometry. Part II consists of three papers on the collision-induced dissociation of selected organosulfur compounds. Each paper is prepared in a format ready for publication. The description of specific experimental conditions are given in each individual section. The dissertation ends with a general conclusion.

# PART I

# UNIMOLECULAR DISSOCIATION STUDIES OF POLYATOMIC MOLECULES BY MOLECULAR BEAM PHOTOIONIZATION MASS SPECTROMETRY

# INTRODUCTION

Photoionization mass spectrometry is a spectroscopic technique for studying the processes following the absorption of a VUV photon by a molecule or an atom. When molecules are irradiated with high energy photons, processes such as photoexcitation, photoionization, and photodissociation, are predominant.[2]

Photoionization: $AB + h\nu \rightarrow AB^+ + e^-$

Autoionization: $AB + h\nu \rightarrow AB^* \rightarrow AB^+ + e^-$

Dissociative photoionization: $AB + h\nu \rightarrow AB^+ + e^- \rightarrow A^+ + B + e^-$

By measuring the ionization cross section of a particular dissociation product channel as a function of the variable photon excitation energy, the ionization energy (IE) of the neutral species and the appearance energy (AE) of the fragment ion are obtained. After simple calculations with those values, some basic and useful information such as heat of formation and sequential bond energies can be deduced from the photoionization measurements. The photoionization technique is well known for accurate IE and AE measurement.

The narrowed velocity distribution achieved by forming a molecular beam with a nozzle was first suggested by Kantrowitz and Grey[5] and made successfully by Becker et al [3]. Under the molecular beam condition, the internal energy of the gas in the high-pressure stagnation region is removed collisionally and transferred to translation along the flow streamline direction. Collisions cool the internal degrees of freedom of molecules in the expansion, and

an internal temperature of only a few Kelvin can be achieved.[6,7] Because the local speed of sound in a gas is a measure of the random thermal motion, in the case that motion transverse to the flow, molecules moving along the flow have speeds several times greater than the local speed of sound. Therefor, such a gas expansion is called a "supersonic expansion". In addition to high directionality, the higher number densities of gas in the stagnation region of the expansion leads to higher flux than for an effusive beam. This revolutionary discovery has been widely implemented in studies of molecular reaction dynamics and spectroscopy.[4] Use of the supersonic beam technique in the photoionization mass spectrometric studies has made possible a cooled molecule beam with high intensity in a collision-free environment.

**References**

1. T. Baer. C. Y. Ng, and I. Powis, The Structure, Energetics, and Dynamics of Organic Ions. Wiley (1996)

2. W. J. Rabalais, Principles of Ultraviolet Photoelectron Spectroscoopy, John Wiley & Sons. (1977)

3. E. W. Becker, K. Bier, and W. Henkes, Z. Phys. 146, 333 (1956)

4. J. D. McDonal, P. R. Lebreton, Y. T. Lee, and D. R. Herschback, J. Chem. Phys, 56, 769 (1972)

5. A. Kantrowitz, and J. Grey, Rev. Sci. Instrum. 22, 328 (1951)

6. G. Scoles, Atomic and Molecular Beam Methods, Oxford (1988)

7. J. M. Farrar, and W. H. Saunders, Techniques for the Study of Ion-Molecule Reactions.Wiley (1988)

# I. A MOLECULAR BEAM PHOTOIONIZATION MASS SPECTROMETRIC STUDY OF $CR(CO)_6$, $MO(CO)_6$, AND $W(CO)_6$

A paper published in the Journal of Chemical Physics

Y. J. Chen, C. L. Liao and C. Y. Ng

**Abstract**

The photoionization efficiency (PIE) spectra for $M(CO)_n^+$ (n=0-6) from $M(CO)_6$, M=Cr, Mo, and W, have been measured in the photon energy range of 650-1600 Å. Based on the ionization energies for $M(CO)_6$ and appearance energies (AEs) for $M(CO)_n^+$ (n=0-5) determined here, we have obtained estimates for the sequential bond dissociation energies ($D_0$) for CO-$M(CO)_{n-1}^+$ (n=1-6). The comparison between the $D_0$ values for the $Cr(CO)_6^+$ system obtained here and in the recent collisional induced dissociation and theoretical studies suggests that $D_0$ values for CO-$M(CO)_{n-1}^+$ (n=3-6) based on this PIE experiment are reliable. The PIE results reveal the general trend for individual $D_0$ values that $D_0[CO\text{-}Cr(CO)_{n-1}^+] < D_0[CO\text{-}Mo(CO)_{n-1}^+] < D_0[CO\text{-}W(CO)_{n-1}^+]$ (n=3-6). The comparison of the first $D_0$ values for $M(CO)_6^+$ obtained here and those for $M(CO)_6$ reported previously provides strong support for the theoretical analysis that the importance of relativistic effects, which give rise to more efficient M to CO π-back-donation in $M(CO)_6$, is in the order $W(CO)_6 > Mo(CO)_6 > Cr(CO)_6$.

## Introduction

Neutral and ionic transition metal carbonyl compounds and their fragments are model systems for the detailed experimental[1-7] and theoretical[8-13] investigation of transition metal-ligand bonding. The accurate determination of the successive bond dissociation energies at 0 K ($D_0$) for neutral and ionic transition metal carbonyl compounds is still a challenge for both

state-of-the-art experimental techniques[3-7] and theoretical[8-12] calculations. Due to the complexity of these experimental systems and finite limitations of individual experimental techniques, the accurate determination of successive $D_0$ values requires careful comparisons of results obtained using different experimental methods[1-7] and predictions from high level theoretical calculations.[8-12]

Photoionization[2,4,5,14] and electron-ionization[15-19] mass spectrometry are traditional techniques for obtaining estimates of the sequential $D_0$ values for ligated transition metal cations, such as $CO\text{-}M(CO)_{n-1}^+$ (n=1-6), M=Cr, Mo, and W. Due to the finer control in ionization energy and the more favorable threshold law for photoionization,[14] photoionization mass spectrometry is preferred over electron-ionization mass spectrometry. In a photoionization mass spectrometric study of $M(CO)_6$, the photoionization efficiency (PIE) spectra for $M(CO)_n^+$ (n=0-6) are measured, from which the ionization energy (IE) and appearance energies (AEs) for the following processes are determined.

$$M(CO)_6 + h\nu \rightarrow M(CO)_6^+ + e^- \quad (1)$$

$$\rightarrow M(CO)_5^+ + CO + e^- \quad (2)$$

$$\rightarrow M(CO)_4^+ + 2CO + e^- \quad (3)$$

$$\rightarrow M(CO)_3^+ + 3CO + e^- \quad (4)$$

$$\rightarrow M(CO)_2^+ + 4CO + e^- \quad (5)$$

$$\rightarrow MCO^+ + 5CO + e^- \quad (6)$$

$$\rightarrow M^+ + 6CO + e^- \quad (7)$$

In principle, the differences of successive AE values yield the $D_0$ values for $M(CO)_6^+$. In reality, the accuracy for the $D_0$ values obtainable in such an experiment is affected by hot bands and kinetic shift effects.[14] The hot band effect is due to thermal excitation of rotational and low frequency vibrational modes of the precursor molecule. As a result, the observed onset is lower than the true IE or AE value. It is possible to lessen the hot band effect by using the supersonic molecular beam technique to introduce the gas sample into the photoionization source so that the rotational and low frequency vibrational populations of the sample molecules are partially relaxed prior to photoionization.[20,21] The kinetic shift effect is statistical in nature. For a polyatomic molecule, the kinetic shift effect may restrict the dissociation rate of the excited cation to a negligible level near the dissociation threshold, making it difficult to observe the true dissociation threshold. Since the hot band and kinetic shift effects are counteracting factors, a quantitative assessment of these effects on the measured onset is difficult to make. For this reason, the accuracy of $D_0$ values obtained by PIE measurements requires confirmation with other experimental and theoretical studies. Despite the difficulties mentioned above, previous PIE results[1,2,4,5] have provided valuable energetic information on selected metal carbonyl cation systems.

The photoionization processes (1-7) for $Cr(CO)_6$ have been investigated previously by PIE[1] and photoelectron-photoion coincidence (PEPICO)[4] measurements. The photoionization studies for $M(CO)_6$, M=Mo and W, have also been made without mass selection. The main objective of this article is to present PIE data for $M(CO)_n^+$ (n=0-6), M=Cr, Mo, and W, formed in processes (1-7). The analysis of these data yields estimates for the sequential $D_0$ values for $CO\text{-}M(CO)_{n-1}^+$ (n=1-6). The successive $D_0$ values for CO-

$Cr(CO)_{n-1}^+$ (n=1-6) were determined in a recent collision-induced dissociation (CID) study.[7] The comparison between the $D_0$ values for $CO\text{-}Cr(CO)_{n-1}^+$ (n=1-6) obtained here and in the CID study suggests that the $D_0$ values for $CO\text{-}M(CO)_{n-1}^+$ (n=3-6) determined in the photoionization mass spectrometric study are more reliable than those for $CO\text{-}M(CO)_{n-1}^+$ (n=1-2), M=Mo and W. The sum of the PIE (total PIE) spectra for the individual $M(CO)_n^+$ (n=0-6) systems are also compared here with the corresponding HeI photoelectron spectra for $M(CO)_6$, M= Cr, Mo, and W.[22]

**Experiment**

The experimental arrangement of the molecular beam photoionization apparatus used in this experiment has been described in detail previously.[20,21] Briefly, the apparatus consists of a 3 m near normal incidence vacuum ultraviolet (VUV) monochromator, a capillary discharge lamp, a tungsten photoelectric VUV light detector, a differentially pumped supersonic molecular beam production system, and a quadrupole mass spectrometer for ion detection.

The grating employed in this study was a Bausch and Lomb 1200 lines/mm Os coated aluminum grating blazed at 1360 Å. Either the hydrogen many-lined pseudocontinuum or the helium Hopfield continuum was used as the light source, depending on the wavelength region desired. All PIE data were taken at an optical resolution of 1.5 Å (full width at half maximum).

The $Cr(CO)_6$, $Mo(CO)_6$, and $W(CO)_6$ samples were obtained from Alfa Products with a stated purity of 98%, and were used without purification. In this experiment, a continuum $Cr(CO)_6$ [or $Mo(CO)_6$ or $W(CO)_6$] beam seeded in Ar was produced by supersonic expansion

through a home-built quartz oven beam source. This oven beam source consisted of a quartz sample cell and a quartz nozzle (diameter ≈ 127 μm) which were heated by separated heaters. Two microprocessor based temperature controllers were used to independently set the temperature of the sample cell and nozzle. The sample cell was maintained at temperatures of 85 °C, 110 °C, and 120 °C, yielding partial pressures of 68 Torr, 25 Torr, and 15 Torr for $Cr(CO)_6$, $Mo(CO)_6$, and $W(CO)_6$, respectively. In order to avoid condensation at the nozzle, the nozzle was kept at a temperature about 10 °C higher than that of the sample cell. When the cell and nozzle were heated to a temperature >130 °C, noticeable decomposition of the metal carbonyl compounds was observed as monitored by the photoionization mass spectrometer. The total stagnation pressure of the Ar and metal carbonyl vapor was maintained at ≈200 Torr. The molecular beam was collimated by a conical skimmer (diameter=1 mm) before entering the photoionization chamber. During the experiment, the beam source and photoionization chambers were maintained at $1x10^{-4}$ Torr and $\leq 2x10^{-5}$ Torr, respectively.

In this experiment, the dispersed VUV photon beam from the monochromator is modulated by a 150 Hz tuning fork chopper.[20] The difference between the counts corresponding to the VUV photon beam on and off was taken to be the ion signal. Due to the low ion signal near the IE and AEs, the modulation technique is essential in reducing the background of the ion detector. The PIE data presented here represent the averages of at least two reproducible scans.

## Results

### A. $Cr(CO)_n^+$ (n=0-6)

The PIE spectra for $Cr(CO)_n^+$ (n=0-6) from $Cr(CO)_6$ measured in the wavelength range from 700-1600 Å are depicted in Figs. 1(a) and 1(b). The fragment ions observed are assumed to result from processes (1-7) for M = Cr. We note that the same PIE scale is used for for all $Cr(CO)_n^+$ (n=0-6) spectra. Thus, the PIE spectra of Figs. 1(a) and 1(b) show the relative fragment ion intensities as a function of ionizing photon energy.

The PIE curve for $Cr(CO)_6^+$ rises above the background level at ≈1530 Å and increases gradually as photon energy is increased. The gradual rise in the ionization threshold is consistent with the interpretation that the geometries for $Cr(CO)_6$ and its cation are different, resulting in poor Franck-Condon factors for the ionization transition. This behavior of a very gradual ionization onset is also observed in photoionization thresholds of other transition metal carbonyl compounds.[1,2,4,5] The linear extrapolation of the PIE data near the ionization threshold yields a value of 1520±5 Å (8.16±0.03 eV) for the adiabatic IE of $Cr(CO)_6$. The nonlinear rise of the PIE spectrum from 1530 to 1520 Å is attributed to the hot band effect. The IE value determined in this study is in good agreement with previous photoionization results.[1,4] (see Table I). The onsets for $Cr(CO)_n^+$ (n=2-5) are relatively distinct, whereas the onsets for $CrCO^+$ and $Cr^+$ are very gradual. The formation of smaller $Cr(CO)_n^+$ fragment ions is likely the result of sequential dissociation processes. On the basis of statistical consideration, we expect that the probability or rate of dissociation at the true threshold decreases as the extent of dissociation increases because the neutral fragments carry away finite energy. Thus, the increasingly gradual onset observed for smaller $Cr(CO)_n^+$ fragment ions is consistent with this expectation.

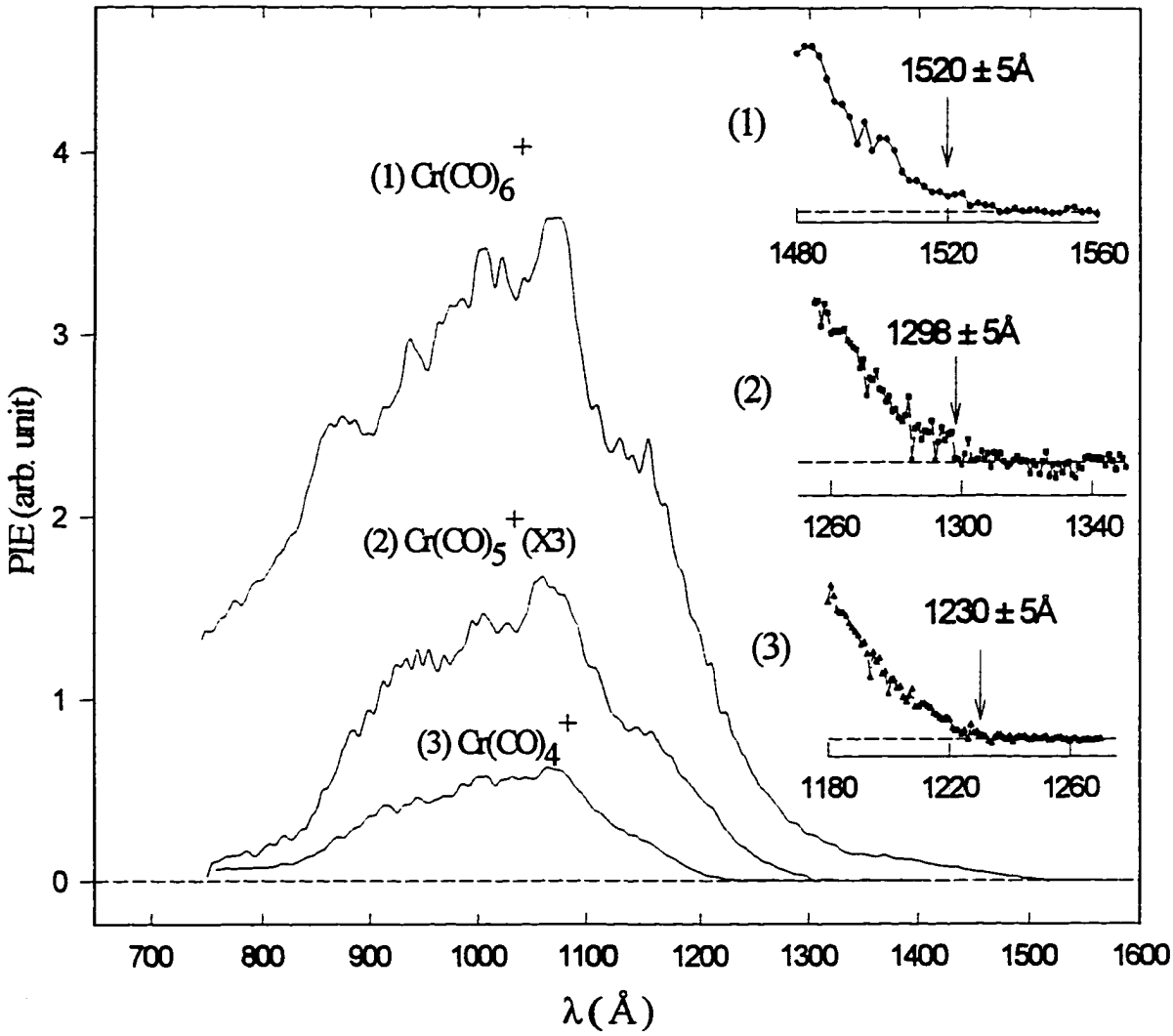


Figure 1(a) PIE spectra for $Cr(CO)_n^+$ n=4-6 from $Cr(CO)_6$ in the wavelength (λ) range of 650 - 1600 Å. Note that the relative PIE scale are the same for (a) and (b).

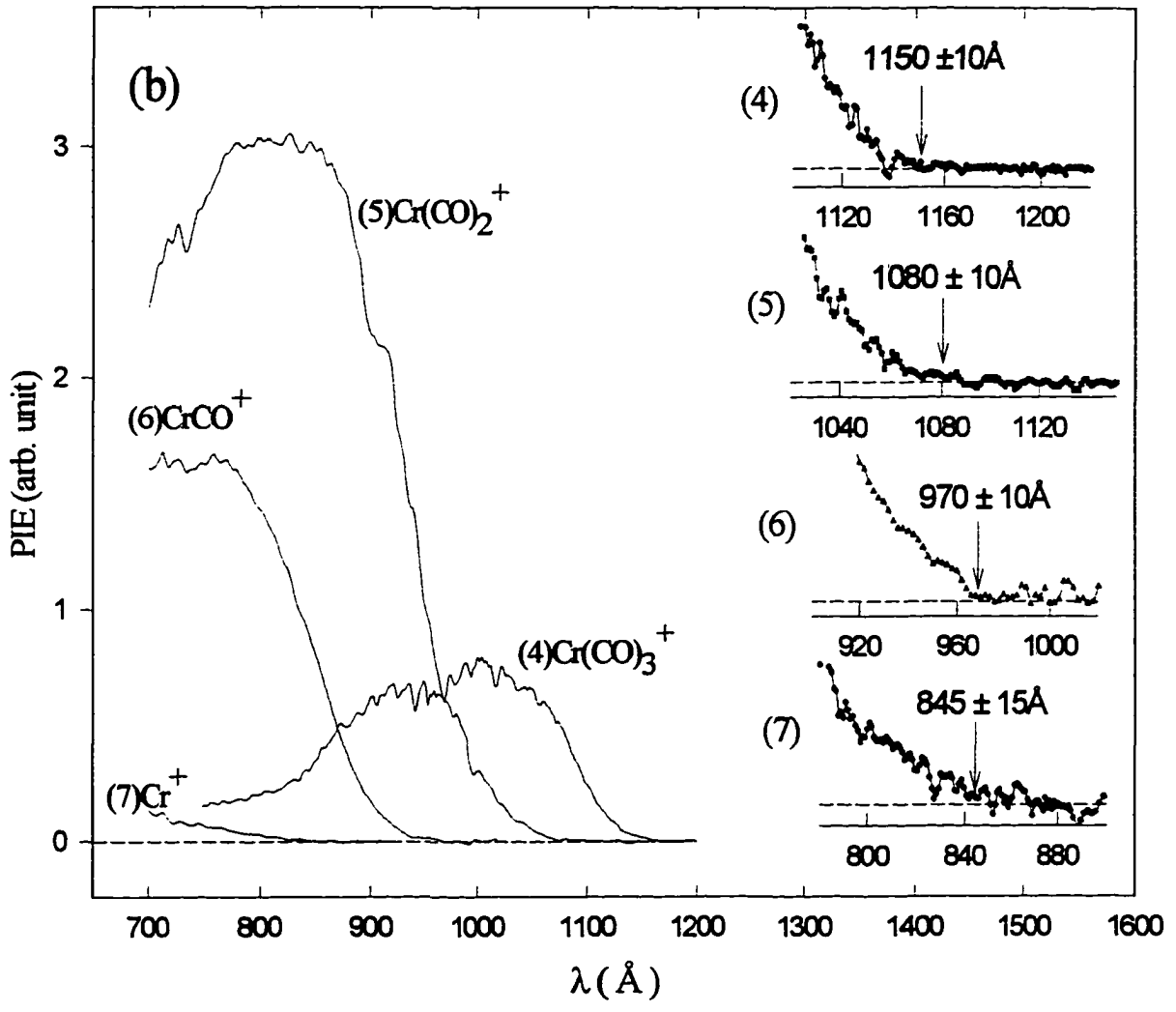


Figure 1(b) PIE spectra for $Cr(CO)_n^+$, n=0-3 from $Cr(CO)_6$ in the wavelength (λ) range of 650-1600 Å. Note that the relative PIE scale are the same for (a) and (b).

**Table I** Ionization energies (IEs) and heats of formation at 0 K ($\Delta_f H^\circ_0$) and at 298 K ($\Delta_f H^\circ_{298}$).[a]

| Species | $\Delta_f H^\circ_0$ (kcal/mol) | $\Delta_f H^\circ_{298}$ (kcal/mol) | IE(eV) |
|---|---|---|---|
| CO | -27.20±0.04 | -26.42±0.04 | 14.0139 |
| Cr | 94.3±1.0 | 94.8±1.0 | 6.766 |
| $Cr^+$ | 250.3±1.0 | 252.5±1.0 | |
| Mo | 156.9 | 157.3 | 7.099 |
| $Mo^+$ | 320.6 | 321.0 | |
| W | 203.7±1.5 | 203.4±1.5 | 7.60 |
| $W^+$ | 378 | 379 | |
| $Cr(CO)_6$ | -218.4±0.4 | -217.1±0.4 | 8.16±0.03[b]<br>8.142±0.017c<br>8.24±0.07[d] |
| $Mo(CO)_6$ | -219 | -218 | 8.21±0.03[b]<br>8.227±0.011[c] |
| $W(CO)_6$ | -213 | -212±1 | 8.24±0.03[b]<br>8.242±0.006[c] |

a) Unless specified, the values given in the table are obtained from Ref. 22.

b) This work.

c) Reference 1.

d) Reference 4.

The IE and AEs determined by the PIE spectra of Figs. 1(a) and 1(b) are compared to previous electron-ionization[15-19] and photoionization[4] results in Table II. Although the vibrational relaxation for $M(CO)_6$, M=Cr, Mo, and W, under the beam expansion conditions of the present experiment is likely to be incomplete, we assumed that the IEs and AEs determined here are 0 K values. Taking into account the experimental uncertainties, the AEs for $Cr(CO)_n^+$ (n=1-5) obtained here and those in the previous PEPICO experiment[4] are in agreement. However, the AE of 14.67 eV for $Cr^+$ observed here is significantly higher than the PEPICO value of 14.13 eV.[4] The deviations between AE values obtained in previous electron-ionization studies are large,[15-19] indicating the lack of precision in the electron-ionization method. The AEs for $Cr(CO)_n^+$ (n=0-2) based on electron-ionization are significantly higher than the corresponding photoionization values.

The heats of formation at 0 K ($\Delta_f H^\circ_0$) and at 298 K ($\Delta_f H^\circ_{298}$) for $Cr^+$, CO, and $Cr(CO)_6$ are known (see Table I).[23] Using these values, we calculated a value of 13.26 eV (13.50 eV) for the heat of reaction at 0 K (298 K) for the formation of $Cr^+(^6S)$ + 6CO from $Cr(CO)_6$. This, the thermochemical threshold for the ground state $Cr^+(^6S)$ ion, is significantly lower than the $AE(Cr^+)$ value observed here, indicating that this $AE(Cr^+)$ is an upper limit. It was suggested that the electron-ionization[24,25] and photoionization[26] of $Cr(CO)_6$ leads to production of $Cr^+$ in an excited state. Since the first excited $Cr^+(^6D)$ state is 1.52 eV higher than the ground $Cr^+(^6S)$ state,[27] we calculate a thermochemical theshold of 14.78 eV for the formation of $Cr^+(^6D)$. The agreement between the latter value and the PIE $AE(Cr^+)$ of 14.67±0.26 eV seems to support the proposal that $Cr^+$ is formed in the first excited $Cr^+(^6D)$ in the dissociative photoionization of $Cr(CO)_6$. Using the thermochemical threshold (13.26 eV) of process (7) for M=Cr and $IE[Cr(CO)_6]$=8.16±0.03 eV, we calculate a value of 0.85 eV for the average Cr-CO bond dissociation energy for $Cr(CO)_6^+$.

The successive $D_0$ values for CO-$Cr(CO)_{n-1}$ (n=1-6) calculated using the AEs of this experiment are compared to those of the PEPICO[4] and CID[7] studies in the last column of Table II. Taking into account the experimental uncertainties, the $D_0$ values for CO-$Cr(CO)_{n-1}$ (n=3-6) determined here are in good accord with those of the CID study. We have included in Table II the theoretical[28] $D_0$ values for CO-$CrCO^+$ (0.98 eV) and $Cr^+$-CO (0.93 eV) predicted by high level *ab initio* calculations.[8] These latter values are in excellent agreement with the CID values. On the basis of the comparison of $D_0$ values in Table I, we conclude that the PIE AE($CrCO^+$) value of 12.78 eV obtained here is also higher than the true threshold for the formation of $CrCO^+$ + 5CO in their ground states from $Cr(CO)_6$. Using the 0 K thermochemical threshold of 13.26 eV for the formation of $Cr^+(^6S)$ + 6CO and the AE($CrCO^+$) (≤12.78 eV), we calculate a lower bound of 0.47 eV for $D_0(Cr^+$-CO). Assuming that $D_0$[CO-$CrCO^+$] ≈ $D_0(Cr^+$-CO) as predicted by the theoretical caluclations[8] and using the AE[$Cr(CO)_2^+$] = 11.48 eV and the thermochemical threshold for $Cr^+(^6S)$ (13.26 eV), we obtain an estimate of 0.89 eV for $D_0$[CO-$CrCO^+$] and $D_0(Cr^+$-CO), which is in reasonable agreement with the CID[7] and theoretical[8] results.

Armentrout and co-workers[7] rationalized the observed trend in the sequential $D_0$ values for $Cr(CO)_6^+$ as due to spin changes induced by the increasing ligand field. The strong bonds are associated with a dissociation process which obeys spin conservation.[29,30] That is, the higher values for $D_0$[CO-$CrCO^+$] and $D_0(Cr^+$-CO) are attributed to the fact that the ground electronic states for $Cr^+$, $CrCO^+$ and $Cr(CO)_2^+$ have the same spin multiplicity, namely the $Cr^+(^6S)$, $CrCO(^6\Sigma^+)$, and $Cr(CO)_2^+(^6\Sigma_g^+)$ sextet states.[8,26] The higher $D_0$[CO-$Cr(CO)_5^+$], $D_0$[CO-$CrCO^+$], and $D_0(Cr^+$-CO) values indicate that $Cr(CO)_6^+$, $Cr(CO)_2^+$, and $CrCO^+$ are more stable compared to other fragment ions. It is interesting to note that the maximum PIEs for $Cr(CO)_6^+$, $Cr(CO)_2^+$, and $CrCO^+$ are

**Table II** Ionization energies (IEs) or appearance energies (AEs) of $Cr(CO)_n^+$, n=0-6, from $Cr(CO)_6$ and bond dissociation energies $D_0$ for $CO\text{-}Cr(CO)_{n-1}^+$, n=1-5.

| | IE or AE (eV) | | | | | | | |
|---|---|---|---|---|---|---|---|---|
| Species | This work | Ref. 4 | Ref. 15 | Ref. 19 | Ref. 17 | Ref. 18 | Ref. 16 | $D_0$ (eV)[a] |
| $Cr(CO)_6^+$ | 8.157±0.026 (1520±5 Å) | 8.24±0.07 | 8.15 | 8.42 | 8.48 | 8.43 | 8.18 | 1.39±0.05[b]<br>1.49±0.25[c]<br>1.35±0.08[d] |
| $Cr(CO)_5^+$ | 9.55±0.04 (1298±5 Å) | 9.73±0.24 | 9.5 | 9.85 | 8.95 | 9.32 | 9.17 | 0.53±0.6[b]<br>0.22±0.26[c]<br>0.64±0.03[d] |
| $Cr(CO)_4^+$ | 10.08±0.04 (1230±5 Å) | 9.95±0.10 | 10.7 | 10.45 | 9.64 | 9.52 | 9.97 | 0.70±0.10[b]<br>0.83±0.17[c]<br>0.53±0.08d |
| $Cr(CO)_3^+$ | 10.78±0.09 (1150±10 Å) | 10.78±0.14 | 12.0 | 11.35 | 11.00 | 10.42 | 10.62 | 0.70±0.14[b]<br>0.66±0.19c<br>0.56±0.06[d] |
| $Cr(CO)_2^+$ | 11.48±0.11 (1080±10 Å) | 11.44±0.13 | 13.1 | 12.51 | 11.94 | 12.56 | 11.56 | ≤1.30±0.17[b]<br>1.36±0.16[c]<br>0.98±0.03[d]<br>0.98[e]<br>≈0.89[f] |
| $CrCO^+$ | ≤12.78±0.13 (>970±10 Å) | 12.80±0.10 | 14.9 | 14.03 | 13.63 | 14.12 | 13.3 | >0.47[b]<br>1.33±0.05[c]<br>0.95±0.04[d]<br>0.93[e]<br>≈0.89[f] |
| $Cr^+$ | <14.67±0.26 (>845±15 Å) | 14.13±0.11 | 17.7 | 15.36 | 15.10 | 17.07 | 14.7 | |

a) Bond dissociation energies at 0 K ($D_0$) for $CO\text{-}Cr(CO)_{n-1}^+$ (n=1-6).

Table II (continued)

b) PIE values. This work.

c) PEPICO values. Reference 4.

d) CID values. Reference 7.

e) Theoretical values. Reference 8. These values have not been corrected for zero-point vibrational energes.

f) Assuming that $D_0[CO\text{-}CrCO^+] \approx D_0(Cr^+\text{-}CO)$ as predicted by the theoretical caluclations (Ref. 8) and using the $AE[Cr(CO)_2^+] = 11.48$ eV and the thermochemical reshold for $Cr^+(^6S)$ (13.26 eV), we obtain an estimate of 0.89 eV for $D_0[CO\text{-}CrCO^+]$ and $D_0(Cr^+\text{-}CO)$.

significantly higher than those for other fragment ions as shown in Figs. 1(a) and 1(b).

We show in Fig. 2(a) the plot of the sum of the PIEs, i.e., total PIE, for $Cr(CO)_n^+$ (n=0-6) in the photon energy range of 7.7-19.0 eV. The HeI photoelectron spectrum for $Cr(CO)_6$ in a similar energy range obtained from Ref. 22 is reproduced in Fig. 2(b) for comparison with the total PIE spectrum of Fig. 2(a). The first photoelectron band centered at 8.5 eV has been assigned to the removal of an electron from the highest occupied $t_{2g}$ orbital of $Cr(CO)_6$, which has mostly the Cr(3d) and CO($2\pi$) characters. The broad photoelectron band in the photon region of 13-16 eV is assigned to ionization from molecular orbitals with the CO($1\pi$ and $5\sigma$) characters. The rise in total PIE observed in the photon region of 9.5-13 eV is likely due to autoionization from Rydberg states of $Cr(CO)_6$. The autoionization mechanism[31] should make possible the efficient formation of vibrationally excited $Cr(CO)_6^+$ precursor ions prior to fragmentation according to processes (1-6).

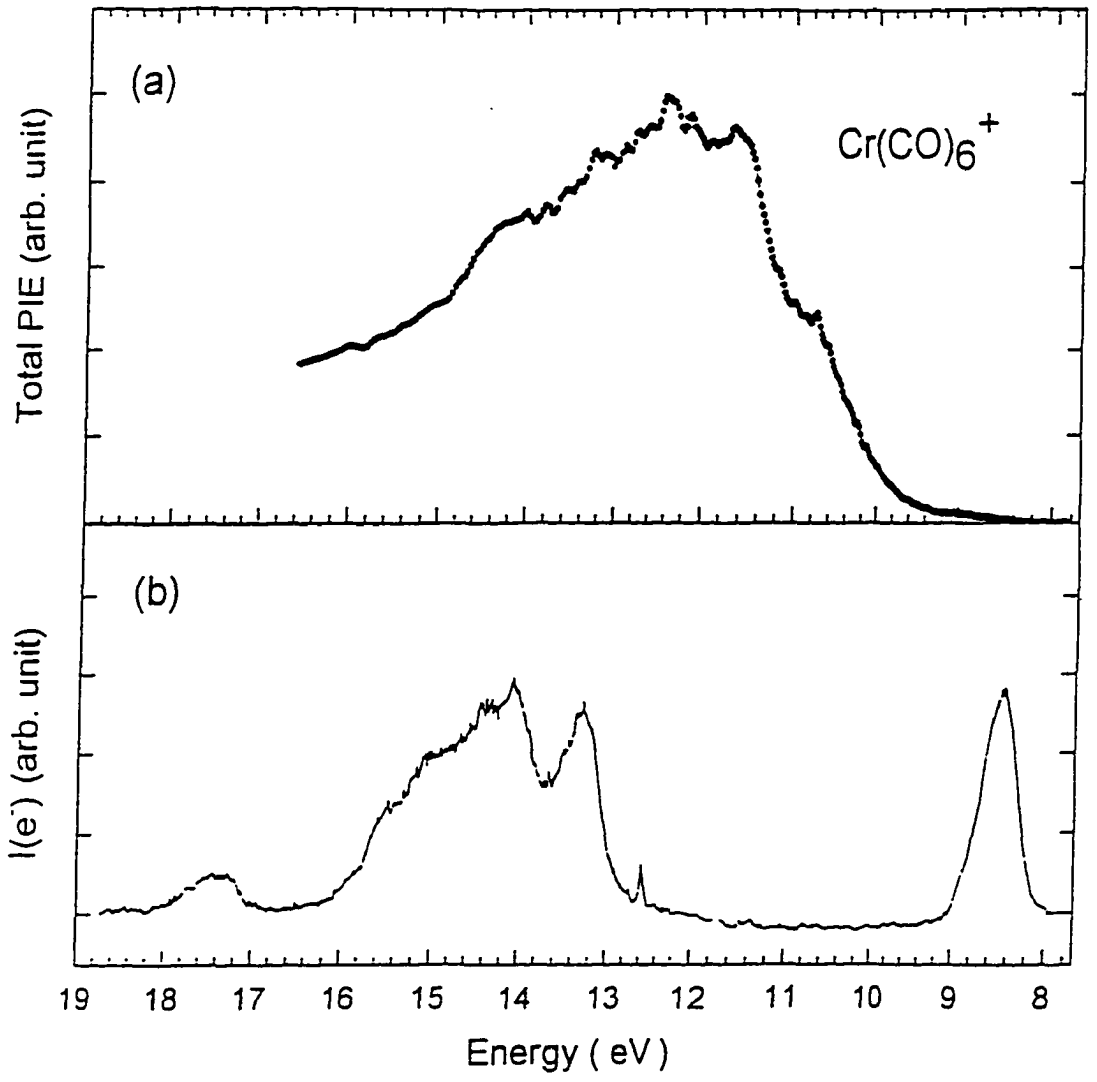


Figure 2 (a) The sum of the PIE (total PIE) for $Cr(CO)_n^+$ (n=0-6) in the photon energy range from 7.7-19.0 eV range.

(b) HeI photoelectron spectrum for $Cr(CO)_6$ in the energy range 7.7-19.0 eV (Ref. 22). $I(e^-)$ is the photoelectron intensity.

**B. $Mo(CO)_n^+$ (n=0-6)**

Figures 3(a) and 3(b) show the PIE spectra for $Mo(CO)_n^+$ (n=0-6) formed in the photoionization of $Mo(CO)_6$ in the wavelength range of 620-1600 Å using the same relative PIE scale. The PIE spectra for $Mo(CO)_6^+$ and $Mo(CO)_5^+$ reveal strong autoionization features at ≈1010 and ≈1080 Å. These features are also discernible, though less prominent, in the PIE spectra for $Cr(CO)_6^+$ and $Cr(CO)_5^+$ [see Fig. 1(a)].

The PIE spectrum for $Mo(CO)_6^+$ rises above the background at 1520 Å. A linear extrapolation of the PIE data near the threshold yields an adiabatic IE[$Mo(CO)_6$] value of 1510±5 Å (8.21±0.03 eV). The latter value is in excellent agreement with that obtained in the previous photoionization study of Ref. 1. The AE values for $Mo(CO)_n^+$ (n=2-5) obtained by the linear PIE extrapolation method are listed in Table III for comparison with AE values obtained in previous electron-ionization studies.[15-19] We note that the PIE spectrum for $MoCO^+$ rises above the background level at ≈798 Å and increases very gradually in the region of 768-798 Å. To account for this, we have assigned a relatively large uncertainty (±15 Å) to the AE($MoCO^+$). Using the known $\Delta_f H^\circ_0$ ($\Delta_f H^\circ_{298}$) values for $Mo^+$, CO, and $Mo(CO)_6$ (Table I), we calculate a value of 16.32 eV (16.50 eV) for the 0 K (298 K) thermochemical threshold for the formation of $Mo^+(^6S)$ + 6CO from $Mo(CO)_6$. The latter value is significantly lower than the AE($Mo^+$) values ranging from 18.18 to 20.7 eV obtained in this PIE and previous electron-ionization studies,[15-19] indicating that these AE($Mo^+$) values are upper limits. Since the first excited $Mo^+(^6D)$ state is 1.47 eV higher than the ground $Mo^+(^6S)$ state, the threshold for the formation of the excited $Mo^+(^6D)$ + 6CO channel is expected to be 17.78 eV. Thus, the observed IE AE ($Mo^+$) value is also consistent

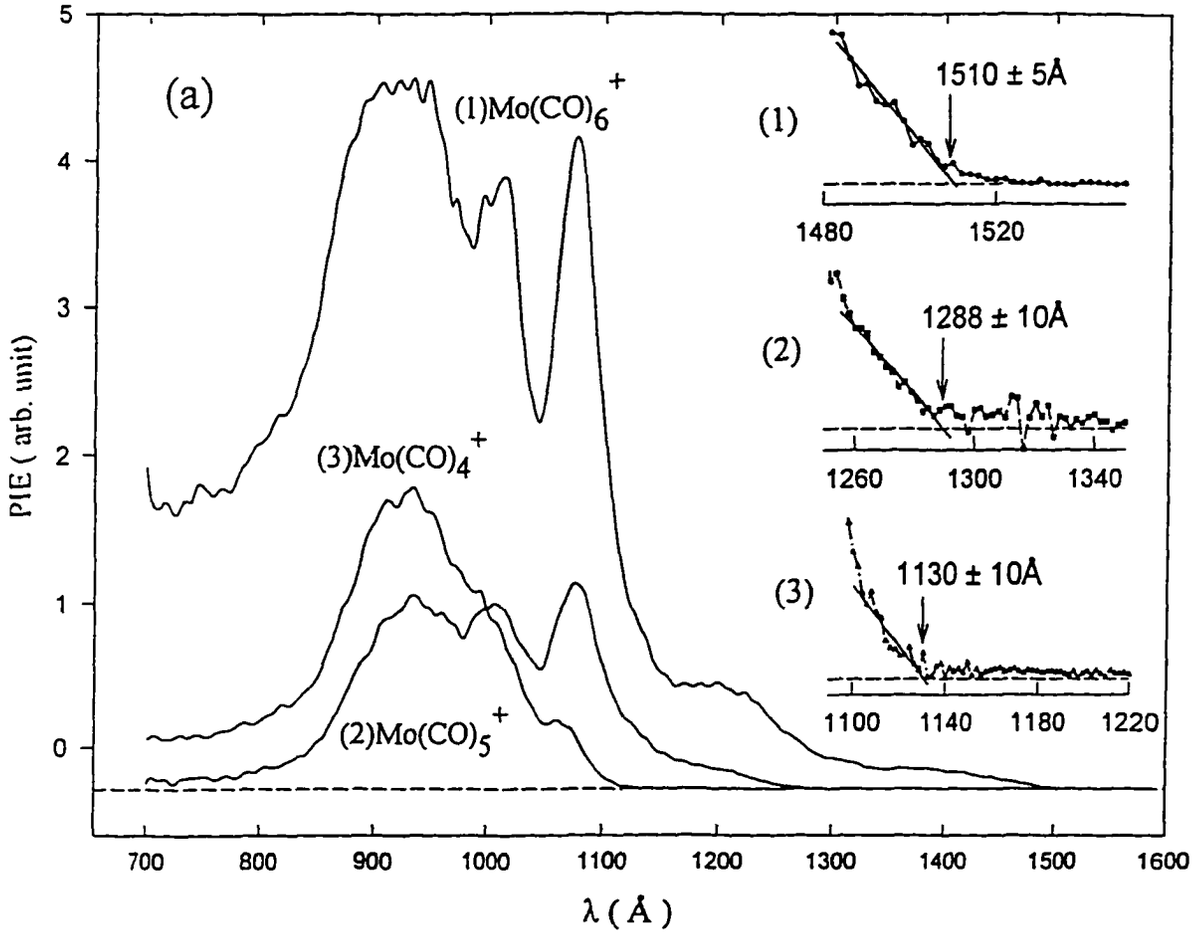


Figure 3 (a) PIE spectra for $Mo(CO)_n^+$, n=4-6, from $Mo(CO)_6$ in the wavelength (λ) range of 650-1600 Å. Note that the relative PIE scale are the same for (a) and (b).

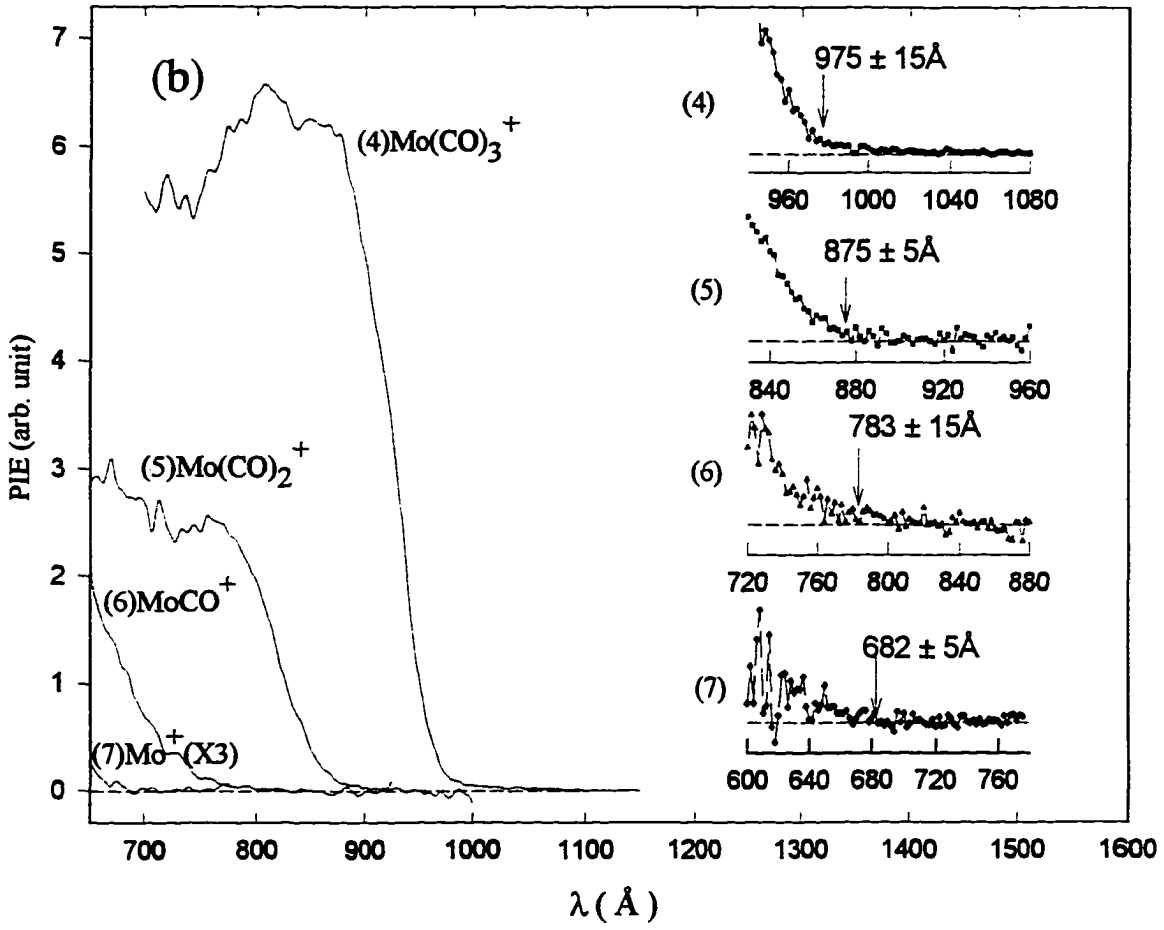


Figure 3(b) PIE spectra for $Mo(CO)_n^+$ , n=0-3, from $Mo(CO)_6$ in the wavelength (λ) range of 650-1600 Å. Note that the relative PIE scale are the same for (a) and (b).

**Table III** Ionization or appearance energies (IE or AE) of $Mo(CO)_n^+$, n=0-6, from $Mo(CO)_6$ and bond dissociation energies $D_0$ for $CO\text{-}Mo(CO)_{n-1}^+$, n=1-5.

| | IE or AE (eV) | | | | | | |
|---|---|---|---|---|---|---|---|
| Species | This work | Ref. 15 | Ref. 19 | Ref. 17 | Ref. 18 | Ref. 16 | $D_0$ (eV)[a] |
| $Mo(CO)_6^+$ | 8.21±0.03 (1510±5 Å) | 8.23 | 8.46 | 8.32 | 8.46 | 8.30 | 1.42±0.08[b] |
| $Mo(CO)_5^+$ | 9.63±0.07 (1288±10 Å) | 9.8 | 9.43 | 9.14 | 10.02 | 9.64 | 1.34±0.06[b] |
| $Mo(CO)_4^+$ | 10.97±0.10 (1130±10 Å) | 11.9 | 10.63 | 10.72 | 11.62 | 11.28 | 1.74±0.22[b] |
| $Mo(CO)_3^+$ | 12.71±0.20 (975±15 Å) | 13.7 | 12.82 | 13.18 | 13.29 | 12.36 | 1.46±0.22[b] |
| $Mo(CO)_2^+$ | 14.17±0.08 (875±5 Å) | 15.6 | 14.5 | 14.76 | 14.86 | 13.90 | ≤1.66±0.31[b]<br>0.92[c]<br>≈1.08[d] |
| $MoCO^+$ | ≤15.83±0.30 (783±15 Å) | 18.1 | 15.7 | 15.61 | 16.52 | 15.80 | >0.49[b]<br>0.82[c]<br>≈1.08[d] |
| $Mo^+$ | <18.18±0.13 (682±5 Å) | 20.7 | 18.6 | 19.63 | 18.24 | 18.30 | |

a) Bond dissociation energies at 0 K for $CO\text{-}Mo(CO)_{n-1}^+$ (n=1-6).

b) PIE values. This work.

c) Theoretical values. Reference 8. These values have not been corrected for the zero-point vibratioanl energies.

d) Assuming that $D_0[CO\text{-}MoCO^+] \approx D_0(Mo^+\text{-}CO)$ as predicted by the theoretical caluclations (Ref. 8) and using the $AE[Mo(CO)_2^+] = 14.17$ eV and the thermochemical reshold for

Table III (continued)

$Mo^+(^6S)$ (16.32 eV), we obtain an estimate of 1.08 eV for $D_0[CO\text{-}MoCO^+]$ and $D_0(Mo^+\text{-}CO)$.

with the proposal[24-26] that $Mo^+$ is formed in excited electronic states in the dissociative photoionization and electron-ionization of $Mo(CO)_6$.On the basis of the known thermochemical threshold (16.32 eV) for the formation of $Mo^+(^6S)$ + 6CO from $Mo(CO)_6$ and the IE[$Mo(CO)_6$] = 8.21 eV, the average Mo-CO bond dissociation energy for $Mo(CO)_6^+$ is calculated to be 1.35 eV.

The sequential $D_0$ values for $Mo(CO)_6^+$ calculated using the measured AE values determined in the present experiment are given in Table III. Similar to the observation for the $D_0$ values for $Cr(CO)_6^+$, the second Mo-CO bond is found to be weaker than the first Mo-CO bond in $Mo(CO)_6^+$. The $CO\text{-}Mo(CO)_3^+$ bond seems to be the strongest Mo-CO bond in $Mo(CO)_6^+$. While the $D_0[CO\text{-}Mo(CO)_5^+]$ value of 1.42±0.09 eV is close to the $D_0[CO\text{-}Cr(CO)_5^+]$ value of 1.39±0.06 eV, the $D_0[CO\text{-}Mo(CO)_{n-1}^+]$ (n=3-5) values are significantly greater than the corresponding $D_0[CO\text{-}Cr(CO)_{n-1}^+]$ (n=3-5) values. The sequential $D_0[CO\text{-}Mo(CO)_{n-1}^+]$ (n=2-6) determined here fall in the range of 1.34-1.74 eV, and are close to the average $D_0$ of 1.35 eV. The variation of the sequental $D_0$ values for $Mo(CO)_6^+$ is smaller than that observed for $Cr(CO)_6^+$. We have included in Table III the respective theoretical predictions[8] of 0.92 and 0.82 eV for $D_0[CO\text{-}MoCO^+]$ and $D_0(Mo^+\text{-}CO)$. It is interesting that these values are lower than the corresponding theoretical predictions[8] for $D_0[CO\text{-}CrCO^+]$ = 0.98 eV and $D_0[CO\text{-}Cr^+]$ = 0.93 eV. Using the thermochemical threshold of 16.32 eV for the formation of $Mo^+(^6S)$ + 6CO from $Mo(CO)_6$, together with the PIE AE($MoCO^+$) of 15.83 eV, we calculate a value of 0.49 eV for $D_0(Mo^+\text{-}CO)$, which is significantly

lower than the theoretical prediction of 0.82 eV. This observation indicated that the AE($Mo^+$-CO) value obtained here is likely an upper limit. If we take the difference between the thermochemical threshold of 16.32 eV for $Mo^+(^6S)$ + 6CO from $Mo(CO)_6$ and the PIE AE[$Mo(CO)_2^+$] = 14.17 eV, we obtained the sum of $D_0$[CO-$MoCO^+$] and $D_0$($Mo^+$-CO) to be 2.15 eV.

If we assume that $D_0$[CO-$MoCO^+$] ≈ $D_0$($Mo^+$-CO) as predicted by the theoretical calculation,[8] we arrive at an estimate of 1.07 eV for $D_0$[CO-$MoCO^+$] and $D_0$($Mo^+$-CO), which is close to the theoretical predictions in the range of 0.82-0.92 eV.

Figure 4(a) depicts the total PIE spectrum for $Mo(CO)_n^+$ (n=0-6) in the photon energy range of 7.7-17.7 eV. The HeI photoelectron spectrum for $Mo(CO)_6$ in a similar energy range obtained from Ref. 22 is reproduced in Fig. 4(b) for comparison with the total PIE spectrum of Fig. 4(b). The HeI photoelectron spectra for $Cr(CO)_6$ and $Mo(CO)_6$ have essentially the same features. The assignment for the HeI photoelectron spectrum for $Mo(CO)_6$ is similar to that for $Cr(CO)_6$. That is, the first photoelectron band centered at 8.5 eV is attributed to the removal of an electron from the highest occupied $t_{2g}$ orbital of $Mo(CO)_6$, which has mostly the Mo(4d) and CO($2\pi$) characters. The broad photoelectron band in the photon region of 13-16 eV is assigned to ionization from molecular orbitals with mainly the CO($1\pi$ and $5\sigma$) characters. The increase in total PIE observed in the photon energy region of 9.5-13 eV is most likely contributed by autoionization from Rydberg states of $Mo(CO)_6$. Autoionization in this photon energy region is expected to produce vibrationally excited $Mo(CO)_6^+$ precursor ions for further dissociation according to processes (1-3).

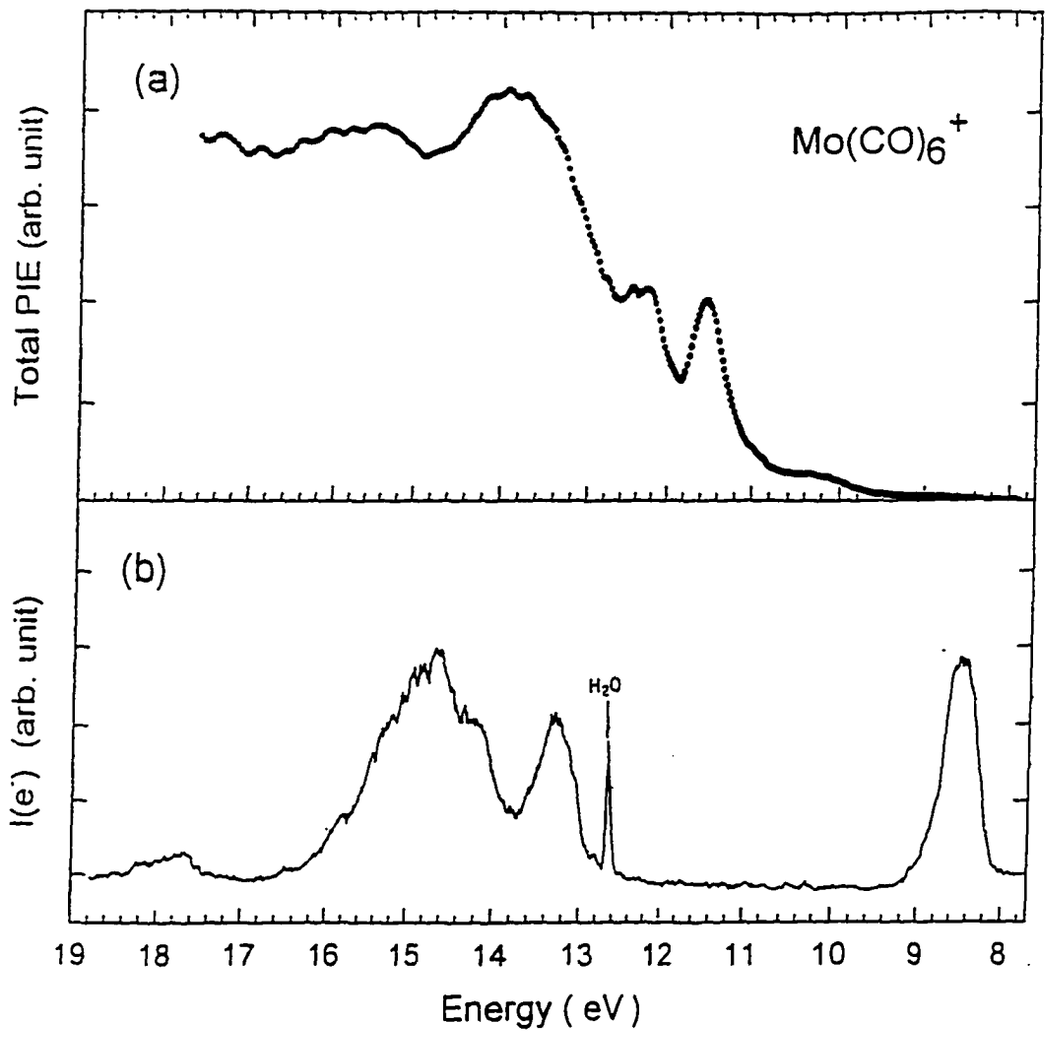


Figure 4 (a) The sum of the PIE (total PIE) for $Mo(CO)_n^+$ (n=0-6) in the photon energy range from 7.7-19.0 eV range. (b) HeI photoelectron spectrum for $Mo(CO)_6$ in the energy range 7.7-19.0 eV (Ref. 22). $I(e^-)$ is the photoelectron intensity.

## C. $W(CO)_n^+$ (n=1-6)

The PIE spectra for $W(CO)_n^+$ (n=1-6) formed in the photoionization of $W(CO)_6$ [processes (1-6) for M=W] in the wavelength range of 650-1600 Å are plotted in Figs. 5(a) and 5(b). Within the sensitivity of this experiment, the $W^+$ ion was not observed in this wavelength region.

The gross features observed in the PIE spectra for $W(CO)_n^+$ (n=1-6) are similar to those found in the corresponding spectra for $Mo(CO)_n^+$ (n=1-6). The autoionization peaks observed at ≈1070 Å in the PIE spectra for $W(CO)_n^+$ (n=5,6) are less pronounced than those found in the $Mo(CO)_n^+$ (n=5,6) spectra. The PIE spectrum for $W(CO)_6^+$ rises above the background level at 1513 Å. The adiabatic IE[$W(CO)_6$] of 1505±5 Å (8.24±0.03 eV) determined here is also in excellent agreement with the photoionization value of Ref. 1. The AEs for $W(CO)_n^+$ (n=1-5) determined in the present PIE experiment are compared with those obtained in previous electron-ionization studies[15-19] in Table IV. Using the known $\Delta_f H^\circ_0$ ($\Delta_f H^\circ_{298}$) values for $W^+(^6D)$, CO, and $W(CO)_6$ (see Table I), we calculate the 0 K (298 K) thermochemical threshold for the formation of $W^+(^6D)$ + 6CO from $W(CO)_6$ to be 18.55 eV (18.76 eV). Based on the latter value and IE[$W(CO)_6$]= 8.24 eV, we obtained a value of 1.71 eV for the average W-CO bond dissociation energy for $W(CO)_n^+$. The ground $W^+(^6D)$ state corresponds to the electronic configuration of $5d^46s$, whereas the first excited $W^+(^6S)$ state has the electronic configuration of $5d^5$. The $W^+(^6S)$ state is 0.92 eV above the ground $W^+(^6D)$ state.[27] Thus, the thermochemical threshold for the formation of the excited $W^+(^6S)$ + 6CO channel from $W(CO)_6$ is 19.47 eV. The fact that $W^+$ was not observed at photon energies up to 19.68 eV (630 Å) may indicate that the probability for the formation of $W^+(^6D)$ ions by photoionization is low.

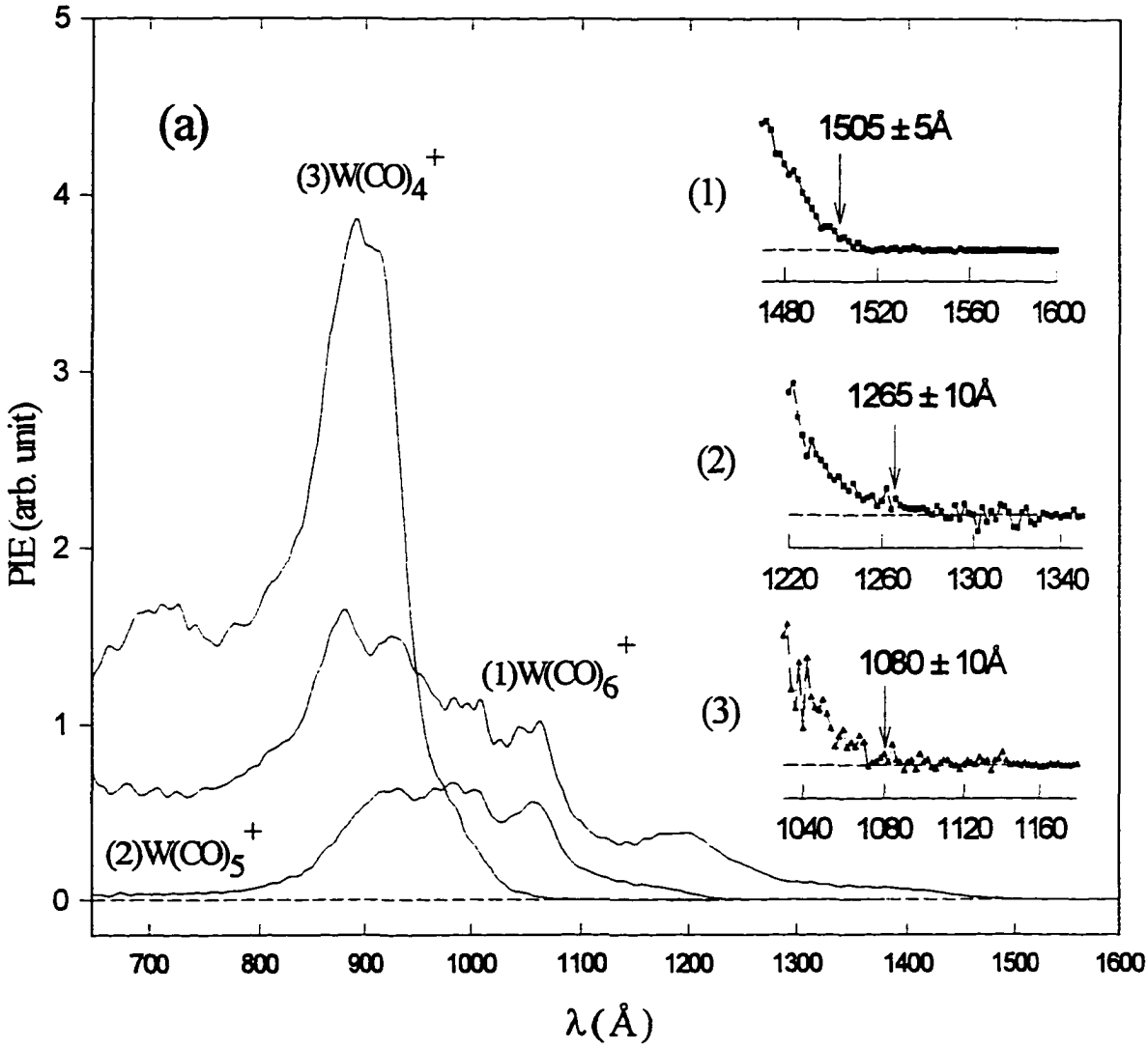


Figure 5(a) PIE spectra for $W(CO)_n^+$, n=0-3, from $W(CO)_6$ in the wavelength (λ) range of 650-1600 Å. Note that the relative PIE scale are the same for (a) and (b).

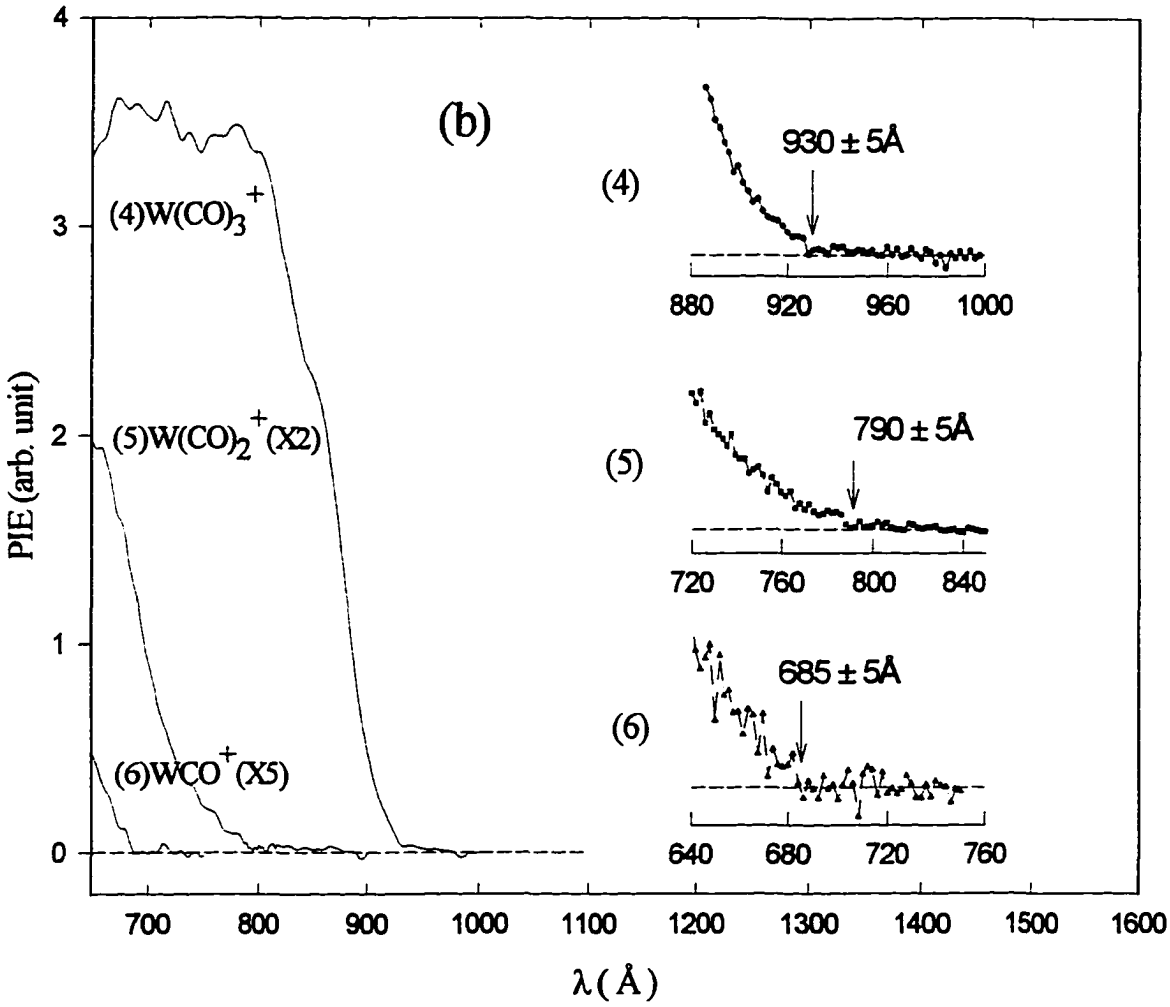


Figure 5(b) PIE spectra for $W(CO)_n^+$, n=0-3, from $W(CO)_6$ in the wavelength (λ) range of 650-1600 Å. Note that the relative PIE scale are the same for (a) and (b).

**Table IV** Ionization or appearance energies (IE or AE) of $W(CO)_n^+$, n=0-6, from $W(CO)_6$ and bond dissociation energies $D_0$ for $CO\text{-}W(CO)_{n-1}^+$, n=1-5.

| | IE or AE (eV) | | | | | | |
|---|---|---|---|---|---|---|---|
| Species | This work | Ref. 15 | Ref. 19 | Ref. 17 | Ref. 18 | Ref. 16 | $D_0$ (eV)[a,b] |
| $W(CO)_6^+$ | 8.24±0.03 (1505±5 Å) | 8.56 | 8.47 | 8.43 | 8.60 | 8.46 | 1.56±0.09 |
| $W(CO)_5^+$ | 9.80±0.08 (1265±10 Å) | 9.8 | 9.86 | 9.21 | 10.03 | 9.97 | 1.68±0.14 |
| $W(CO)_4^+$ | 11.48±0.11 (1080±10 Å) | 12.7 | 11.93 | 12.05 | 12.22 | 11.82 | 1.85±0.13 |
| $W(CO)_3^+$ | 13.33±0.07 (930±5 Å) | 14.9 | 13.7 | 13.87 | 14.06 | 13.60 | 2.36±0.13 |
| $W(CO)_2^+$ | 15.69±0.10 (790±5 Å) | 17.6 | 15.8 | 16.08 | 16.29 | 16.07 | ≤2.41±0.16 ≈1.43[c] |
| $WCO^+$ | ≤18.10±0.13 (685±5 Å) | 20.2 | 18.7 | 18.51 | 18.36 | 18.50 | <0.45 ≈1.43[c] |
| $W^+$ | — | 22.9 | 21.7 | 22.25 | 21.01 | | |

a) Bond dissociation energies at 0 K for $CO\text{-}W(CO)_{n-1}^+$ (n=1-6).

b) PIE values. This work.

c) Assuming that $D_0[CO\text{-}WCO^+] \approx D_0(W^+\text{-}CO)$ and using the $AE[Cr(CO)_2^+] = 15.69$ eV and the thermochemical threshold for $Cr^+(^6D)$ (18.55 eV), we obtain an estimate of 1.43 eV for $D_0[CO\text{-}WCO^+]$ and $D_0(W^+\text{-}CO)$.

The sequential $D_0$ values for $W(CO)_6^+$ calculated using the IE and AEs of the present PIE experiment are included in Table IV. Based on the 0 K thermochemical threshold (18.55 eV) for $W^+$ and PIE AE($WCO^+$)=18.10 eV, we estimate that $D_0(W^+\text{-}CO) = 0.45$ eV. The theoretical predictions and experimental values for $D_0(Mo^+\text{-}CO)$ and $D_0(Cr^+\text{-}CO)$ are in the range of 0.8-1.0 eV. The value of 0.45 eV for $D_0(W^+\text{-}CO)$ is most likely too low. Thus, the AE($W^+$-CO) = 18.1 eV and $D_0[CO\text{-}WCO^+]$=2.41 eV obtained here are probably upper limits. If $D_0[CO\text{-}WCO^+] \approx D_0(W^+\text{-}CO)$ as in the case of the Mo and Cr systems, we expect that $D_0[CO\text{-}WCO^+]$ and $D_0(W^+\text{-}CO)$ have a value of ≈1.43 eV which is lower than the average W-CO bond dissociation energy of 1.71 eV for $W(CO)_6^+$. We note that the higher $D_0[CO\text{-}W(CO)_2^+]$ and $D_0[CO\text{-}W(CO)_3^+]$ also seems to correlate with the higher PIEs for $W(CO)_3^+$ and $W(CO)_4^+$ as shown in Figs. 5(a) and 5(b).

The total PIE spectrum for $W(CO)_n^+$ (n=1-6) in the photon energy range of 7.5-19.1 eV is shown in Fig. 6(a). The HeI photoelectron spectrum of $W(CO)_6$ reported in Ref. 22 is reproduced in Fig. 6(b) for comparison with the total PIE spectrum of Fig. 6(b). The first photoelectron peak at 8.5 eV is associated with ionization of an electron from the highest occupied $t_{2g}$ orbital of $W(CO)_6$, which has mostly the W(5d) and CO($2\pi$) characters. The broad photoelectron band in the photon region of 13-16 eV is assigned to ionization from molecular orbitals with mainly the CO($1\pi$ and $5\sigma$) characters. The rise in the total PIE observed in the photon region of 9.5-13 eV can be attributed to autoionization from Rydberg states of $W(CO)_6$. Vibrationally excited $W(CO)_6^+$ initially formed by autoionization in this photon energy region may subsequently decompose to $W(CO)_5^+ + CO$. As shown in Figs. 2(b), 4(b) and 6(b), the HeI spectra for $Cr(CO)_6$, $Mo(CO)_6$, and $W(CO)_6$ have essentially the same structures. Thus, it is not surprising that the total PIE spectra for $W(CO)_n^+$ and $Mo(CO)_n^+$ (n=0-6) are also similar.

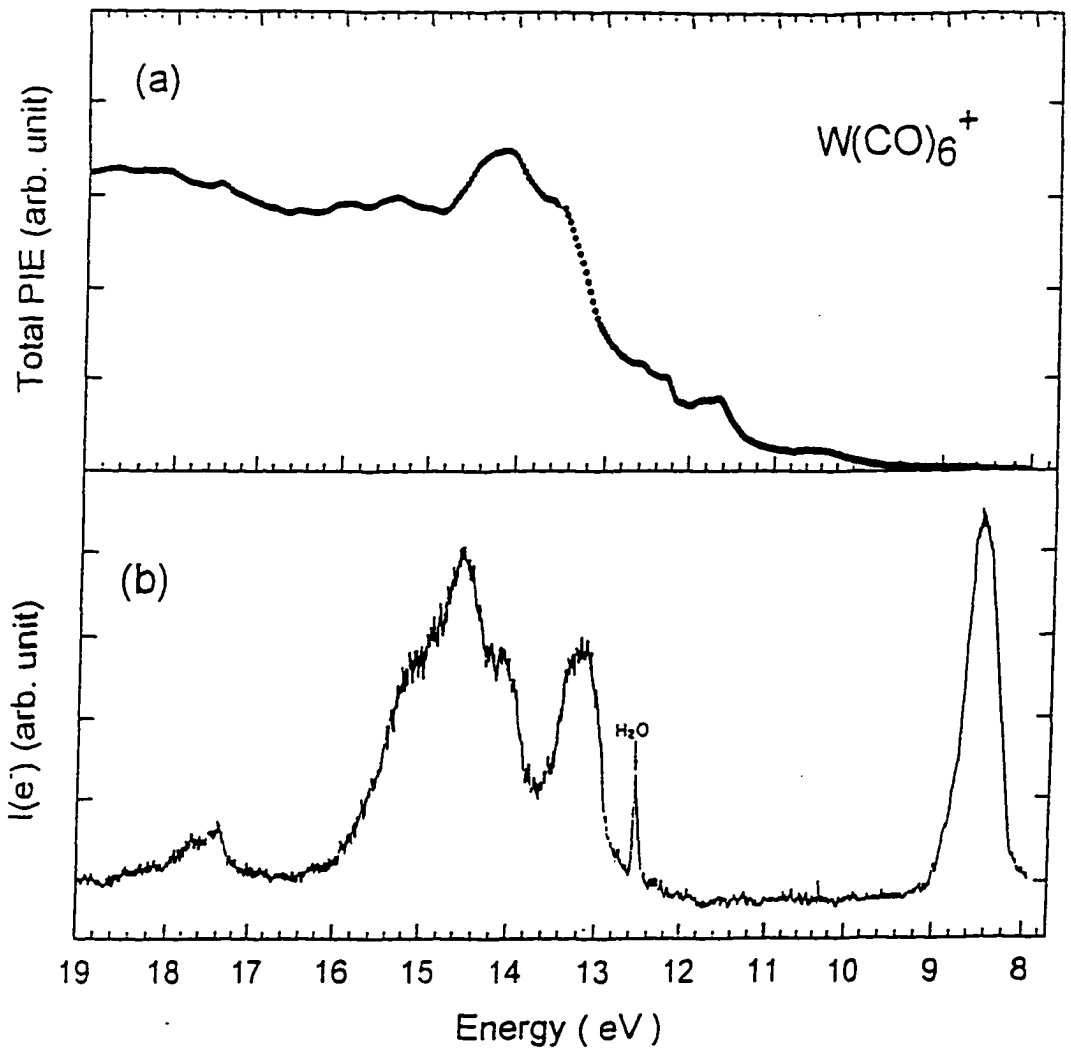


Figure 6 (a) The sum of the PIE (total PIE) for $W(CO)_n^+$ (n=0-6) in the photon energy range from 7.7-19.0 eV range. (b) HeI photoelectron spectrum for $W(CO)_6$ in the energy range 7.7-19.0 eV (Ref. 22). $I(e^-)$ is the photoelectron intensity.

**Discussion**

Due to the large difference in IE(M) [IE(Cr)=6.77 eV, IE(Mo)=7.10 eV, IE(W)=7.60 eV] and IE(CO) (14.014 eV),[23] the bonding interactions between M and CO are expected to be inefficient, and should be mostly electrostatic in nature. This picture is reflected by the small $D_0$ values for $M(CO)_6$ and $M(CO)_6^+$, M=Cr, Mo, and W. Since the highest occupied molecular orbital is expected to be dominated by the atomic orbitals of M, we expect that the IE value for $M(CO)_6$ is similar to that of M. Stemming from this consideration, the IE for $M(CO)_6$ should have the trend: $IE[Cr(CO)_6] < IE[Mo(CO)_6] < IE[W(CO)_6]$. Furthermore, as the IE is increased from Cr to Mo to W, the bonding interaction between M and CO should become more favorable. Thus, we expect that the $D_0$(M-CO) values for $M(CO)_6$ and $M(CO)_6^+$ are in the order: $D_0$(Cr-CO) < $D_0$(Mo-CO) < $D_0$(W-CO). As shown in Fig. 7, this trend for individual $D_0[CO\text{-}M(CO)_{n-1}^+]$ (n=3-6) values is observed in the present experiment. The average M-CO bond dissociation energies for $M(CO)_6^+$, M=Cr, Mo, and W, certainly obey this trend. Although the trend for the IEs is also observed, the IE differences for $M(CO)_6$ are surprisingly slight and significantly smaller than the differences for IE(Cr), IE(Mo), and IE(W).

The complication in describing the bonding for group 6B transition metal carbonyl species arises in part due to the small energy gap between the metal nd and (n+1)s atomic orbitals. The increasing importance of relativistic effects (such as spin-orbit interaction) as M is changed from Cr to Mo to W can account for the observed variation in $D_0$ values for M-CO. A more refined bonding picture for group 6B transition metal carbonyl species takes into account the possible interactions between the highest occupied and lowest unoccupied orbials of M and CO. The lowest energy electronic configuration for Cr, Mo, and W are $3d^54s$, $4d^55s$, and $5d^46s^2$,

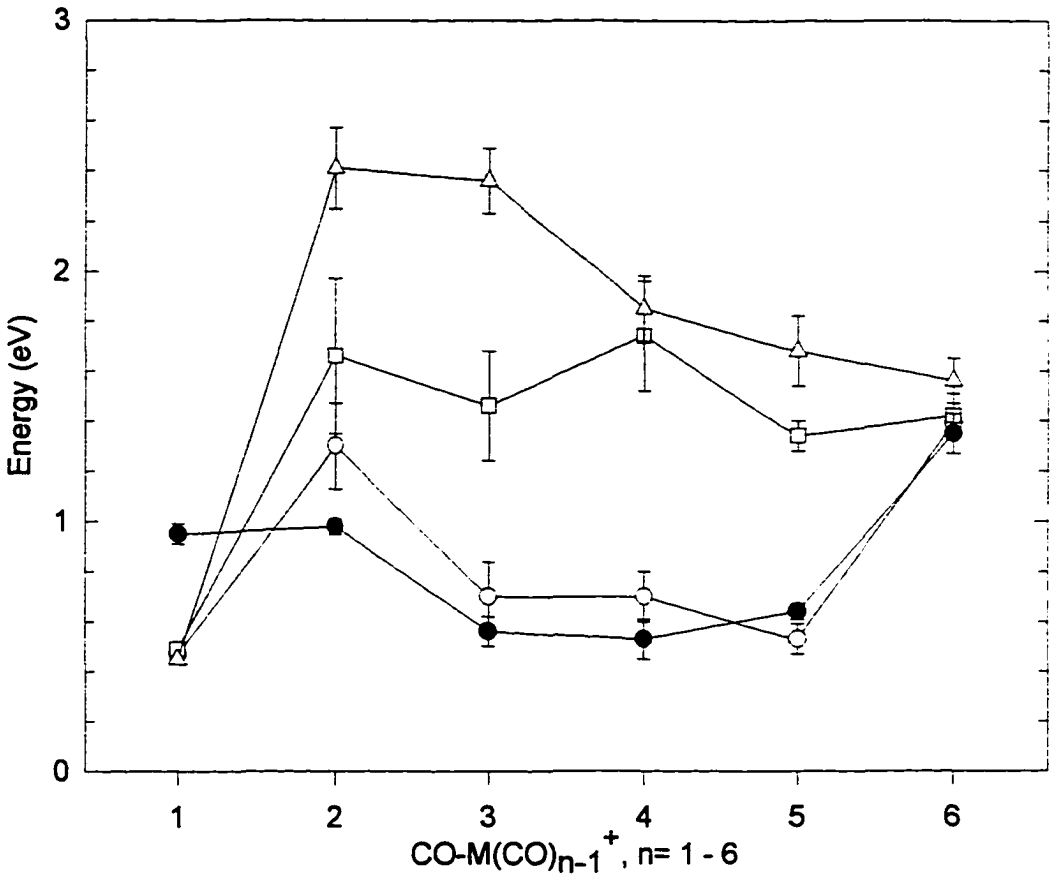


Figure 7 The bond dissociation energies ($D_0$) for $CO\text{-}M(CO)_{n-1}^+$ (n=1-6), M= Cr (O), Mo ( ), and W (Δ) determned in the present PIE experiment. Note that the $D_0[CO\text{-}MCO^+]$ values are upper limits, while the $D_0(M^+\text{-}CO)$ values are lower limits (see the text). The $D_0$ values obtained in the CID study of Ref. 7 are shown as (●).

respectively, whereas the cations $Cr^+$, $Mo^+$, and $W^+$ have the respective ground state electronic configurations of $3d^5$, $4d^5$, and $5d^46s$. Based on the molecular orbital scheme, the stability of $M(CO)_6$ is largely derived from two types of bonding interactions. One involves σ-type bonding, which arises from the donation of an σ-type electron pair from the C atom end of CO to vacant metal orbitals. The other is π-type bonding interactions, resulting from the back donation of electrons from filled metal dπ orbitals into the unoccupied 2π (antibonding $\pi^*$-orbital) of CO. The π-back-donation has the effect of strengthening the M-C bond and weakening of the C-O bond. The recent theoretical analysis of Ziegler and co-workers[12] shows that relativistic effects play a key role in the periodic trends among M-CO bond dissociation energies and bond distances. The inclusion of relativistic effects in the calculations are seen to strengthen the M-CO bonds. Depending on the level of theory, for $Cr(CO)_6$, $Mo(CO)_6$, and $W(CO)_6$, the relativistic effects increase the first $D_0$(M -CO) values by 0.3-0.9, 1.5-2.4, and 4.9-8.4 kcal/mol, respectively. Relativistic effects also diminish the steric repulsive interactions between $M(CO)_5$ and CO as a result of the reduction in electronic kinetic energy due to the relativistic mass-velocity correction.[12] The relativistic effects, which raise the metal d-orbitals, reduce the energy gap between the M(dπ) and CO($\pi^*$) orbitals, and thus enhance the π-back-donation stabilization factor. The increase in the M(dσ) orbital energy will on the other hand increase the energy gap between the M(dσ) and CO(σ) orbitals, and thus reduce the CO to M σ-donation bonding interaction. However, it is concluded that the stabilization factor due to enhancing π-back-donation prevails over the destabilization factor due to reducing the σ-donation. We note that the formation of $M(CO)_6^+$ involves the removal of an electron from the highest occupied molecular orbital of $M(CO)_6$. Thus, the

comparison of the first $D_0$ values for $M(CO)_6$ and $M(CO)_6^+$ should be most sensitive in probing the stabilization factors due to the $\pi$-back-donation and $\sigma$-donation bonding interactions.

The first bond dissociation energies at 298 K for $Cr(CO)_6$, $Mo(CO)_6$, and $W(CO)_6$ have been measured using pulsed pyrolysis techniques to be 36.8±2.0, 40.5±2.0, and 46.0±2.0 kcal/mol, respectively.[3] After thermal corrections,[11] we estimated that $D_0[CO\text{-}Cr(CO)_5]$= 34.8±2.0 kcal/mol, $D_0[CO\text{-}Mo(CO)_5]$= 38.5±2.0 kcal/mol, and $D_0[CO\text{-}W(CO)_5]$= 44.0±2.0 kcal/mol. In comparison, the first $D_0$ values for $Cr(CO)_6^+$, $Mo(CO)_6^+$, and $W(CO)_6^+$ determined here are: 32.1±1.4, 32.7±2.1, and 36.0±2.1 kcal/mol, respectively. The corresponding differences in the first $D_0$ values for the neutrals and cations are 2.7 kcal/mol for $Cr(CO)_6^+$, 5.8 kcal/mol for $Mo(CO)_6^+$, and 8.0 kcal/mol for $W(CO)_6^+$. These losses in stability by removal of an electron from the highest occupied $t_{2g}$ molecular orbital of $M(CO)_6$ are consistent with the trend expected for the importance of relativistic effects on $Cr(CO)_6$, $Mo(CO)_6$, and $W(CO)_6$. This observation can be taken as strong support for the theoretical analysis[12] that the stabilization factor due to $\pi$-back-donation is more important for heavier transition metal elements.

**Conclusion**

We have measured the PIE spectra for $M(CO)_n^+$ (n=0-6), M=Cr, Mo, and W, in the photon energy range of 7.75-19.07 eV. The sequential $D_0$ values for $M(CO)_6^+$ have been calculated using the observed IEs for $M(CO)_6$ and AEs for $[M(CO)_n^+]$ (n=0-6), M=Cr, Mo, and W. The comparison between the $D_0$ values for the $Cr(CO)_6^+$ system obtained here and in the previous CID and theoretical studies indicates that the values for $D_0[CO\text{-}M(CO)_{n-1}^+]$ (n=3-6) are likely to be more reliable than those for $D_0[CO\text{-}M(CO)_{n-1}^+]$ (n=1-2), M=Mo and W.

The observed decreases of the first $D_0$ values for $M(CO)_6^+$ compared to those for $M(CO)_6^+$, M=Cr, Mo, and W, support the theoretical analysis of Ziegler and co-workers[12] that the stabilizing factors due to relativistic effects are more important for heavier transition metal elements. We hope that this experiment will stimulate rigorous theoretical studies of group 6B transition metal carbonyl species.

**References**


1. D. R. Lloyd and E. W. Schlag, *Inorg. Chem.* **8**, 2544 (1969).
2. G. Distefano, *J. Res. Natl. Bur. Stand.* **74A**, 233 (1970).
3. K. E. Lewis, D. M. Golden, and G. P. Smith, *J. Am. Chem. Soc.* **106**, 3905 (1984).
4. P. R. Das, T. Nishimura, G. G. Meisels, *J. Phys. Chem.***89**, 2808 (1985).
5. K. Norwood, A. Ali, G. D. Flesch, and C. Y. Ng, *J. Am. Chem. Soc.* **112**, 7502 (1990).
6. L. S. Sunderlin, D. Wang, R. R. Squires, *J. Am. Chem. Soc.* **114**, 2788 (1992).
7. F. A. Khan, D. E. Clemmer, R. H. Schultz, and P. B. Armentrout, *J. Phys. Chem.* **97**, 7978 (1993).
8. L. A. Barnes, M. Rosi, and C. W. Bauschlicher, Jr., *J. Chem. Phys.* **93**, 609 (1990).
9. A. Ricca and C. W. Bauschlicher, Jr., *J. Phys. Chem.* **99**, 5922 (1995).
10. A. Ricca and C. W. Bauschlicher, Jr., *J. Phys. Chem.* **98**, 12899 (1994).
11. A. W. Ehlers and G. Frenking, *J. Am. Chem. Soc.* **116**, 1514 (1994).
12. J. Li, G. Schreckenbach and T. Ziegler, *J. Phys. Chem.* **98**, 4838 (1994).
13. M. Elian and R. Hoffmann, *Inorg. Chem.* **14**, 1058 (1975).

14. H. M. Rosenstock, K. Draxl, B. W. Steiner, and J. T. Herron, *J. Phys. Ref. Data 6. Suppl. 1* (1977).

15. R. E. Winters and R. W. Kiser, *Inorg. Chem.* **4**, 157 (1965).

16. A. Foffani, S. Pignataro, B. Cantone, F. Grasso, *Z. Physik. Chem.* **45**, 79 (1965).

17. D. R. Bidinosti, N. S. McIntyre, *Can. J. Chem.* **45**, 641 (1967).

18. G. A. Junk and H. J. Svec, *Z. Naturforsch, B* **23**, 1 (1968).

19. G. D. Michels, G. D. Flesch, and H. J. Svec, *Inorg. Chem.* **19**, 479 (1980).

20. C. Y. Ng, *Adv. Chem. Phys.* **52**, 265 (1983).

21. C. Y. Ng, in "Vacuum Ultraviolet Photoionization and Photodissociation of Molecules and Clusters", edited by C. Y. Ng (World Scientific, Singapore, 1991), p. 169.

22. D. W. Turner, C. Baker, A. D. Baker, C. R. Brundle, "Molecular Photoelectron Spectroscopy" (Wiley, London 1970).

23. S. G. Lias, J. E. Bartmess, J. F. Liebman, J. L. Holmes, R. D. Levin, and W. G. Mallard, *J. Phys. Ref. Data, Suppl. 1*, **14** (1988).

24. R. B. Freas and D. P. Ridge, *J. Am. Chem. Soc.***102**, 7129 (1980).

25. P. B. Armentrout, L. F. Halle, and J. L. Beauchamp, *J. Am. Chem. Soc.* **103**, 501 (1981).

26. S. K. Huang and M. L. Gross, *J. Phys. Chem.***89**, 4422 (1985).

27. C. E. Moore, "Atomic Energy Levels", Natl. Bur. Stand. (U.S.) (U.S. GPO, Washigton, D.C.), Vol. II (1952); ibid., Vol. III (1953); ibid, Vol. III (1958).

28. The theoretical values of 0.93 and 0.98 eV for bond dissociation energies of $Cr^+$-CO and CO-$CrCO^+$, respectively, have not been corrected for zero point vibration energies.

29. T. A. Seder, S. P. Church, A. J. Ouderkirk, and E. Weitz, *J. Am. Chem. Soc.* **107**, 1432 (1985); T. A. Seder, S. P. church, and E. Weitz, *J. Am. Chem. Soc.* **108**, 4721 (1986); T. A. Seder, A. J. Ouderkirk, and E. Weitz, *J. Chem. Phys.* **85**, 1977 (1986).

30. T. R. Fletcher and R. N. Rosenfield, *J. Am. Chem. Soc.* **108**, 1686 (1986).

31. P. M. Guyon, T. Baer, and I. Nenner, *J. Chem. Phys.* **78**, 3665 (1983).

## II. COMBINING EXPERIMENT AND THEORY: THERMOCHEMISTRY OF $SF_N$, $SF_N^+$, AND $SF_N^-$, N=1-6

A paper published in the Journal of American Chemical Society

Y. S. Cheung, Y. J. Chen, C. Y. Ng, S. W. Chiu, and W. K. Li

**Abstract**

The appearance energies for the formation of $SF_3^+$, $SF_4^+$, and $SF_5^+$ from $SF_6$, and for the formation of $SF_2^+$ and $SF_3^+$ from $SF_4$ have been reexamined by the molecular beam photoionization mass spectrometric (PIMS) method. The heats of formation at 0 K ($\Delta_fH°_0$) for $SF_n^+$ (n=2-4) derived from this and previous PIMS studies are in agreement with G2 and G2(MP2) predictions. The G2 and G2(MP2) calculations allow the examination of the consistency of experimental thermochemical data for $SF_n$, $SF_n^+$, and $SF_n^-$ (n = 1-6) in the literature. Based on comparisons between G2 and G2(MP2) theoretical predictions and experimental measurements, we recommend the following self-consistent set of experimental $\Delta_fH°_0$ values for $SF_n$, $SF_n^+$, and $SF_n^-$ (n = 1-6): $\Delta_fH°_0(SF)$ = 2.9±1.4 kcal/mol, $\Delta_fH°_0(SF^+)$ = 240.9±1.2 kcal/mol, $\Delta_fH°_0(SF^-)$ = -43±13 kcal/mol, $\Delta_fH°_0(SF_2)$ = -67.5±3.5 kcal/mol, $\Delta_fH°_0(SF_2^+)$ = 164.9±3.3 kcal/mol, $\Delta_fH°_0(SF_3)$ = -103.6±2.5 kcal/mol, $\Delta_fH°_0(SF_3^+)$ = 85.0±1.9 kcal/mol, $\Delta_fH°_0(SF_3^-)$ = -175.1±5.2 kcal/mol, $\Delta_fH°_0(SF_4)$ = -182.5±2.5 kcal/mol, $\Delta_fH°_0(SF_4^+)$ = 91.9±2.5 kcal/mol, $\Delta_fH°_0(SF_4^-)$ = -217.1±5.2 kcal/mol, $\Delta_fH°_0(SF_5)$ = -205.9±3.4 kcal/mol, $\Delta_fH°_0(SF_5^+)$ = 16.4±3.6 kcal/mol, $\Delta_fH°_0(SF_5^-)$ = -291±5.7 kcal/mol, $\Delta_fH°_0(SF_6)$ = -288.4±0.2 kcal/mol, and $\Delta_fH°_0(SF_6^-)$ = -314.5± 2.4 kcal/mol. For $\Delta_fH°_0(SF_2^-)$, which is not known experimentally, we recommend a G2 value of -102.7 kcal/mol. At the MP2/6-31+G(d) level, $SF_6^+$ is found to be unstable with respect to

dissociation forming lower sulfur fluoride cations. We have rationalized the theoretical structures for $SF_n$, $SF_n^+$, and $SF_n^-$ (n=1-6) using the valence-shell-electron-pair-repulsion theory. The alternating patterns of high and low values observed for the $SF_{n-1}$-F (n=2-6), $SF_{n-1}^+$-F (n=3-5), and $SF_{n-1}^-$-F (n=2-6) bond dissociation energies at 0 K and for the IEs and EAs of $SF_n$ (n=1-6) are attributed to special stabilities for closed-shell molecular species, ($SF_3^+$, $SF_2$, and $SF^-$), ($SF_5^+$, $SF_4$, and $SF_3^-$), and ($SF_6$ and $SF_5^-$), with fully-filled eight, ten, and twelve valence electron shells around the central S atoms, respectively.

**Introduction**

Reliable thermochemical data are among the most fundamental and useful information for chemical species and are used to predict their chemical reactivities. Fluorinated molecules such as $SF_6$ have found widespread use as gaseous dielectrics in the electric power industry and as plasma etching gases in the semiconductor industry. For sulfur hexafluoride, $SF_n$, $SF_n^+$, and $SF_n^-$ (n=1-5) are expected to be formed as byproducts.[1-12] Sulfur hexafluride has also been suggested as a tracer in hazardous waste incineration systems.[13] The toxic nature of breakdown byproducts of $SF_6$ in these applications is of environmental concern.[14,15] Accurate thermochemical data for F- and S-containing neutral and ionic species are critical for understanding the complex kinetics involved in these applications.

In addition to practical industrial applications, sulfur fluorides are excellent examples of hypervalent[16] compounds. The studies[17-19] of the neutral and ionic sulfur fluoride species have also been motivated to understand their structures as a model system for achieving deeper insight into the bonding of hypervalent species.

Despite the existence of a large body of thermochemical data for the $SF_n$ and $SF_n^+$ (n=1-6) systems, general agreement among previous measurements for many sulfur fluorides is lacking.[20] Several recent reports address the inconsistency of the literature thermochemistry for the $SF_n$ and $SF_n^+$ systems.[20-24] The ion collision-induced dissociation (CID) and endothermic charge transfer study of $SF_n^+$ (n=1-5) by Fisher, Kickel, and Armentrout[20] represents the most comprehensive measurements of the IEs for $SF_n$ (n=1-6) and the sequential bond dissociation energies at 0 K ($D°_0$) for $SF_{n-1}^+$-F. They have also made a detailed summary of the literature thermochemical data for $SF_n$ and $SF_n^+$ (n=1-6) published before 1992.

Traditionally, the sequential bond dissociation energies for $SF_{n-1}^+$-F (n=1-6) are measured by electron impact[25-27] or photoionzation[28-33] mass spectrometry (PIMS). In these experiments, the IE for $SF_6$ and the appearance energies (AEs) for $SF_n^+$ (n=1-5) formed in the dissociative ionization of $SF_6$ are measured. The parent $SF_6^+$ ion has not been observed experimentally.[20,25,30,32] This, together with the observation that the ionization onset for $SF_6$ observed by photoelectron (PE) spectroscopy[34-37] is nearly identical to the AE for $SF_5^+$ from $SF_6$ measured by PIMS experiment,[28-30,32] indicates that $SF_6^+$ is unstable with respect to $SF_5^+$ + F. We note that $SF_6^+$ may exist in the form of an ion complex, $SF_5^+\cdots F$.

Regardless of the minor difficulties due to the rotational and vibrational hot band effects and the poor Franck-Condon factor for ionization excitations, the most serious problem encountered in AE measurements is the kinetic shift effect, which may prevent observation of the true AE for a given product species.[38] Depending on the dissociation dynamics of the parent ion produced in photoionization, the photofragments may be formed in an excited state. If the excited state cannot be identified, the $D°_0$ deduced from the

experimental AE is erroneous. Since the kinetic shift effect is statistical in nature, it does not depend on the mode of energization of the precursor ions. Thus, the kinetic shift effect may affect the AEs measured in the ion CID[20] as well as in the PIMS experiments. Considering that each experimental technique has its own advantages and limitations, reliable thermochemical data for a complex system such as the sulfur fluorides require the application of as many experimental methods as possible.

When thermochemical data obtained by different experimental methods do not agree, theoretical predictions calculated using a reliable *ab initio* quantum chemical procedure help to reveal possible experimental problems. It has been shown that the Gaussian-2 *ab initio* procedure[39] yields accurate predictions for bond dissociation energies, adiabatic ionization energies (IE), adiabatic electron affinities (EA), and proton affinities of molecules and radicals consisting of the first- and second-row elements. Most recently, Curtiss *et al.* have introduced two variations of the G2 theory at reduced Møller-Plesset (MP) perturbation orders.[40] The basis-set extension energy corrections obtained at the 2nd and 3rd orders are referred to as the G2(MP2) and G2(MP3) theories, respectively. These theories give slightly poorer results but require significantly less computational time and disk storage than the G2 theory does. In recent experimental and theoretical studies, we have performed G2, G2(MP3), and G2(MP2) *ab initio* calculations of the energetics for sulfur-containing polyatomic neutral species $CH_3S$ (Ref. 41), $CH_3SS$ (Ref. 42), $C_2H_5S$ (Ref. 43), and $CH_3SSCH_3$ (Ref. 44) and their ions for comparison with experimental measurements. These comparisons indicate that G2 predictions for the adiabatic IEs and heats of formation of these species at 0 K ($\Delta_fH°_0$) and at 298 K ($\Delta_fH°_{298}$) are accurate to ±0.15 eV.

In this report, we present the results of a combined experimental and theoretical investigation of the $SF_n$, $SF_n^+$, and $SF_n^-$ (n=1-6) systems. The AEs for $SF_n^+$ (n=3-5) from $SF_6$ and those for $SF_n^+$ (n=2,3) from $SF_4$ have been reexamined using the modulated molecular beam PIMS method.

$$SF_6 + h\nu \rightarrow SF_5^+ + F + e^- \quad (1)$$

$$\rightarrow SF_4^+ + 2F + e^- \quad (2)$$

$$\rightarrow SF_3^+ + 3F + e^- \quad (3)$$

$$SF_4 + h\nu \rightarrow SF_4^+ + e^- \quad (4)$$

$$\rightarrow SF_3^+ + F + e^- \quad (5)$$

$$\rightarrow SF_2^+ + 2F + e^- \quad (6)$$

We note that the photoionization efficiency (PIE) spectra for $SF_n^+$ (n=3-5) from $SF_6$ have been examined previously in gas cell[28-30] and effusive beam[32] PIMS experiments. The AEs for processes (1),[28,30] (2),[32] and (3)[30] have been reported. Processes (4), (5), and (6) have also been investigated recently using the photoionization and photoelectron-photoion coincidence techniques.[45] Since the $\Delta H^\circ_{f0}$ values determined for $SF_3^+$ and $SF_4^+$ in the CID experiment[20] are found to be incompatible with those derived from previous photoionization experiments, we decided to reexamine these processes, focusing on the AE determinations.

We have performed extensive *ab initio* calculations on $SF_n$, $SF_n^+$, and $SF_n^-$ (n=1-6) using the G2 and G2(MP2) procedures. A preliminary report on the G2(MP2) calculations of the energetics for $SF_n$ (n=4-6) and $SF_n^+$ (n=4,5) and their comparison with the literature

thermochemical data for these species has been published.[23] Here, we present a thorough analysis of the results of the previous and present PIMS experiments. The good agreement between experimental results obtained in the PIMS studies and predictions calculated using the G2 and G2(MP2) procedures indicates that AE measurements using PIMS can provide accurate thermochemical data for complex systems such as $SF_6^+$. The G2 and G2(MP2) calculations make possible a thorough assessment of the literature thermochemical data[46] for the $SF_n$, $SF_n^+$, and $SF_n^-$ (n=1-6) systems. The detailed comparison presented here allows the selection of a self-consistent, possibly more reliable, set of experimental values for the IEs and EAs of $SF_n$ and $\Delta_fH°_0$'s of $SF_n$ and $SF_n^+$ (n=1-6). The G2 and G2(MP2) $\Delta_fH°_0$ values for $SF_n$, $SF_n^-$, and $SF_n^-$ (n=1-6) are found to be in good agreement with available experimental results.

The theoretical structures for $SF_n$, $SF_n^+$, and $SF_n^-$ (n=1-6) optimized at the MP2/6-31G(d) level are presented. We rationalize these structures based on the valence-shell-electron-pair-repulsion (VSEPR) theory.[47] The experimental trends observed for the $D°_0$'s, IEs, and EAs of these molecular species are also rationalized.

## Experimental and Theoretical Methods

### A. Photoionization mass spectrometric measurements

The PI measurements of $SF_6$ and $SF_4$ are performed using the molecular beam photoionization mass spectrometer which has been described in detail previously.[48-50] Briefly, the apparatus consists of a 3 m near normal incidence vacuum ultraviolet (VUV) monochromator (McPherson 2253), a capillary discharge lamp, a VUV light detector, and a quadrupole mass spectrometer for ion detection.

A quartz nozzle with a diameter of 0.127 mm is used to introduce the neutral $SF_6$ ($SF_4$) at room temperature. The supersonic beam is produced by the expansion of 14% $SF_6$ (25% $SF_4$) seeded in Ar (total stagnation pressure = 415 Torr) through the quartz nozzle. The gas beam is skimmed by a conical skimmer before entering the photoionization region of a quadrupole mass spectrometer. Photoionization sampling of the $SF_6$ ($SF_4$) beam takes place ≈6 cm from the nozzle tip.

Sulfur hexafluoride is supplied by Aldrich with a purity of ≥99.75% and sulfur tetrafluride is obtained from Air Products with a purity of 94.0%. The major impurity in the $SF_4$ sample is $S_2F_2$. Both $SF_6$ and $SF_4$ samples are used without further purification.

Photoions are produced by dispersed vacuum ultraviolet (VUV) radiation at a wavelength resolution of ≈1.5 Å (Full-width-at-half-maximum). Within the sensitivity of this experiment, $SF_6^+$ from $SF_6$ is not observed. Because of the limited photon energy range of our photon source, the photoionization efficiency (PIE) spectra for $S^+$, $SF^+$, and $SF_2^+$ from $SF_6$ cannot be measured. The formation of $SF_4^+$, $SF_3^+$, and $SF_2^+$ from $SF_4$ are observed. A chopper operated at 150 Hz is used to chop the VUV light. The photoion signal is taken to be the difference between the ion intensity observed when the VUV light is on and that when the VUV light is off. We find that by modulating the VUV radiation, the influence in the AE measurements due to the dark counts of the ion detector is greatly minimized. The counting time at each wavelength is typically 20-40 sec. The PIE spectra reported here represent the average of at least two reproducible scans.

**B. *Ab initio* calculations**

The *ab initio* G2 theoretical procedure has been described in detail by Curtiss et al.[39] Briefly, at the G2 level of theory, molecular structures are optimized using MP2 perturbation

calculations with the 6-31G(d) basis set and all the electrons are included [MP2(full)/6-31G(d)]. Equilibrium structures are found for all sulfur fluoride species except $SF_6^+$, where attempts to locate an equilibrium structure at the MP2/6-31G(d) and MP2/6-31+G(d) levels have been unsuccessful. All single-point calculations involved are based on the MP2/6-31G(d) optimized structures. The G2 method, an approximation of a QCISD(T)/6-311+G(3df,2p) calculation, requires single-point calculations at the MP4/6-311G(d,p), MP4/6-311+G(d,p), MP4/6-311G(2df,p), QCISD(T)/6-311G(d,p), and MP2/6-311+G(3df,2p) levels. A small semiempirical correction is applied to account for high level correlation effects. The MP2/6-31G(d) harmonic vibrational frequencies, scaled by 0.93, are used to correct zero-point vibrational energies (ZPVE).[41] The total energy at 0 K ($E_0$) is equal to $E_e$ + ZPVE, where $E_e$ is the total electronic energy. All calculations are carried out on IBM RS6000-320h and RS6000/340 work stations or CRAY-YMP and CRAY-2 using the Gaussian 90 and Gaussian 92 package programs.[51]

Recently, Curtiss et al. have introduced two variations of G2 theory [G2(MP2) and G2(MP3)] at reduced Møller-Plesset (MP) perturbation orders.[40] The G2(MP2) and G2(MP3) theories, which provide substantial savings in computational time and disk storage, have been tested on the same set of 125 systems used for validation of the G2 theory.[39,40] The average absolute deviations of G2(MP2) and G2(MP3) theories from experiment are only 0.4 kcal/mol greater than that observed for G2 theory.

Due to the relatively large size of the molecule, we have performed calculations for $SF_n$, $SF_n^+$, and $SF_n^-$ (n=3-6) only at the G2(MP2) levels of theory. In order to verify the accuracy of G2(MP2) and G2(MP3) predictions as compared to G2 predictions, we have compared the results obtained by G2(MP2) and G2(MP3) on $SF_n$, $SF_n^+$, and $SF_n^-$ (n=1,2) with those calculated

using the G2 procedure, since the energetics for the $SF_n$, $SF_n^+$, and $SF_n^-$ (n=1,2) species are relatively well known. This comparison of G2 predictions and experimental molecular energies for these smaller sulfur fluorides also serves to verify the accuracy of the G2 procedure.

Among the closed-shell species, only $SF^+$ is found to be RHF unstable,[52] i.e., the UHF wavefunction yields lower energy than the RHF wavefunction. Hence, in the optimization and subsequent single-point energy calculations, the UHF wavefunction is employed for $SF^+$. Restricted HF wavefunctions are used for other closed-shell species, $SF^-$, $SF_2$, $SF_3^+$, $SF_3^-$, $SF_4$, $SF_5^+$, $SF_5^-$, and $SF_6$.

Because of the very large size of $SF_6^-$, the UQCISD(T)/6-311G(d,p) single-point energy calculation is computationally very demanding. Hence, we obtain the G2(MP2) energy by approximating the UQCISD(T)/6-311G(d,p) energy using the following approximated additivity rule:

$$\begin{aligned} &E[\text{QCISD(T)/6-311G(d,p)}] \\ &= E[\text{MP4/6-311G(d,p)} + \{E[\text{QCISD(T)/6-311G(d,p)}] - E[\text{MP4/6-311G(d,p)}]\} \\ &. E[\text{MP4/6-311G(d,p)} + \{E[\text{QCISD(T)/6-31G(d,p)}] - E[\text{MP4/6-31G(d,p)}]\} \end{aligned} \quad (7)$$

The same approximation is repeated for other sulfur fluoride species in verification calculations. Comparisons are made between IE, EA, and $)H_{f0}$ predictions calculated using this approximated G2(MP2) [AG2] and G2(MP2) schemes are made.

**Results and Discussion**

**A. Theoretical structures for $SF_n$, $SF_n^+$, and $SF_n^-$ (n=1-6)**

Figure 1 shows the equilibrium structures for $SF_n$, $SF_n^+$, and $SF_n^-$ (n=1-6) optimized at the MP2/6-31G(d) level. Bond distances (*r*) are in C and bond angles (*p*) are in degrees. Many of these molecules are hypervalent species and their structures can be rationalized by the VSEPR model.[47] Traditionally, the bonding and structures for some of these hypervalent sulfur fluorides are described by VSEPR along with the valence bond $sp^3d$ and $sp^3d^2$ hypbridization schemes. However, recent reliable *ab initio* investigations[53] of main group hypervalent species indicate that the *d*-orbital participation in the bonding of $SF_4$ and $SF_6$ is insignificant. Thus, the equilibrium structures for $SF_n$, $SF_n^+$, and $SF_n^-$ (n=1-6) are rationalized below using the VSEPR model without invoking the $sp^3d$ and $sp^3d^2$ hypbridization schemes. We note that *r*(S-F) increases from $SF^+$ to SF to $SF^-$. This trend is expected since the nonbonding electron density on sulfur increases from $SF^+$ to SF to $SF^-$, and hence the repulsion between the nonbonding electrons on S and F and *r*(S-F) increases accordingly.

The *r*(S-F) increases and ∠F-S-F decreases from $SF_2^+$ to $SF_2$. As both S atoms in $SF_2^+$ and $SF_2$ are $sp^3$ hybridized, the higher nonbonding electron density localized in the S $sp^3$ orbital in $SF_2$ leads to longer *r*(S-F) and smaller ∠F-S-F. In the case of $SF_2^-$, *r*(S-F) is longer and ∠F-S-F is greater than those for $SF_2^+$ and $SF_2$. The anion $SF_2^-$ is a hypervalent species with 42 electron pairs around the S atom. The VSEPR model predicts that the two F atoms occupy the axial positions and that the two and a half lone pairs occupy the equatorial positions of a trigonal bipyramidal structure. Since the three equatorial lone pair lobes are only partially filled, the 3-fold axis cannot be maintained and the anion is distorted from linearity. The increasing nonbonding electron density at the S atom in $SF_2^-$ is also responsible for *r*(S-F) (1.67-1.80 C) being longer for $SF_2^-$ than for

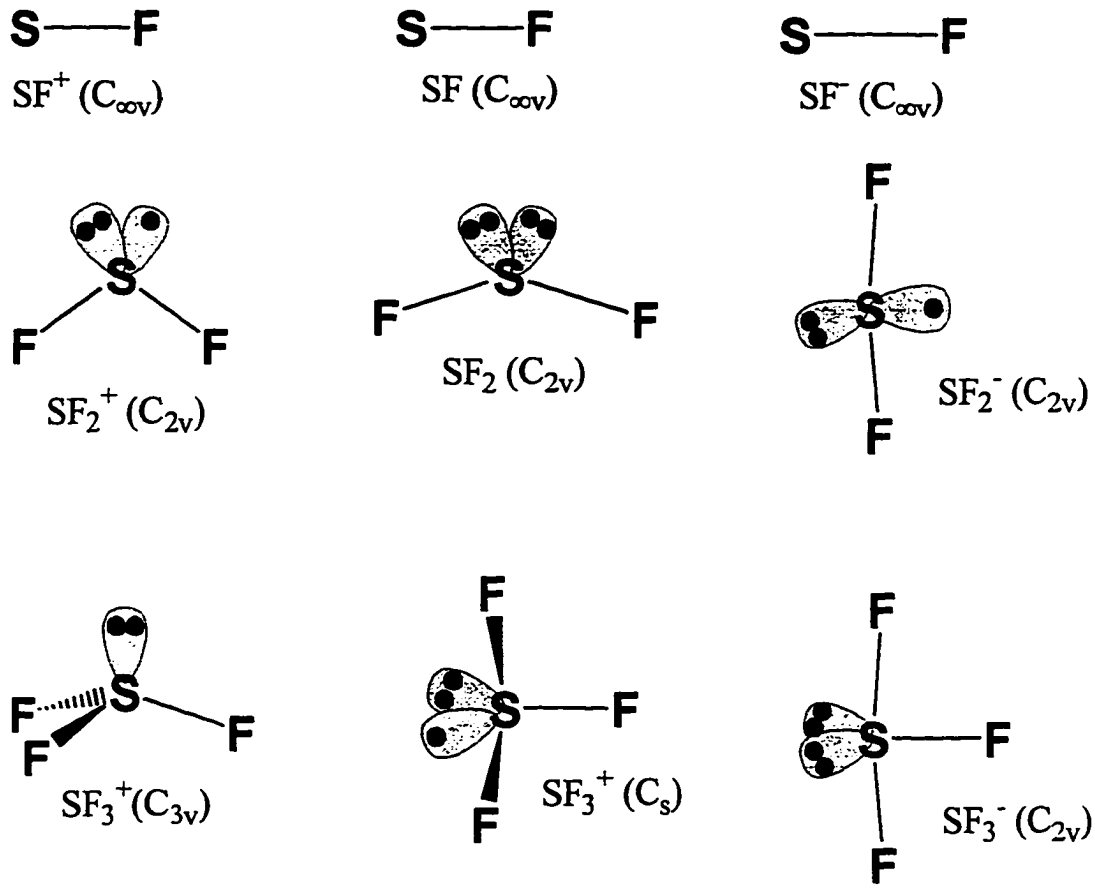


Figure 1(a) Theoretical equilibrium structures for $SF_n$ (n=1-3), $SF_n^+$ (n=1-3), and $SF_n^-$ (n=1-3) optimized at the MP2/6-31G(d) levels. Bond distances are in Å and bond angles are in degrees.

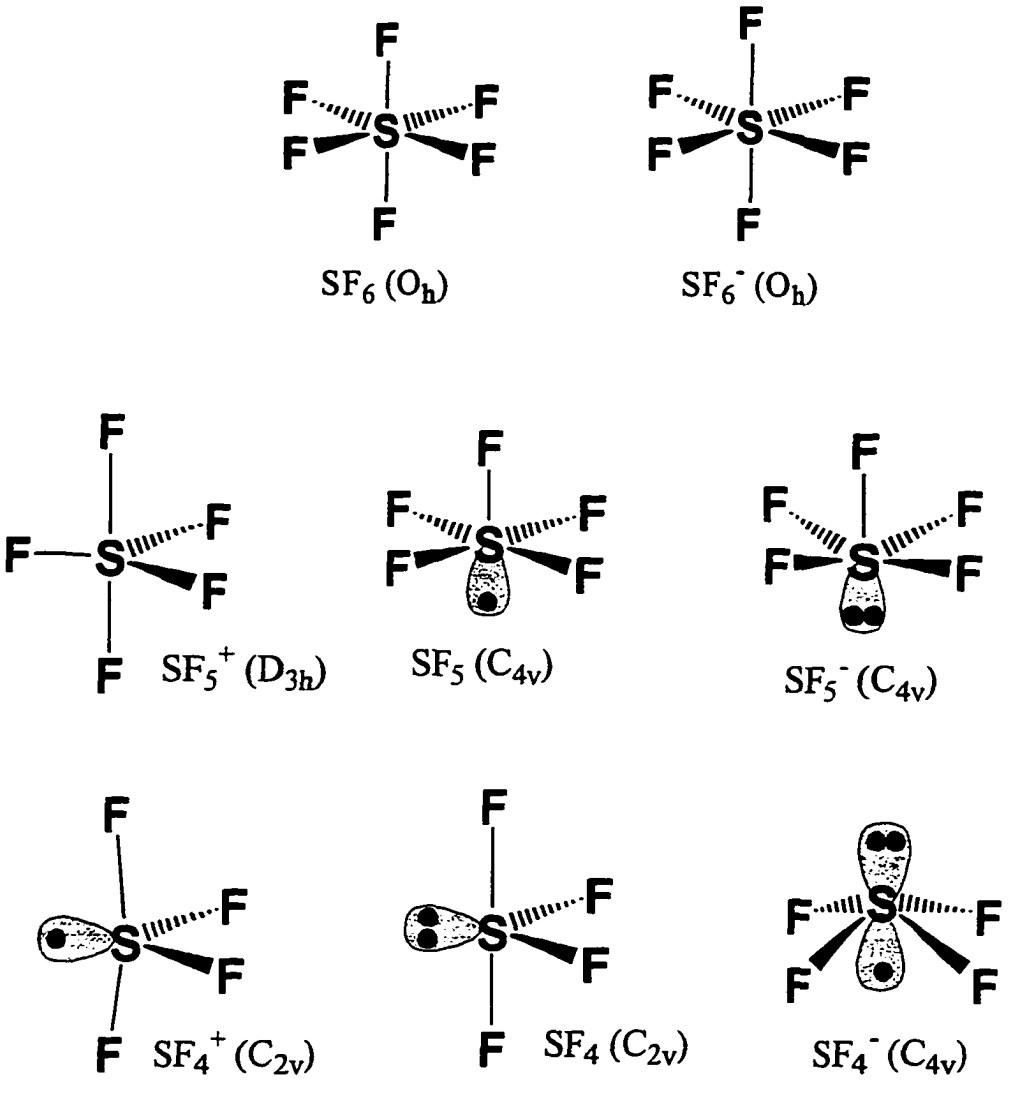


Figure 1(b). Theoretical equilibrium structures for $SF_n$ (n=4-6), $SF_n^+$ (n=4-5), and $SF_n^-$ (n=4-6) optimized at the MP2/6-31G(d) levels. Bond distances are in Å and bond angles are in degrees.

$SF_2^+$ (1.535 C) and $SF_2$ (1.60-1.67 C).

The bonding of F atoms to S in $SF_3^+$ obeys the octet rule, and the $sp^3$ hybridization on the S atom leads to a trigonal pyramidal molecule with $C_{3v}$ symmetry. Both $SF_3$ and $SF_3^-$ are hypervalent species with $4\frac{1}{2}$ and 5 electron pairs, respectively, around the S atoms. In $SF_3^-$, the two lone pairs on the S atom occupy two of the equatorial positionsof a trigonal bypyramidal arrangement, resulting in a T-shaped structure. When one electron is taken from a sulfur lone pair, the nonbonding electron densities associated with the two equatorial lobes are no longer equivalent. The two axial F atoms are expected to be distorted out of the molecular plane, yielding a structure with $C_s$ symmetry for $SF_3$.

Similarly, the $C_s$ symmetry structures of $SF_4^+$ and $SF_4$ are easily understood via the VSEPR theory. In these cases, the half-filled and the lone pair reside in an equatorial position of a trigonal bipyramidal arrangement around the S atoms in $SF_4^+$ and $SF_4$, respectively. Two structures with $C_{4v}$ and $C_{2v}$ symmetries are located for $SF_4^-$. There are $5\frac{1}{2}$ electron pairs (4 bonded pairs and $1\frac{1}{2}$ lone pairs) around the S atoms in $SF_4^-$. To arrange the electron pairs in an octahedral arrangement in $SF_4^-$, the one and half lone pair lobes can be in either a *trans* or a *cis* configuration, which corresponds to the $SF_4^-(C_{4v})$ or $SF_4^-(C_{2v})$ isomer, respectively. If the two non-equivalent lobes are in the *cis* configuration, the axial F atoms are expected to distort from the plane containing these F atoms, as in the case of $SF_3$. The three nonbonding electrons on S in the $SF_4^-(C_{2v})$ isomer are subject to greater inter-electron repulsion than those in the $SF_4^-(C_{4v})$ isomer, where the two lobes of the nonbonding electrons point in opposite directions. This picture is consistent with the G2(MP2) prediction that the $SF_4^-(C_{4v})$ isomer is more stable than the $C_{2v}$ isomer by 11.3 kcal/mol.

The point group for $SF_5^+$ is $D_{3h}$, while those for $SF_5$ and $SF_5^-$ are $C_{4v}$. Since $SF_5^+$ is isoelectronic with $PF_5$, the five bonded electron pairs in $SF_5^+$ are expected to be distributed around the S atom in a normal trigonal bipyramidal structure. The neutral $SF_5$ and anionic $SF_5^-$ have a half-filled pair and a filled lone pair, respectively, and their roles in the molecular geometry are similar to that of the lone pair in $ClF_5$. Thus, $SF_5$ and $SF_5^-$, similar to $ClF_5$, are predicted by the VSEPR theory to possess a square pyramidal ($C_{4v}$) structure.

Sulfur hexafluoride has six bonded electron pairs around the S atom and is predicted by the VSEPR model to have $O_h$ symmetry. As indicated above, an equilibrium structure for $SF_6^+$ is not found because the cation tends to dissociate to $SF_4^+ + F_2$ at the MP2/6-31G(d) and MP2/6-31G+(d) levels. We note that the highest occupied molecular orbital for $SF_6$ has $T_{1g}$ symmetry. Upon ionization, the resulting electronic configuration [...$(t_{1g})^5$] corresponds to a triply degenerate state. The fact that this state is subject to Jahn-Teller distortion may be the source of the instability of $SF_6^+$. Although $SF_6^+$ may not be chemically bound, it may exist as $SF_4^+\cdots F_2$, stabilized by long range forces such as the charge-induced-dipole interaction. The formation of $SF_6^-$ can be considered by adding an electron to the lowest unoccupied molecular orbital (LUMO). Since this LUMO has $A_{1g}$ symmetry, the $O_h$ structure is preserved for $SF_6^-$. However, the anti-bonding character of the $a_{1g}$ orbital causes $r$(S-F) to lengthen by 0.118 Å in $SF_6^-$ compared to that in $SF_6$.

**B. Comparison of G2, G2(MP3), and G2(MP2) predictions**

In order to verify the accuracy of the G2(MP2) procedure which is applied to predict the energetics of higher sulfur fluorides $SF_n$, $SF_n^+$ and $SF_n^-$ (n=3-6), we have compared the predictions for the IEs, EAs, $\Delta_fHE_0$'s, and $\Delta_fHE_{298}$'s of $SF_n$, $SF_n^+$, and $SF_n^-$ (n=1,2) obtained using the G2 and G2(MP2) procedures. These predictions, together with those calculated using the G2(MP3) procedure, are listed in Table I. The available experimental results for $SF_n$, $SF_n^+$, and $SF_n^-$ (n=1,2)

**Table I.** Comparisons between G2, G2(MP3), and G2(MP2) $E_0$, $\Delta_fHE_0$, IE, and EA values and experimental $\Delta_fHE_0$, IE, and EA values for $SF_n$, $SF_n^+$, and $SF_n^-$ (n = 1 and 2).

| | G2 | G2(MP3) | G2(MP2) | Δ[G2-G2(MP2)][a] | Expt[b] |
|---|---|---|---|---|---|
| | | | **SF** | | |
| $E_0$ (hartree) | -497.41824 | -497.41336 | -497.40726 | -0.01098 | ... |
| $H_{298}$ (hartree) | -497.41486 | -497.40998 | -497.40387 | -0.01099 | ... |
| $\Delta_fHE_0$ (kcal/mol)[c] | 2.3 | 3.7 | 1.7 | 0.6 | **2.9±1.4** |
| | | | | | **6.6±4.1**[d] |
| | | | | | 8.3±2.6[d] |
| | | | | | 8.0[e] |
| $\Delta_fHE_{298}$ (kcal/mol)[f] | 2.5 | 3.9 | 1.9 | 0.6 | **3.1±1.4** |
| IE (eV) | 10.40 | 10.33 | 10.31 | 0.09 | **10.16±0.17**[d] |
| | | | | | **10.09±0.10**[g] |
| EA (eV) | 2.33 | 2.33 | 2.29 | 0.04 | **2.0±0.5**[h] |
| | | | **$SF^+$** | | |
| $E_0$ (hartree) | -497.03622 | -497.03391 | -497.02850 | -0.00772 | ... |
| $H_{298}$ (hartree) | -497.03288 | -497.03056 | -497.02516 | -0.00772 | ... |
| $\Delta_fHE_0$ (kcal/mol)[c] | 242.0 | 241.8 | 239.4 | 2.6 | **240.9±1.2**[d] |
| | | | | | 235.6±"4.0 |
| $\Delta_fHE_{298}$ (kcal/mol)[f] | 242.2 | 242.0 | 239.6 | 2.6 | ... |
| | | | **$SF^-$** | | |
| $E_0$ (hartree) | -497.50372 | -497.49692 | -497.49130 | -0.01242 | ... |
| $H_{298}$ (hartree) | -497.50028 | -497.49347 | -497.48786 | -0.01242 | ... |
| $\Delta_fHE_0$ (kcal/mol)[c] | -51.4 | -48.7 | -51.0 | -0.4 | ... |
| $\Delta_fHE_{298}$ (kcal/mol)[f] | -51.1 | -48.5 | -50.8 | -0.3 | **-43±13**[i] |
| | | | **$SF_2(C_{2v})$** | | |
| $E_0$ (hartree) | -597.19238 | -597.18512 | -597.17896 | -0.01342 | ... |
| $H_{298}$ (hartree) | -597.18804 | -597.18077 | -597.17461 | -0.01343 | ... |
| $\Delta_fHE_0$ (kcal/mol)[c] | -67.9 | -65.5 | -69.3 | 1.4 | **-67.5±3.5**[j] |
| | | | | | **-69.2±2.8**[d] |
| | | | | | **-70.4±4.0** |
| $\Delta_fHE_{298}$ (kcal/mol)[f] | -68.1 | -65.7 | -69.6 | 1.5 | ... |
| IE (eV) | 10.15 | 10.06 | 10.07 | 0.08 | **10.08±0.05**[k] |
| EA (eV) | 1.51 | 1.35 | 1.43 | 0.08 | ... |

Table I (continued)

Table I (continued)

| | | | | | |
|---|---|---|---|---|---|
| | | | $SF_2^+(C_{2v})$ | | |
| $E_0$ (hartree) | -596.81927 | -596.81525 | -596.80878 | -0.01049 | ... |
| $H_{298}$ (hartree) | -596.81505 | -596.81102 | -596.80455 | -0.01050 | ... |
| $\Delta_fHE_0$ (kcal/mol)[c] | 166.2 | 166.6 | 163.0 | 3.2 | **<u>164.9±3.3</u>**[l] **167±11**[m] **163.2±2.6**[d] 162.0 |
| $\Delta_fHE_{298}$ (kcal/mol)[f] | 165.9 | 166.3 | 162.7 | 3.2 | **<u>164.6± 3.3</u>**[n] 161.6 |
| | | | $SF_2^-(C_{2v})$ | | |
| $E_0$ (hartree) | -597.24780 | -597.23456 | -597.23163 | -0.01617 | ... |
| $H_{298}$ (hartree) | -597.24295 | -597.22970 | -597.22677 | -0.01618 | ... |
| $\Delta_fHE_0$ (kcal/mol)[c] | -102.7 | -96.5 | -102.4 | -0.3 | ... |
| $\Delta_fHE_{298}$ (kcal/mol)[f] | -102.6 | -96.4 | -102.3 | -0.3 | ... |

a) Difference between G2 and G2(MP2) values.

b) Experimental values. Unless specified, values are from Ref. 46. The underlined values are recommended values. The values in bold font are consistent with the G2 and G2(MP2) predictions.

c) Calculated using $\Delta_fHE_0$ values of S (65.6 kcal/mol) and F (18.5 kcal/mol) from Ref. 46; $E_o$(G2) values S (-397.65495 hartree) and F (-99.63282 hartree) from Ref. 39; $E_0$[G2(MP3)] values of S (-397.65326 hartree) and F (-99.63194 hartree) from Ref. 40; and $E_0$[G2(MP2)] values of S (-397.64699 hartree) and F (-99.62894 hartree) from Ref. 40.

d) Reference 20.

e) Reference 54.

f) Calculated using the $\Delta_fHE_{298}$ values of S (66.2 kcal/mol) and F (19.0 kcal/mol) from Ref. 46. $H_{298}$[G2, G2(MP3), or G2(MP2)] values for these atoms are obtained by adding $E_{trans}$ + PV (= 5/2 RT = 2.36 milli-hartree at 298 K) to their $E_0$[G2, G2(MP3), or G2(MP2)] values.

Table I (continued)

g) References 25 and 46.

h) 298 K value. G2 and G2(MP2) calculations show that EA(0 K) is essentially identical to EA(298 K).

i) Calculated using EA(298 K) = 2.0±0.5 eV and $\Delta_fHE_{298}(SF) = 3.1\pm1.4$ kcal/mol (Ref. 46).

j) This work. Calculated using $IE(SF_2) = 10.08\pm0.05$ eV (Ref. 55) and $\Delta HE_{f0}(SF_2^+) = 164.9\pm3.3$ kcal/mol derived from the AE of $SF_2^+$ from $SF_4$ (see Table II).

k) Reference 55.

l) This work. Value converted from $\Delta_fHE_{298}(SF_2^+) = 164.6\pm3.3$ kcal/mol. See footnote (n) of this table.

m) Reference 56.

n) This work. Value determined using the AE for $SF_2^+$ from $SF_4$ and $\Delta_fHE_{298}(SF_2) = -183.7\pm2.5$ kcal/mol $\Delta_fHE_0(F) = 19$ kcal/mol (Ref. 46). See Table II.

are also included in the table.[20,25,46,54-56] Detailed comparisons between the experimental and theoretical results are made in a later section. Here, we just point out that the G2, G2(MP3), and G2(MP2) predictions for the $\Delta_fHE_0$'s, $\Delta_fHE_{298}$'s, IEs, and EAs of $SF_n$, $SF_n^+$, and $SF_n^-$ (n=1,2) fall within the range of the experimental measurements reported in the literature. The deviation between the G2 and G2(MP2) values, Δ[G2-G2(MP2)], for $E_0$'s, $\Delta_fHE_0$'s, IEs, and EAs of $SF_n$, $SF_n^+$, and $SF_n^-$ (n=1,2) are shown in Table I. The theoretical $E_0$'s are found in the order $E_0(G2) < E_0[G2(MP3)] < E_0[G2(MP2)]$, a trend consistent with the expectation that $E_0$ is lower as the degree of correlation increases. The $E_0(G2)$ values are lower than the corresponding $E_0[G2(MP2)]$ values by 0.007-0.016 hartree. The differences between the G2 and G2(MP2) predictions for the

IEs and EAs of SF and $SF_2$ are ≤0.09 eV. The absolute values for Δ[G2-G2(MP2)] of $_fHE_0$ [or $\Delta_fHE_{298}$] are 1.5 kcal/mol for SF, $SF^-$, $SF_2$, and $SF_2^-$. Higher Δ[G2-G2(MP2)] values of 2.6 and 3.2 kcal/mol are observed for $\Delta_fHE_0(SF^+)$ and $\Delta_fHE_0(SF_2^+)$ [or $\Delta_fHE_{298}(SF^+)$ and $\Delta_fHE_{298}(SF_2^+)$], respectively. Based on these and previous comparisons of experimental and G2(MP2) results, we conclude that the G2(MP2) procedure provides reliable energetic predictions for the sulfur fluorides and their ions of interest.

**C. $\Delta_fHE_0(SF_n^+)$ (n=2-5) from PIMS studies and their comparison to G2 predictions**

Figure 2(a) shows the PIE spectra for $SF_3^+$, $SF_4^+$, and $SF_5^+$ from $SF_6$ obtained in the wavelength region of 600-850 Å. The relative PIEs of these spectra have been calibrated by measuring the relative intensities for $SF_3^+$, $SF_4^+$, and $SF_5^+$ at selected wavelengths. These spectra are in excellent agreement with those observed previously,[28-30,32] except that the intensities of $SF_3^+$ and $SF_4^+$ relative to that of $SF_5^+$ are greater than those found in Ref. 28. The PIEs for $SF_n^+$ (n=3-5) near their onsets are magnified in the figure to show the assignments of the experimental AEs for processes (1)-(3). The AEs measured in this study are compared to previous PIMS results[28-30,32] in Table II. Although the adiabatic IE of $SF_6$ cannot be measured in the PIMS experiments, the literature IE determined by PE spectroscopy is included in the table. After taking into account the experimental uncertainties, the values for the AEs of $SF_3^+$ and $SF_5^+$ from $SF_6$ determined here are in excellent agreement with those observed previously.[28,30] The AE of 18.23±0.05 eV observed for $SF_4^+$ from $SF_6$ is also consistent with the PIE measurement of Ref. 29, which indicates that the $SF_4^+$ signal appears at 18.1 eV.

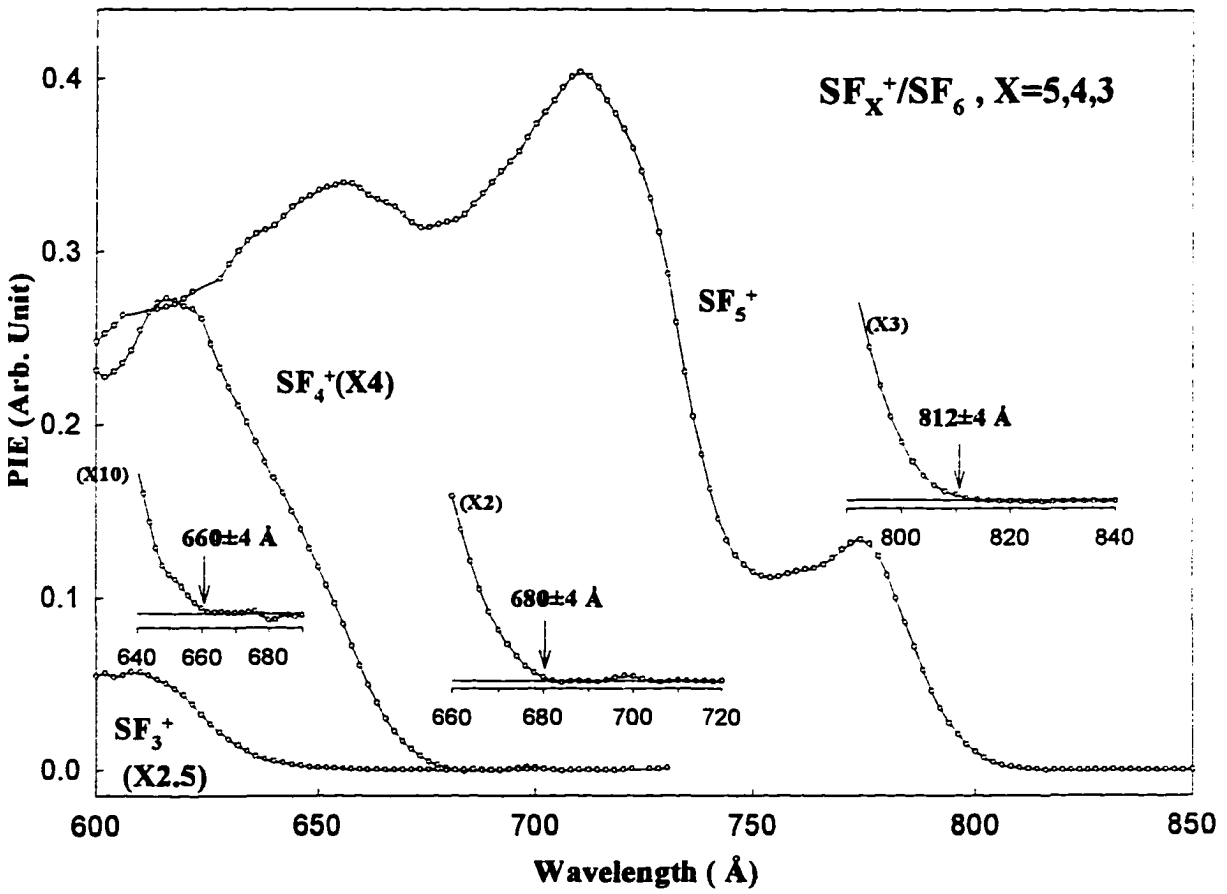


Figure 2 (a) PIE spectra for $SF_3^+$, $SF_4^+$, and $SF_5^+$ from $SF_6$ in the wavelength range of 600 -850 Å.

**Table II.** AEs for $SF_n^+$ (n=3-6) from $SF_6$ and $SF_n^+$ (n=2-4) from $SF_4$ measured using PIMS and PE spectroscopy, and comparison between $)_fHE_0(SF_n^+)$ (n=2-5) derived from these PIMS experiments and G2 calculations.

| Reactants | Product Channels | AE(expt)[a] (eV) | $\Delta_fHE_{298}$(expt)[b] (kcal/mol) | $\Delta_fHE_0$(expt)[c] (kcal/mol) | $\Delta_fHE_0$(Theor)[d] (kcal/mol) |
|---|---|---|---|---|---|
| $SF_6 + h\nu \rightarrow$ | $SF_6^+ + e^-$ | IE = 15.35[e] | .. | ... | ... |
| | $SF_5^+ + F + e^-$ | 15.27±0.08 (812±4 Å)[f]<br>15.32±0.04[g]<br>15.29[h] | ≤41.9[f] | ≤43.8[e] | 20.3 |
| | $SF_4^+ + 2F + e^-$ | 18.23±0.05 (680±4 Å)[f]<br>18.5±0.1 (670±5 Å)[i]<br>18.1 (685 Å)[j] | 90.7±2.5[f] | 91.9±2.5[e] | 91.1 |
| | $SF_3^+ + 3F + e^-$ | 18.79±0.11 (660±4 Å)[f]<br>18.79±0.14 (660±5 Å)[g]<br>19.5±0.1 (635±5 Å)[i]<br>18.9 (655 Å)[j] | 84.6±2.5[f]<br>84.6±3.2[g] | 85.5±2.5[e]<br>85.5±3.2[e] | 85.5 |
| $SF_4 + h\nu \rightarrow$ | $SF_4^+ + e^-$ | IE = 11.90[k] | 90.9[k]<br>92.2[k,l] | 92.2[h]<br>93.5[h,k] | 91.1 |
| | $SF_3^+ + F + e^-$ | 12.41±0.05 (999±4 Å)[f]<br>12.40[k] | 83.7±3.9[f]<br>85.0±5.1[f,l]<br>83.5±2.8[m] | 84.6±3.9[e]<br>85.9±5.1[e,k]<br>84.4±2.8[m] | 85.5 |
| | $SF_2^+ + 2F + e^-$ | 16.75±0.09 (740±4 Å)[f]<br>16.90[k] | 164.8±4.2[f]<br>166.1±5.4[f,l]<br>164.6±3.3[m] | 165.1±4.2[f]<br>166.4±5.4[f,l]<br>164.9±3.3[m] | 163.0<br>166.2[n] |

a) The AEs are assumed to be 298 K values.

b) $\Delta_fHE_{298}$ values for $SF_n^+$ (n=2-5) calculated using the AEs, $\Delta_fHE_{298}(F)$ = 19.0 kcal/mol from Ref. 46, $\Delta_fHE_{298}(SF_4)$ = -183.5±3.7 kcal/mol, and $\Delta_fHE_{298}(SF_6)$ = -291.7±0.2

Table II (continued)

kcal/mol from Ref. 46. The value for $\Delta_fHE_{298}(SF_4)$ is converted from $\Delta_fHE_0(SF_4)$ = -182.3±3.7 kcal/mol from Ref. 20 using MP2/6-31G(d) vibrational frequencies for $SF_4$.

c) $\Delta_fHE_0$(expt) values converted from corresponding $\Delta_fHE_{298}$(expt) values for $SF_n^+$ (n=2-5) using MP2/6-31G(d) vibrational frequencies for $SF_n^+$ (n=2-5).

d) G2(MP2) predictions unless specified. See Ref. 23.

e) Reference 34.

f) This work.

g) Reference 30.

h) Reference 28.

i) Reference 32

j) Reference 29. Cited in Ref. 32.

k) Reference 45.

l) Values calculated using $\Delta_fHE_{298}(SF_4)$ = -182.2±5.0 kcal/mol, which is calculated using $\Delta_fHE_0(SF_4)$ = -180.9±5.0 kcal/mol from Ref. 56 and MP2/6-31G(d) vibrational frequencies for $SF_4$.

m) Values calculated using $\Delta_fHE_{298}(SF_4)$ = -183.7±2.5 kcal/mol, which is obtained by combining $\Delta_fHE_{298}(SF_4^+)$ = 90.7±2.5 kcal/mol (this work) and IE($SF_4$) = 11.90 eV (Ref. 45). See the text.

n) G2 value.

The PIE spectra for $SF_2^+$ and $SF_3^+$ from $SF_4$ in the wavelength region of 600-1020 C are depicted in Fig. 2(b). The PIEs near the onsets of $SF_2^+$ and $SF_3^+$ are also magnified in the figure to show the experimental AEs for processes (3) and (4). While the AE for $SF_3^+$ is in excellent agreement with that obtained in Ref. 45, the AE (16.75±0.09 eV) of $SF_2^+$ is lower than that of Ref. 45 by 0.15 eV (see Table II).

The AEs measured in previous PIMS experiments[28,30,45] are 298 K values. Under the molecular beam expansion conditions of the present experiments, the relaxation of the vibrational excitations of $SF_4$ and $SF_6$ is expected to be inefficient. Although the rotational excitations are partially relaxed, it is a good assumption that the AEs determined here also correspond to 298 K values. However, the partial rotational relaxation is expected to reveal more distinct AEs than those measured in previous PIMS studies. Using the AEs, together with the literature thermochemical data $\Delta_fHE_{298}(F)$ = 19.0 kcal/mol,[46] $\Delta_fHE_{298}(SF_4)$ = -183.5±3.7 kcal/mol[20] [or $\Delta_fHE_{298}(SF_4)$ = -182.3±3.7 kcal/mol[56]],[57] and $\Delta_fHE_{298}(SF_6)$ = -291.7±0.2 kcal/mol,[46] we have obtained the experimental $\Delta_fHE_{298}(SF_n^+)$ (n=2-5) values shown in Table II. The experimental $\Delta_fHE_0(SF_n^+)$ (n=2-5) values in the table are converted from corresponding $\Delta_fHE_{298}$ values using MP2/6-31G(d) vibrational frequencies for $SF_n^+$ (n=2-5). The observation that the $\Delta_fHE_0(SF_n^+)$ (n=3,4) values derived from the AEs of $SF_n^+$ (n=3,4) from $SF_6$ are in excellent agreement with those derived from $SF_4$ is taken as strong support that these experimental data are reliable.

The value $\Delta_fHE_{298}(SF_4)$ = -183.5"3.7 kcal/mol [$\Delta_fHE_0(SF_4)$ = -182.3"3.7 kcal/mol] used to calculate $\Delta_fHE_{298}(SF_3^+)$ = 83.7"3.9 kcal/mol and $\Delta_fHE_{298}(SF_2^+)$ = 164.8"4.2 kcal/mol (see Table II) is obtained by combining $\Delta_fHE_0(SF_4^+)$ = 87.2"3.4 kcal/mol and IE($SF_4$) = 11.69±0.06 eV determined in the recent CID and charge transfer study.[20] The latter IE value is lower than the

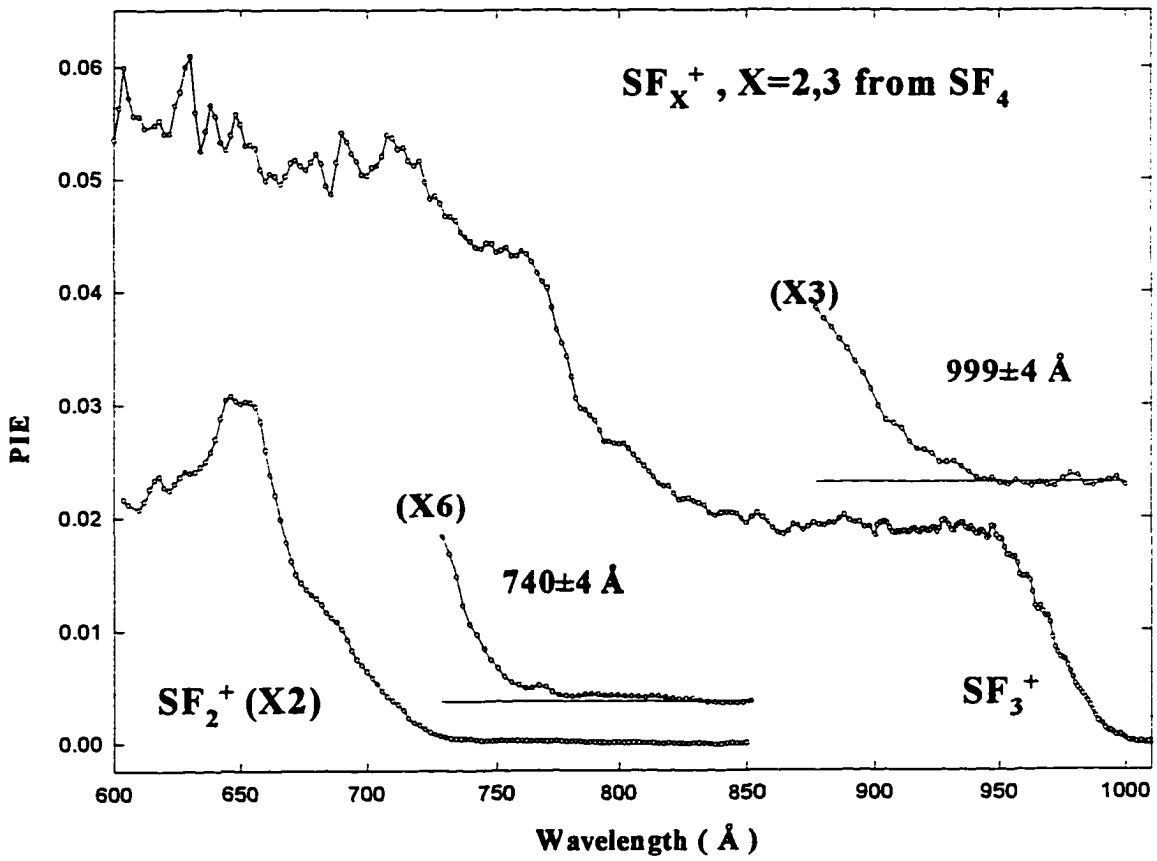


Fig. 2(b) PIE spectra for $SF_2^+$ and $SF_3^+$ from $SF_4$ in the wavelength range of 600-1020 Å.

value of 11.90 eV determined in the PIMS and PE spectroscopy study.[45] Furthermore, the $\Delta_fHE_0(SF_4^+)$ = 87.2±3.4 kcal/mol is also lower than the value of 91.9±2.5 kcal/mol determined here. We derive a value of -183.7±2.5 kcal/mol for $\Delta_fHE_{298}(SF_4)$ by combining IE($SF_4$) = 11.90 eV and $\Delta_fHE_{298}(SF_4^+)$ = 90.7±2.5 kcal/mol based on the AE of $SF_4^+$ from $SF_6$ determined in this study. We note that although the value $\Delta_fHE_{298}(SF_4)$ = -183.5±3.7 kcal/mol derived from the CID and charge transfer experiment is essentially the same as that derived using the PIMS data, we recommend the PIMS value, i.e., $\Delta_fHE_{298}(SF_4)$ = -183.7±2.5 kcal/mol [$\Delta_fHE_{f0}(SF_4)$ = -182.5±2.5 kcal/mol] on basis of the analysis presented above. Using $\Delta_fHE_{298}(SF_4)$ = -183.7"2.5 kcal/mol, we obtain $\Delta_fHE_{298}(SF_3^+)$ = 83.5±2.8 kcal/mol [$\Delta_fHE_0(SF_3^+)$ = 84.4±2.8 kcal/mol] and $\Delta_fHE_{298}(SF_2^+)$ = 164.6±3.3 kcal/mol [$\Delta_fHE_0(SF_2^+)$ = 164.9±3.3 kcal/mol] (see Table II). These latter experimental values for $\Delta_fHE_0(SF_3^+)$ and $\Delta_fHE_0(SF_2^+)$ are recommended.

The G2(MP2) predictions for $SF_n$, $SF_n^+$, and $SF_n^-$ (n=2-5) are included in Table II for comparison with the experimental $\Delta_fHE_0(SF_n^+)$ (n=2-5) values derived from the PIMS experiments. As pointed out previously, the observation that the IE of $SF_6$ determined by PE spectroscopy is nearly identical with the AE for $SF_5^+$ from $SF_6$ indicates that the AE value for $SF_5^+$ is an upper limit. This in turn yields an upper bound of 41.9 kcal/mol for $\Delta_fHE_{298}(SF_5^+)$ [or 43.8 kcal/mol for $\Delta_fHE_0(SF_5^+)$], which is consistent with the G2(MP2) prediction of $\Delta_fHE_0(SF_5^+)$ = 20.3 kcal/mol.[23] Other than for $\Delta_fHE_0(SF_5^+)$, the agreement between the G2(MP2) predictions for $\Delta_fHE_0(SF_n^+)$ (n=2-4) and the PIMS results is excellent. This comparison lends additional support to the reliability of G2(MP2) predictions for the sulfur fluorides.

**D. Comparison of experimental and theoretical results for $SF_n$, $SF_n^+$, and $SF_n^-$ (n=1-6)**

The main motivation for performing G2 and G2(MP2) calculations for $SF_n$, $SF_n^+$, and $SF_n^-$ (n=1-6) is to help choose reliable experimental data from widely scattered experimental

measurements. The comparisons of theoretical and experimental[18,20,22,24,56,58] results for $SF_n$, $SF_n^+$, and $SF_n^-$ (n=3-6) are made in Tables I and III. Where G2 and G2(MP2) predictions are available, the G2 value is preferred for comparison with experimental values. After considering the experimental uncertainties and estimated errors for G2 and G2(MP2) calculations, we have highlighted in bold font the experimental values which are in reasonable accord with the corresponding G2 and G2(MP2) predictions. The underlined experimental IE, EA, and $)_fHE_0$ values are recommended values for $SF_n$, $SF_n^+$, and $SF_n^-$ (n=1-6) based on these comparisons.

The experimental values for $\Delta_fHE_0(SF)$ range from 2.9 to 8.0 kcal/mol. The lowest value 2.9 ± 1.4 kcal/mol, is closest to the G2 prediction of 2.3 kcal/mol for $\Delta_fHE_0(SF)$, and is recommended for $\Delta_fHE_0(SF)$. Taking into account the experimental uncertainties, the value 6.6 ±4.1 kcal/mol determined in the recent CID and charge transfer study[20] is also consistent with the G2 prediction. The experimental IE(SF) = 10.16±0.17 eV, EA(SF) = 2.0"0.5 eV, $\Delta_fHE_0(SF^+)$ = 240.9±1.2 kcal/mol, and $\Delta_fHE_{298}(SF^-)$ = -43±13 kcal/mol [$\Delta_fHE_0(SF^-)$ = -43±13 kcal/mol][59] are consistent with the corresponding G2 predictions.

The experimental $\Delta_fHE_0(SF_2^-)$ and $EA(SF_2)$ are unknown. However, the experimental $IE(SF_2)$ =10.08±0.05 eV agrees very well with the IE(G2) value of 10.15 eV. The experimental$\Delta_fHE_0(SF_2^+)$ = 164.9"3.3 kcal/mol is also in excellent accord with the G2 prediction of 166.2 kcal/mol. Combining these experimental values, a value of -67.5±3.5 kcal/mol is calculated for $\Delta_fHE_0(SF_2)$, which compares well with the G2 value of -67.9 kcal/mol. We note that after taking into account of experimental uncertainties, the other experimental values[20,46] of -69.2±2.8 and -70.4±4.0 kcal/mol for $\Delta_fHE_0(SF_2)$ and $\Delta_fHE_0(SF_2^+)$ are also consistent with the G2 predictions.

**Table III.** $E_0$, $\Delta_fH°_0$, IE, and EA values obtained at the G2(MP2) levels and experimental $\Delta_fH°_0$ [$\Delta_fH°_0$(exp)], IE [IE(exp)] and EA [EA(exp)] values for $SF_n$, $SF_n^+$, and $SF_n^-$, n=3-6.

| Species | $E_0$[G2(MP2)] (hartree) | $\Delta_fH°_0$[G2(MP2)][a] (kcal/mol) | $\Delta_fH°_0$(exp)[b] (kcal/mol) | IE/EA[G2(MP2)] (eV) | IE(exp)[b] (eV) | EA(exp)[b] (eV) |
|---|---|---|---|---|---|---|
| Neutrals | | | | | | |
| $SF_3(C_s)$ | -696.89453 | -105.2 (-105.8) | **-103.6±2.5**[c] | 8.27/3.09 | **8.18±0.07** | **3.1±0.2** |
| | | | -111.6±3.6[d] | | | 2.9±0.1 |
| | | | -115.2±5.8[e] | | | |
| $SF_4(C_{2v})$ | -796.67566 | -182.2 (-183.4) | **-182.5±2.5**[f] | 11.85/1.52[g], 1.02[g] | **11.90** | **1.5±0.2** |
| | | | **-182.3±3.7**[d] | | **12.03±0.05** | |
| | | | **-181±5** | | **11.69±0.06** | |
| $SF_5(C_{4v})$ | -896.36530 | -201.8 (-203.6) | **-205.9±3.4**[c,h] | 9.63/4.07 | **9.60±0.05**[l] | **3.70±0.2** |
| | | | -215.7±3.2[e] | | | **>3.7±0.3** |
| | | | -221.8±4.3 | | | 3.01±0.29 |
| $SF_6(O_h)$ | -996.16457 | 290.2 (-292.8) | **-288.4±0.2** | .../1.04 | ≤15.27 | **1.05±0.10**[j] |
| | | | | | | 15.35 |
| Cations | | | | | | |
| $SF_3^+(C_{3v})$ | -696.59058 | 85.5 (84.7) | **85.6±1.9**[k] | ... | ... | ... |
| | | | 93.8±8.0[l] | | | |
| | | | 77.0±3.2[d] | | | |
| $SF_4^+(C_{2v})$ | -796.24009 | 91.1 (89.9) | **91.9±2.5**[f] | ... | ... | ... |
| | | | **87.2±3.4**[d] | | | |
| | | | 96.7±5.0 | | | |
| $SF_5^+(D_{3h})$ | -896.01141 | 20.3 (18.3) | **16.4±3.6**[m] | ... | ... | ... |
| | | | ≤25.0±2.0[n] | | | |
| | | | 5.6±3.5[i] | | | |
| | | | -0.4±4.1[d] | | | |
| | | | ≤43.8[f] | | | |
| $SF_6^+$ | ... | ... | | ... | ... | ... |
| Anions | | | | | | |
| $SF_3^-(C_{2v})$ | -697.00818 | -176.5 (-177.0) | **-175.1±5.2**[p] | ... | ... | ... |
| | | | **-187.1±10.5**[q] | | | |

Table III ( continued)

| | | | | | | |
|---|---|---|---|---|---|---|
| $SF_4^-(C_{2v})$ | -796.71324 | -205.8 (-206.6) | ... | ... | ... | ... |
| $SF_4^-(C_{4v})$ | -796.73136 | -217.1 (-217.8) | **-217.1±5.2**[f] | | | |
| $SF_5^-(C_{4v})$ | -896.51473 | -295.6 (-297.0) | **-291.2±5.7**[g]<br>**-275.3±7.5**[h] | ... | ... | ... |
| $SF_6^-(O_h)$ | -996.20296[a] | -314.3[a] (-315.6)[a] | **-314.5±2.4**[w] | ... | ... | ... |

a) Calculated using $\Delta_f H°_0$ values of S (65.6 kcal/mol) and F (18.5 kcal/mol) from Ref. 46, and $E_o$[G2(MP2)] values of S (-397.64699 hartree), and F (-99.62894 hartree) from Ref. 40. The values in parentheses are $\Delta_f H°_{298}$[G2(MP2)] values.

b) Experimental values. Unless specified, values are from Ref. 46. The underlined values are recommended values. The values in bold font are consistent with the G2(MP2) predictions.

c) This work. Calculated using the $\Delta_f H°_0(SF_3^-)$ = 85.0±1.9 kcal/mol (see footnote k of this table) and IE($SF_3$) = 8.18±0.07 eV.

d) Reference 20.

e) Reference 18.

f) This work.

g) The EA[G2(MP2)] values of 1.52 and 1.02 eV correspond the processes, $SF_4^-(C_{4v}) \rightarrow SF_4(C_{2v}) + e^-$ and $SF_4^-(C_{4v}) \rightarrow SF_4(C_{2v}) + e^-$, respectively.

h) Value calculated using the experimental $D°_0(SF_5\text{-}F)$ = 101 kcal/mol.

Table III ( continued)

Table III ( continued)

i) Reference 22.

j) Reference 58.

k) Average value of 85.5±2.5 kcal/mol and 84.4±2.8 kcal/mol for $\Delta_f H°_0(SF_3^-)$ determined using the AEs of $SF_3^+$ from $SF_6$ and $SF_4$, respectively. See Table II.

l) Reference 56.

m) Value calculated using the experimental $D°_0(SF_5\text{-}F)$ = 101 kcal/mol and $IE(SF_5)$ = 9.60±0.05 eV (Ref. 22).

n) Reference 24.

o) Equilibrium structure for $SF_6^+$ is not found.

p) Calculated using $\Delta_f H°_0(SF_3)$ = 103.6±2.5 kcal/mol and $EA(SF_3)$ = 3.1±0.2 eV.

q) Reference 46. Converted from $\Delta_f H°_{298}$ values.

r) Calculated using $\Delta_f H°_0(SF_4)$ = -182.5±2.5 kcal/mol and $EA(SF_4)$ = 1.5±0.2 eV.

s) Calculated using $\Delta_f H°_0(SF_5)$ = -205.9±3.4 kcal/mol and $EA(SF_5)$ = 3.7±0.2 eV.

t) Calculated using $\Delta_f H°_0(SF_5)$ = -205.9±3.4 kcal/mol and $EA(SF_5)$ = 3.01±0.29 eV.

u) Calculated using the approximated G2(MP2), i.e., AG2, scheme.

w) Converted from $\Delta_f H°_{298}(SF_6^-)$ = -315.9±2.4 kcal/mol, which is calculated using $\Delta_f H°_{298}(SF_6)$ = -291.7±0.2 kcal/mol (Ref. 46) and $EA(SF_6)$ = 1.05±0.10 eV (Ref. 46, 298 K value).

The experimental IE($SF_3$) (= 8.18±0.07 eV) and EA($SF_3$) (= 3.1±0.2 eV) are in good accord with IE[G2(MP2)] (= 8.27 eV) and EA[G2(MP2)] (= 3.10 eV). The value $\Delta_fHE_0(SF_3^+)$ = 85.0±1.9 kcal/mol is the average of the two values 85.5±2.5 and 84.4±2.8 kcal/mol determined using the AEs of $SF_3^+$ from $SF_6$ and $SF_4$ (see Table II), and is in excellent agreement with the G2(MP2) value of 85.5 kcal/mol. Combining this average value and the experimental IE($SF_3$), we obtain $\Delta_fHE_0(SF_3)$ = -103.6±2.5 kcal/mol, which agrees with the IE[G2(MP2)] value of 105.2 kcal/mol. Using $\Delta_fHE_0(SF_3)$ = -103.6±2.5 kcal/mol and EA($SF_3$) = 3.1±0.2 eV,[46] we obtain $\Delta_fHE_0(SF_3^-)$ = -175.1±5.2 kcal/mol, in close agreement with EA[G2(MP2)] = -176.5 kcal/mol.

As pointed out above, IE($SF_4$) = 11.90 eV determined in the previous PIMS and PE spectroscopy experiment[45] and $\Delta_fHE_0(SF_4^+)$ = 91.9±2.5 kcal/mol and $\Delta_fHE_0(SF_4)$ = -182.5±2.5 kcal/mol obtained in this study are in excellent agreement with the G2[(MP2)] values of 11.85 eV, 91.1 kcal/mol, and -182.2 kcal/mol, respectively. Because $SF_4^-$ is found to have two stable structures, two EAs are predicted by G2(MP2) calculations. The EA[G2(MP2)] values of 1.52 and 1.02 eV are measures of the transition energies for the detachment reactions, $SF_4^-(C_{4v}) \rightarrow SF_4(C_{2v}) + e^-$ and $SF_4^-(C_{2v}) \rightarrow SF_4(C_{2v}) + e^-$, respectively. Since the structures for $SF_4(C_{2v})$, $SF_4^-(C_{2v})$, and $SF_4^-(C_{4v})$ are quite different, the Franck-Condon factors for these detachment processes are not favorable. Because $SF_4^-(C_{4v})$ is the more stable isomer, the experimental EA($SF_4$) = 1.5±0.2 eV is associated with the process, $SF_4^-(C_{4v}) \rightarrow SF_4(C_{2v}) + e^-$. Combining this experimental EA($SF_4$) and $\Delta_fHE_0(SF_4)$ = -182.5±2.5 kcal/mol, we calculate $\Delta_fHE_0(SF_4^-)$ = -217.1±5.2 kcal/mol, compared to the G2(MP2) prediction of -217.1 kcal/mol.

The previous experimental determinations of $\Delta_fHE_0(SF_5)$ and $\Delta_fHE_0(SF_5^+)$ are the most controversial. This issue is the subject of several recent reports.[19-24] This difficulty is partly due to the failure of the traditional PIMS method to find the AE of $SF_5^+$ from $SF_6$. The previously

accepted $\Delta_f HE_0(SF_5)$ = -215.7±3.2 kcal/mol is based on the upper limit of 91.1±3.2 kcal/mol for $D^o_0(SF_5\text{-}F)$ obtained in a study of the chemiluminescent reaction $Sr(^3P) + SF_6$.[18] In the same experiment, an upper limit of 101.0±3.4 kcal/mol was obtained for $DE_0(SF_5\text{-}F)$ by the $Ca(^3P) + SF_6$ reaction. No logical arguments are given in Ref. 18 for the rejection of the $Ca(^3P) + SF_6$ results. Cheung et al.[23] point out that the latter limit is close to the G2(MP2) prediction of 106.9 kcal/mol for $D^o_0(SF_5\text{-}F)$. The $Ca(^3P) + SF_6$ result translates into a value of -205.9±3.4 kcal/mol for $\Delta_f HE_0(SF_5)$, which is in reasonable accord with the G2(MP2) prediction of -201.8 kcal/mol after taking into account the experimental uncertainties and the estimated accuracy of the G2(MP2) procedure. One possible difficulty in the chemiluminescence experiment[18] is the existence of higher long-lived excited states such as the $Ca(^1D)$ [$Sr(^1D)$] state in the Ca (Sr) atomic beams. The presence of such higher excited states is expected to result in a lower value for the upper bound of $D^o_0(SF_5\text{-}F)$.

The IE($SF_5$) = 9.60±0.05 is in good agreement with IE[G2(MP2)] = 9.63 eV. The value $\Delta_f HE_0(SF_5^-)$ = 16.4±3.6 kcal/mol derived by combining the experimental IE($SF_5$) and $\Delta_f HE_0(SF_5)$ = -205.9±3.4 kcal/mol is again considered to be in accord with the $\Delta_f HE_0$[G2(MP2)] value of 20.3 kcal/mol. We note that in the most recent proton affinity study of $SF_6$, Latimer and Smith[24] report an upper limit of 25.0±2.0 and 20.9±2.0 kcal/mol for the heats of formation of $SF_5^+$ at 0 K and 298 K, respectively. The experimental EA($SF_5$) values are in the range from >3.7±0.3 to 3.01±0.29 eV. The G2(MP2) calculation yields an EA value of 4.07 eV for $SF_5$, suggesting the actual EA($SF_5$) is likely >3.7 eV. Without newer experimental measurements, we recommend EA($SF_5$) = 3.7±0.2 eV.[56] Combining this latter value and $\Delta_f HE_0(SF_5)$ = -205.9±3.4 kcal/mol, we calculate an EA($SF_5$) value of -291.2±5.7 kcal/mol, which is in agreement with the G2(MP2) prediction of -295.6 kcal/mol after taking into account the experimental uncertainties.

The experimental value $\Delta_fHE_0(SF_6) = -288.4\pm0.2$ kcal/mol is well established. As pointed out above, the adiabatic IE for $SF_6$, and thus $\Delta_fHE_0(SF_6^+)$, are unknown both experimentally and theoretically. In the previous PIMS study[28] of $SF_6$, observation of a very low intensity of $SF_6^+$ is reported. We find that the intensity of $SF_6^+$ is in the noise level of our experiment, in agreement with the observations of previous PIMS[30,32,60] and electron impact[27,61] experiments. The results of the PIMS and electron impact experiments are consistent with the conclusion that $SF_6^+$ is unstable with respect to $SF_5^+ + F$. As noted above, the theoretical structure optimization of $SF_6^+$ indicates that $SF_6^+$ is unstable with respect to $SF_4^+ + F_2$. As pointed out previously, since the $SF_5^+ \cdots F$ and $SF_4^+ \cdots F_2$ complexes are bound by ion-induced-dipole forces, these ion complexes can in principle be observed if mechanisms exist for relaxing their excess internal energies. Using the recommended $\Delta_fHE_0(SF_6) = -288.4\pm0.2$ kcal/mol[46] and $\Delta_fHE_0(SF_5^+) = 16.4\pm3.6$ kcal/mol,[23] along with $\Delta_fHE_0(F) = 18.5$ kcal/mol[46], we predict the true AE for $SF_5^+$ from $SF_6$, i.e., the threshold for process (1), to be 14.0 eV, which is 1.27 eV lower than the observed AE for $SF_5^+$ from process (1). Using the experimental $EA(SF_6) = 1.05\pm0.10$ eV and $\Delta_fHE_{298}(SF_6) = -291.7\pm0.2$ kcal/mol, we calculate a value of $-315.9\pm2.4$ kcal/mol for $\Delta_fHE_{298}(SF_6^-)$. We convert the latter value to $\Delta_fHE_0(SF_6^-) = -314.5\pm2.4$ kcal/mol using the theoretical MP2/6-31G(d) frequencies for $SF_6^-$.

In order to make possible the UQCISD(T)/6-311G(d,p) single-point energy calculation for $SF_6^-$, we invoke the additivity approximation shown in Eq. (7). To test the reliability of applying this approximation to G2(MP2) calculations i.e., the AG2 procedure, we have compared the $E_0$, IE, EA, $\Delta_fHE_0(SF_6^-)$ values for S, F, $SF_n$, $SF_n^+$, and $SF_n^-$ (n=1-6) using the AG2 and G2(MP2) schemes and find excellent agreement between the two schemes. The AG2 results for $E_0$'s, $_fHE_0$'s, IEs, and EAs of S, F, $SF_n$, $SF_n^+$, and $SF_n^-$ (n=1-6) calculated using the AG2 scheme are summarized in Table IV. The deviation $E_0[G2(MP2)] - E_0(AG2)$ increases roughly as the size of

**Table IV.** Comparison between G2(MP2) and approximated G2(MP2) [AG2] theoretical

**Table IV.** Comparison between G2(MP2) and approximated G2(MP2) [AG2] theoretical energetics for S, F, $SF_n$, $SF_n^+$, and $SF_n^-$ (n=1-6).[a]

| Species | $E_0$[AG2] (hartree) | $E_0$[G2(MP2)]-$E_0$[AG2] (hartree) | $\Delta_f H°_0$(AG2)[b] (kcal/mol) | IE/EA(AG2) (eV) |
|---|---|---|---|---|
| S | -397.64694 | -0.00005 | ... | ... |
| F | -99.62881 | -0.00013 | ... | ... |
| SF | -497.40721 | -0.00005 | 1.7 (1.8) | 10.30/2.29 |
| $SF^+$ | -497.02857 | +0.00007 | 239.3 (239.4) | ... |
| $SF^-$ | -497.49131 | +0.00001 | -51.1 (-50.9) | ... |
| $SF_2(C_{2v})$ | -597.17924 | +0.00028 | -69.7 (-69.9) | 10.07/1.42 |
| $SF_2^+(C_{2v})$ | -596.80901 | +0.00023 | 162.6 (162.3) | ... |
| $SF_2^-(C_{2v})$ | -597.23158 | -0.00005 | -102.6 (-102.4) | ... |
| $SF_3(C_s)$ | -696.89496 | +0.00043 | -105.8 (-106.3) | 8.27/3.10 |
| $SF_3^+(C_{3v})$ | -696.59120 | +0.00062 | 84.9 (84.0) | ... |
| $SF_3^-(C_{2v})$ | -697.00872 | +0.00054 | -177.1 (-177.6) | ... |
| $SF_4(C_{2v})$ | -796.67630 | +0.00064 | -183.0 (-184.2) | 11.86/1.52[c] |
| $SF_4^+(C_{2v})$ | -796.24051 | +0.00042 | 90.5 (89.2) | ... |
| $SF_4^-(C_{4v})$ | -796.73229 | +0.00093 | -206.7 (-207.5) | ... |
| $SF_5(C_{4v})$ | -896.36586 | +0.00056 | -202.6 (-204.4) | 9.62/4.08 |
| $SF_5^+(D_{3h})$ | -896.01217 | +0.00076 | 19.4 (17.4) | ... |
| $SF_5^-(C_{4v})$ | -896.51566 | +0.00093 | -296.6 (-298.0) | ... |
| $SF_6(O_h)$ | -996.16512 | +0.00055 | -291.1 (-293.6) | .../1.04 |
| $SF_6^{+d}$ | ... | ... | ... | ... |

Table VI (continued)

| | | | | |
|---|---|---|---|---|
| $SF_6^-(O_h)$ | -996.20296 | ... | -314.3 (-315.6) | ... |

a) The QCISD(T)/6-311G(d,p) energies for G2(MP2) calculations are calculated using the approximation: [QCISD(T)/6-311G(d,p)] ≈ [QCISD(T)/6-31G(d,p)] + [MP4/6-311G(d,p)] - [MP4/6-31G(d,p)].

b) Values in parentheses are $\Delta_f H^\circ_{298}$ values.

c) EA for $SF_4(C_{2v}) + e^- \rightarrow SF_4^-(C_{4v})$

d) Attempts to determine the $SF_6^+$ structure were unsuccessful.

the molecular species, and has a maximum of 0.00093 hartree for $SF_4^-(C_{4v})$ and $SF_5^-$. Comparing the G2(MP2) predictions for $\Delta_f HE_0$'s in Tables I and III with the corresponding AG2 values in Table IV, we find that the agreement between the two schemes is surprisingly good, with the maximum deviation < 1 kcal/mol. The deviations between G2(MP2) and AG2 predictions for $\Delta_f HE_0$'s also increase with molecular size. The G2(MP2) and AG2 predictions for IEs and EAs for $SF_n$ (n=1-5) are also in excellent accord, with differences < 0.1 eV. The AG2 predictions $\Delta_f HE_0(SF_6^-)$ = -314.3 kcal/mol and $EA(SF_6)$ = 1.04 eV agree with the experimental results of 314.5±2.4 kcal/mol and 1.05±0.10 eV, respectively.

Table V compares the experimental and theoretical sequential $D^\circ_0$'s for $SF_{n-1}$-F (n=1-6), $SF_{n-1}^+$-F (1-5), and $SF_{n-1}^-$-F (n=1-6). These experimental sequential $D^\circ_0$'s are computed using the recommended $\Delta_f HE_0$ values for $SF_n^-$ (n=1-6) shown in Tables I and III. Since $\Delta_f HE_0(SF_6^+)$ is not available experimentally or theoretically, the $D^\circ_0(SF_5^+$-F) is not known. Because the experimental value for $\Delta_f HE_0(SF_2^-)$ is also unavailable, we cannot calculate the $D^\circ_0(SF^-$-F) and $D^\circ_0(SF_2^-$-F)

**Table V.** Comparisons between experimental and G2 or G2(MP2) bond dissociation

**Table V.** Comparisons between experimental and G2 or G2(MP2) bond dissociation energies at 0 K for $SF_{n-1}$-F, $SF_{n-1}^+$-F, and $SF_{n-1}^-$-F (n=1-6).[a,b]

| Bond | Neutral (kcal/mol) | | Cations (kcal/mol) | | Anions (kcal/mol) | |
|---|---|---|---|---|---|---|
| | Experiment | Theory | Experiment | Theory | Experiment | Theory |
| S-F | 81.2±1.4 | 81.8 | 81.6±1.2<br>82.1±1.2[c] | 77.2 | 79.2±13 | 89.3 |
| SF-F | 88.9±3.8 | 88.7 | 94.3±4.4<br>96.2±2.3[c] | 94.3 | ... | 69.8 |
| $SF_2$-F | 54.6±4.3 | 55.8[d]<br>54.4 | 98.6±4.6<br>96.0<br>104.7±1.8[c]<br>100.1±2.3[c] | 99.2[d] | ... | 92.3[d]<br>92.6 |
| $SF_3$-F | 97.4±3.5 | 95.5 | 11.6±3.1<br>8.3±1.2[c]<br>12.9±2.8[c] | 12.9 | 60.5±7.4 | 59.1 |
| $SF_4$-F | 41.9±4.2 | 38.1 | 94.0±4.4<br>106.1±2.3[c] | 89.3 | 92.6±7.9 | 97.0 |
| $SF_5$-F | 101.0±3.4 | 106.9 | ... | ... | 41.8±6.5 | 36.2 |
| Sum | 465.0±8.7 | 466.8 | ... | ... | ... | 444.7 |

a) Unless specified, the experimental $D\,^\circ_0$ values are calculated using experimental $\Delta_f H^\circ_0$ values of S (65.6 kcal/mol), F(18.5 kcal/mol), $S^+$ (304.0 kcal/mol), and $S^-$ (17.7 kcal/mol) from Ref. 46; and the recommended experimental $\Delta_f H^\circ_0$ values (underlined and bolded) for $SF_n$ and $SF_n^+$ (n=1-6) given in Tables I and III.

b) Unless specified, the theoretical $D\,^\circ_0(SF_{n-1}\text{-F})$, $D\,^\circ_0(SF_{n-1}^+\text{-F})$, and $D\,^\circ_0(SF_{n-1}^+\text{-F})$ (n=1, 2) are G2 predictions, and $D\,^\circ_0(SF_{n-1}\text{-F})$, $D\,^\circ_0(SF_{n-1}^+\text{-F})$, and $D\,^\circ_0(SF_{n-1}^+\text{-F})$ (n=3-6) are

Table V (continued)

G2(MP2) predictions. These values are calculated using $E_0$(G2) or $E_0$[G2(MP2)] values or theoretical $\Delta_f H°_0$(G2) or $\Delta_f H°_0$[G2(MP2)] values for $SF_n$ and $SF_n^+$ (n=1-6) given in Table I and III. The value $E_0$(G2) = -397.28016 and -397.72856 hartree for $S^+$ and $S^-$ from Ref. 41 is used in the calculation of $D°_0(S^+\text{-}F)$ and $D°_0(S^-\text{-}F)$.

c) Reference 20.

d) Values calculated using $\Delta_f H°_0$(G2) values for $SF_2$, $SF_2^+$, and $SF_2^-$, and $\Delta_f H°_0$[G2(MP2)] values for $SF_3$, $SF_3^+$, and $SF_3^-$.

e) This work.

values. We note that the EA of the F atom (3.4 eV)[46] is high, so the actual dissociation for the anions may involve the formation of $F^-$. Ion-pair processes producing $F^-$ have been observed in PIMS studies of $SF_6$ (Ref. 30) and $SF_4$ (Ref. 45).

The experimental $D°_0$'s for $SF_{n-1}$-F and $SF_{n-1}^+$-F computed using the recommended experimental heats of formation data (underlined values) in Tables I and III are in excellent agreement with those obtained from theoretical G2 and G2(MP2) calculations. In all cases, the theoretical $D°_0$ values fall within the experimental uncertainties, except those for $S^+$-F, $SF_4^+$-F, and $SF_5$-F. The differences between the experimental and theoretical $D°_0$ values for $S^+$-F, $SF_4^+$-F, and $SF_5$-F are 4.4, 4.7, and 5.9 kcal/mol, respectively. The lower theoretical $D°_0(S^+\text{-}F)$ of 77.2 kcal/mol compared to the experimental value of 81.6±1.2 kcal/mol is partly attributed to the fact that the IE of S calculated by the G2 procedure is lower than the experimental IE(S) by 3.7 kcal/mol. Thus, we conclude that the difference observed between the experimental and theoretical $D°_0(S^+\text{-}F)$ is due to the inaccuracy of the G2 prediction. The sum of 465±9.5 kcal/mol for the

sequential experimental $D^o_0(SF_{n-1}\text{-}F)$ (n=1-6) values agrees with the value of 465 kcal/mol for the enthalpy of reaction at 0 K for the process $SF_6 \rightarrow S + 6F$.

Considering the straight-forward approach of applying PIMS and ion CID techniques to determine the sequential $D^o_0$'s for a system such as $SF_6$, it is interesting to compare the $D^o_0(SF_{n-1}^+\text{-}F)$ (n=1-5) determined in these experiments with those calculated by theoretical procedures and also with those calculated using the recommended $\Delta_fHE_0(SF_n^+)$ data. As shown in Table V, the sequential $D^o_0(SF_{n-1}^+\text{-}F)$ (n=1-5) determined by ion CID and PIMS studies are in general accord with those based on the recommended $\Delta_fHE_0(SF_n^+)$ data. The $D^o_0(SF_4^+\text{-}F)$ = 106.1"2.3 kcal/mol determined in the CID study is likely too high. These comparisons indicate that ion CID and PIMS are good experimental techniques for measuring sequential bond dissociation energies and ion heats of formation for complex systems such as $SF_6^+$.

As shown in Table V, the sequential $D^o_0$'s for the neutral, cationic, and anionic sulfur fluorides all exhibit alternation patterns. The trend of alternating high and low values observed for the neutral S-F bond dissociation energies has been discussed and rationalized previously without invoking the participation of the d-orbitals of the S atom in the bonding.[18,20] The pattern observed for the S-F bond dissociation energies of the sulfur fluoride cations is also discussed in Ref. 20. Interestingly, similar patterns are observed for the IEs and EAs of $SF_n$ (n=1-6) shown in Tables I and III.

The general trends observed for $D^o_0(SF_{n-1}\text{-}F)$ (n=2-6), $D^o_0(SF_{n-1}^+\text{-}F)$ (n=3-5), and $D^o_0(SF_{n-1}^-\text{-}F)$ (n=2-6), and $EA(SF_n)$ (1-6) and $IE(SF_n)$ (n=2-5) are understood by recognizing that molecular species with fully-filled eight, ten, and twelve valence electron shells around the S atoms are more stable than other species. Thus, for the systems of interest here, we have: fully-filled eight electron shells for $SF_3^+$, $SF_2$, and $SF^-$; fully-filled ten electron shells for $SF_5^+$, $SF_4$, and $SF_3^-$; and

fully-filled twelve electron shells for $SF_6$ and $SF_5^-$. Figure 3 is constructed to illustrate and to explain the variations of the observed $D^o_0$'s, IEs, and IEs. The cations $SF_n^+$ (n=2-5), the neutrals $SF_n$ (n=1-6), and the anions $SF_n^-$ (n=1-6), are shown in Fig. 3 in three rows. The values on top of the horizontal arrows are the experimental $D^o_0$'s in kcal/mol for dissociation from $SF_{n-1}$-F to $SF_{n-1}$, $SF_{n-1}^+$-F to $SF_{n-1}^+$, or $SF_{n-1}^-$-F to $SF_{n-1}^-$ except those for $DE_0$($SF^-$-F) and $D^o_0$($SF^-$-F) are theoretical values. The higher $D^o_0$ values correspond to the S-F bond energies for $SF_2$ (88.9±3.8 kcal/mol), $SF_4$ (97.4±3.5 kcal/mol), $SF_6$ (101.0±3.4 kcal/mol), $SF_3^+$ (98.6±4.6 kcal/mol), $SF_5^+$ (94.0±4.4 kcal/mol), $SF_3^-$ (92.3 kcal/mol, theoretical value), and $SF_5^-$ (92.6±7.9 kcal/mol). In each of these cases, the dissociation involves the transformation from a higher and more stable neutral (or cationic, or anionic) sulfur fluoride to a lower and less stable neutral (or cationic, or anionic) sulfur fluoride plus an F atom. The lower S-F dissociation energies correspond to transformation from a high and less stable sulfur fluoride to a low and more stable sulfur fluoride plus an F atom. These latter cases are observed for $SF_3$ [$D°_0(SF_2\text{-}F)$ = 54.6±4.3 kcal/mol], $SF_5$ [$D°_0(SF_4\text{-}F)$ = 41.9±4.2 kcal/mol], $SF_4^+$ [$D°_0(SF_3^+\text{-}F)$ = 11.6±3.1 kcal/mol], $SF_2^-$ [$D°_0(SF^-\text{-}F)$ = 69.8 kcal/mol, theoretical value], $SF_4^-$ [$D°_0(SF_3^-\text{-}F)$ = 60.5±7.4 kcal/mol], and $SF_6^-$ [$D°_0(SF_5^-\text{-}F)$ = 41.8±6.5 kcal/mol].

Ionization energy is a measure of the transition energy from the neutral to its cation, whereas electron affinity measures the transition from an anion to its corresponding neutral. The values in eV shown by the side of the vertical arrows in Fig. 3 are either IEs or EAs. For the ionization transitions $SF_2 \rightarrow SF_2^+ + e^-$ and $SF_4 \rightarrow SF_4^{-+} + e^-$, the transitions correspond to ionization from a stable neutral to a less stable cation, and thus the IEs of $SF_2$ (10.08±0.05 eV) and $SF_4$ (11.90 eV) are expected to be high. The lower IEs for $SF_3$ (8.18±0.07 eV) and $SF_5$ (9.60±0.05 eV) are due to ionization transitions from a less stable neutral to a more stable cation.

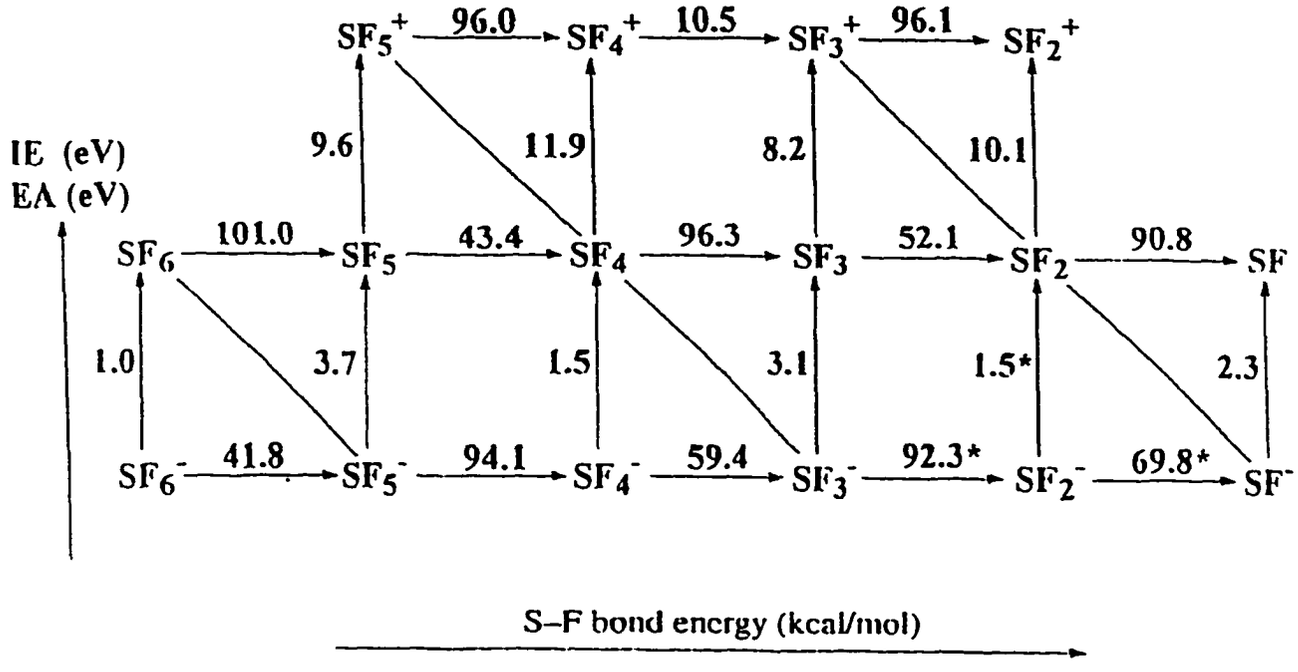


Figure 3 Schematic diagram illustrating the alternating patterns for $D°_0$'s for $SF_{n-1}$-F (n=2-6), $SF_{n-1}^+$-F (n=3-5), and $SF_{n-1}^-$-F (n=2-6), IEs of $SF_n$, and EAs for $SF_n$ (n=1-6). The values marked by asterisks are theoretical values.

Similarly, the electron detachment transitions, $SF^- \rightarrow SF + e^-$, $SF_3^- \rightarrow SF_3 + e^-$, and $SF_5^- \rightarrow SF_5 + e^-$, involve transitions from a more stable to a less stable species. Therefore, we expect the EAs for SF (2.0 eV), $SF_3$ (3.1 eV) and $SF_5$ (3.7 eV) to be higher than those for $SF_2$ (1.5 eV, theoretical value), $SF_4$ (1.5 eV), and $SF_6$ (1.05 eV), which correspond to detachment transitions from a less stable anion to a more stable neutral.

The picture presented above to explain the alternating patterns observed for $D^\circ_0$'s, IEs, and EAs for the $SF_n$ and $SF_n^+$ (n=1-6) systems should also be applicable to similar systems involving other hypervalent species.

**Conclusions**

The comparison of the experimental thermochemical data and G2 [or G2(MP2)] predictions for $SF_n$, $SF_n^+$, and $SF_n^-$ (n=1-6) allows us to recommend a self-consistent set of experimental $\Delta_f HE_0$, IE, EA, $DE_0$ values for these systems. This work shows that for reliable determinations of the thermochemical data for a complex system such as $SF_n$, $SF_n^+$, and $SF_n^-$ (n=1-6), it is necessary to combine both experimental measurements made using different techniques and theoretical predictions calculated using a sufficiently accurate theoretical procedure.

The comparison of experimental and theoretical results in this study further confirms that G2 and G2(MP2) procedures are reliable theoretical methods for providing energetic predictions accurate to 4-5 kcal/mol for complex sulfur-containing molecular species. The study also indicates that traditional CID and PIMS experiments are reliable methods for ion sequential bond energy measurements for complex molecular ions such as $SF_6^+$.

The theoretical equilibrium structures obtained for $SF_n$, $SF_n^+$, and $SF_n^-$ (n=1-6) have been rationalized using the VSEPR theory. Furthermore, we have provided an explanation to account

for the observed alternating patterns in IE, EA and $D^{\circ}_0$ values for $SF_n$, $SF_n^+$, and $SF_n^-$ (n=1-6). Alternating patterns in IE, EA and $D^{\circ}_0$ values are expected for other similar hypervalent species.

**References**


(1) H.-X. Wang, J. H. Moore, J. K. Olthoff, and R. J. Van Brunt, *Plasma Chem. Plasma Process.* **1993**, *13*, 1.

(2) I. Sauers, L. G. Christophorou, and S. M. Spyrou, *Plasma Chem. Plasma Process.* **1993**. *13*, 17.

(3) I. Sauers, H. W. Ellis, and L. G. Christophorou, *IEEE Trans. Electr. Insul.* **1986**, *EI-21*, 111.

(4) I. Sauers, *IEEE Trans. Electr. Insul.* **1986**, *EI-21*, 105.

(5) I. Sauers, *Plasma Chem. Plasma Process.* **1988**, *8*, 247.

(6) N. Mutsukura and G. Turban, *Plasma Chem. Plasma Process.* **1990**, *10*, 27.

(7) K. R. Ryan and E. C. Plumb, *Plasma Chem. Plasma Process.* **1990**, *10*, 207.

(8) P. G. Datskos, L. G. Christophorou, and J. G. Carter, *J. Chem. Phys.* **1993**, *99*, 8607.

(9) A. Picard, G. Turban, and B. Grolleau, *J. Phys. D*, **1986**, *19*, 991.

(10) R. Pinto, K. V. Ramanathan, and R. S. Babu, *J. Electrochem. Soc.* 134, 165 (1987).

(11) V. Premachandran, *Appl. Phys. Lett.* **1991**, *58*, 1600.

(12) M. Zhang, J. Z. Li, I. Adesida, and E. D. Wolf, *J. Vac. Sci. Technol. B*, **1983**, *1*, 1037.

(13) W. Tsang, *ASME Publication 86-WA/HT-27.*

(14) J. K. Olthoff, R. J. Van Brunt, J. T. Herron, and I. Sauers, *Anal. Chem.* **1991**, *63*, 726.

(15) J. T. Herron, *IEEE Trans. Electr. Insul.* EI-22, 523 (1987).

(16) G. Javahery, H. Becker, M. V. Korobov, M. Garber, D. Cooper, D. K. Bohme, *Int. J. Mass Spectrom. Ion Processes*, **1994**, *133*, 73.

(17) J. I. Musher, *Angew Chem. Int. Ed. Eng.* **1969**, *8*, 54.

(18) T. Kiang and R. N. Zare, *J. Am. chem. Soc.* **1980**, *102*, 4024.

(19) H. Becker, J. Hru×<k, and H. Schwarz, *J. Chem. Phys.* **1994**, *100*, 1759.

(20) E. R. Fisher, B. L. Kickel, and P. B. Armentrout, *J. Chem. Phys.* **1992**, *97*, 4859

(21) W. Tsang and J. T. Herron, *J. Chem Phys.* **1992**, *96*, 4272.

(22) L. W. Sieck and P. J. Ausloos, *J. Chem. Phys.* **1990**, *93*, 8374.

(23) Y.-S. Cheung, W.-K. Li, S.-W. Chiu, and C. Y. Ng, *J. Chem. Phys.* **1994**, *101*, 3412.

(24) D. R. Latimer and M. A. Smith, *J. Chem. Phys.* **1994**, *101*, 3410, 10197.

(25) D. L. Hildenbrand, *J. Phys. Chem.* **1973**, *77*, 897.

(26) V. H. Dibeler and F. L. Molhler, *J. Res. Nat. Bur. Stand.* **1948**, *40*, 25.

(27) P. Harland and J. C. J. Thynne, *J. Phys. Chem.* **1969**, *73*, 4031.

(28) V. H. Dibeler and J. A. Walker, *J. Chem. Phys.* **1966**, *44*, 4405.

(29) J. Berkowitz, unpublished data. See J. Berkowitz, *Photoabsorption, Photoionization, and Photoelectron Spectroscopy*; Academic Press: New York, 1979, p. 325.

(30) K. Mitsuke, S. Suzuki, T. Imamura, and I. Koyano, *J. Chem. Phys.* **1990**, *93*, 8717.

(31) H. Baumgartel, H.-W. Jochims, E. Ruhl, O. Losking, and H. Willner, *Z. Naturforsch.* **1989**, *44B*, 21.

(32) J. C. Creasey, I. R. Lambert, R. P. Tuckett, K. Codling, L. J. Frasinski, P. A. Hatherly, and M. Stankiewicz, *J. Chem. Soc. Faraday Trans.* **1991**, *87*, 1287.

(33) I. G. Simm, C. J. Danby, J. H. Eland, and P. I. Mansell, *J. Chem. Soc. Faraday Trans. II*, **1976**, *72*, 426.

(34) D. C. Frost, C. A. McDowell, J. S. Sandhu, and D. A. Vroom, *Adv. Mass Spectrom.* **1986**, *4*, 781.

(35) D. W. Turner, C. baker, A. D. Baker, and C. K. Brundle, *Molecular Photoelectron Spectrosopy*; Wiley: London, 1970, p. 379.

(36) U. Gelius, *J. Electr. Spectr.* **1974**, *5*, 985.

(37) G. Bieri, L. Csbrink, W. Von Niessen, *J. Electron Spectrosc. Relat. Phenom.* **1982**, *27*, 129.

(38) H. M. Rosenstock, K. Draxl, B. W. Steiner, and J. T. Herron, "Energetics of Gaseous Ions", *J. Phys. Chem. Ref. Data*, **1977**, *6*, Suppl. 1, p. 1.

(39) L. A. Curtiss, K. Raghavachari, G.W. Trucks, and J. A. Pople, *J. Chem. Phys.* **1991**, *94*, 7221.

(40) L. A. Curtiss, K. Raghavachari, and J. A. Pople, *J. Chem. Phys.* **1993**, *98*, 1293.

(41) S.-W. Chiu, W.-K. Li, W.-B. Tzeng, and C. Y. Ng, *J. Chem. Phys.* **1992**, *97*, 6557.

(42) Z.-X. Ma, C.-L. Liao, C. Y. Ng, Y.-S. Cheung, W.-K. Li, and T. Baer, *J. Chem. Phys.* **1994**, *100*, 4780.

(43) Z.-X. Ma, C.-L. Liao, H.-M. Yin, C. Y. Ng, S.-W. Chiu, N. L. Ma, and W. K. Li, *Chem. Phys, Lett.* **1993**, *213*, 250.

(44) W.-K. Li, S.-W. Chiu, Z.-M. Ma, C.-L. Liao, and C. Y. Ng, *J. Chem. Phys.* **1993**, *99*, 8440.

(45) H.-W. Jochims, E. Ruhl, and H. Baumhartel, *Z. Naturforsch.* **1989**, *44B*, 13.

(46) S. G. Lias, J. E. Bartmess, J. F. Liebman, J. L. Holmes, R. D. Levin, and W. G. Mallard, *J. Phys. Chem. Ref. Data*, **1988**, *17*, Suppl. No. 1.

(47) R. J. Gillespie and I. Hargittai, *The VSEPR Model of Molecular Geometry*; Allyn and Bacon: Needham Heights, 1991.

(48) Y. Ono, S. H. Linn, H. F. Prest, and C. Y. Ng, *J. Chem. Phys.* **1980**, *73*, 2523.

(49) C. Y. Ng, *Adv. Chem. Phys.* **1983**, *52*, 265.

(50) C. Y. Ng, in *Vacuum Ultraviolet Photoionization and Photodissociation of Molecules and Clusters*; World Scientific: Singapore, 1991, p. 169.

(51) M. J. Frisch et al., *GAUSSIAN 90* (Gaussian Inc., Pittsburg PA, 1990); M. J. Frisch et al., *GAUSSIAN 92* (Gaussian Inc., Pittsburg PA, 1992)

(52) R. Seeger and J. A. Pople, *J. Chem. Phys.* **1977**, *66*, 3045.

(53) See D. L. Cooper, T. P. Cunningham, J. Gerratt, P. B. Kardakov, and M. Raimondi, *J. Am. Chem. Soc.* **1994**, *116*, 4414; and references therein.

(54) G. Di Lonardo and A. Trombetti, *Trans. Faraday Soc.* **1970**, *66*, 2694.

(55) D. M. DeLeeuw, R. Mooyman, and C. A. De Lange, *Chem. Phys.* **1978**, *34*, 287.

(56) M. W. Chase, Jr., C. A. Davies, J. R. Downey, Jr., D. J. Frurip, R. A. McDonald, and A. N. Syverud, *JANAF Therchemical Tables*, 3rd ed., *J. Phys. Chem. Ref. Data*, **1985**, *14*, Suppl. 1.

(57) The $\Delta_f HE_{298}(SF_4)$ = -183.5±3.7 kcal/mol [or $\Delta_f HE_{298}(SF_4)$ = -182.2±5.0 kcal/mol] are converted from known $\Delta_f HE_0(SF_4)$ values of -182.3±3.7 kcal/mol from Ref. 20 [or -180.9±5 kcal/mol from Ref. 5] and using MP2/6-31G(d) vibrational frequencies for $SF_4$.

(58) E. P. Grimsrud, S. Chowdhury, and P. Kebarle, *J. Chem. Phys.* **1985**, *83*, 1059.

(59) $\Delta_f HE_0(SF_4^-)$ is only lower than $\Delta_f HE_{298}(SF_4^-)$ by .0.2 kcal/mol based on the theoretical prediction.

(60) T. Masuoka and J. A. R. Samson, *J. Chem. Phys.* **1981**, *75*, 4946.

(61) A. P. Hitchcock, C. E. Brian, and M. J. Van der Wiel, *J. Phys. B*, **1978**, *11*, 3245.

# PART II

## COLLISION-INDUCED DISSOCIATION OF ORGANOSULFUR COMPOUNDS EVIDENCE OF NON-STATISTICAL BEHAVIOR

## INTRODUCTION

The observation of the decomposition of ions produced by collision-induced dissociation (CID) in the gas phase is as early as 1913 when Thomson[1] observed the decomposition of collisionally activated $H_2^+$ ions, and it was only in 1919 that Aston gave a correct explanation on the observed phenomenon. Although the subject attracts interests of mainly physicists and lead to increasing reports on the fundamentals of the CID process of the small diatomic molecules, the interests of organic mass spectrometry was stimulated by the early work of Jennings[2] and Haddon and McLafferty [3] and the detailed investigation by Cooks et al.[4], Beynon et al.[5], and Kim et al.[6] McLafferty first implemented the CID technique for the structure elucidation of organic ions in the gas phase, and Cooks further explored the potential of CID method for analysis of mixture of organic compounds.[7,8]

The CID process for a polyatomic molecule can be considered to consist of mainly two distinct steps: (a) collisional excitation and following (b) unimolecular dissociation:

$$(AB)^+ + M \rightarrow (AB)^{+\bullet} + M \qquad (a)$$

$$(AB)^{+\bullet} \rightarrow A^+ + B \qquad (b)$$

Collision of high energy ions $(AB)^+$ with a neutral target will usually result in electronic, rotational, or vibrational excitation, depending on the range of the energy. When the ion $(AB)^+$ approaches the neutral target M, a strongly repulsive collision complex will be formed. If the ion and the neutral target approach each other infinitely slowly, the electron density of the system will adjust adiabatically and therefore the ion still remain its electronic ground state

after collision. On the other hand, in the extreme of very short interaction time in the collision complex, the electron can not adjust adiabatically in its excited state. As a result, the nuclear motions can be ignored and the excitation will occur depending on the relative position of the potential curves of $(AB)^+$ and $(AB)^{+\bullet}$.

In general, the mechanism for the collision-induced dissociation can be described well by the statistical quasiequilibrium theory (QET).[9] There are two basic assumptions:

(1) The reaction rate is controlled by the critical configuration of the transition.

(2) The excitation energy will be redistributed over all vibrational degrees of freedom before unimolecular dissociation.

A great deal of evidences supporting the quasiequilibrium theory has been observed. For example, an isotropic distribution of fragments has been observed.[10] The same types of fragments are observed following collisional activation, electron impact excitation, or photon excitation of a molecular ion. However, experimentally, there are examples[10] of incomplete excitation energy sharing among the phase space, i.e., the initially excited state is coupled to significantly fewer levels than the large number of energetically available levels. That a collision proceeds via a long-lived complex doesn't necessarily imply that it is not selective in its energy requirement or that it is not specific in its energy disposal. An example is the elimination of HX molecule from energy-rich alkyl halides, in which a considerable fraction of the energy is deposited into the H-X vibration.[10] Whether energy randomization is in fact complete when the reactant molecular ion dissociates is an important issue requiring further investigation, and it might help us to gain insight into the fundamentals behind the collision-induced dissociation process.

Due to the advantage of soft ionization and high energy resolution achieved in the photoionization , ionization by photoionization is preferred over electron impact ionization for the preparation of state-specific reactant ion.[11] The internal energy of the precursor reactant ion can be better defined by the spectroscopic knowledge of molecules in the vacuum ultraviolet (VUV) region. The precise control of wavelength for ionization of a molecule allows us to produce molecular ions in vibrationally selected states. By the incorporation of jet-cooled molecule beam, the cooling effect, resulting from supersonic expansion, narrows spread in translational energy and makes possible the preparation of neutral reactants in their ground rotational states. The use of the radio frequency (RF) octopole ion guide[12, 13] reaction gas cell in the ion beam- gas cell arrangement allows the absolute total cross section measurement with high accuracy and extends the collision energy to near thermal enrage. By combining VUV light source, molecule beam, RF octopole ion guide reaction cells, we are able to measure the absolute total cross sections with high collection efficiency and well-defined internal energy for the collision-induced dissociation.

Large quantities of sulfur compounds are released by the biosphere, volcanos, and human activities.[14] Such compounds include $H_2S$, COS, $CS_2$ , methyl mercaptan ($CH_3SH$), dimethyl sulfide ($CH_3SCH_3$), and dimethyl disulfide ($CH_3SSCH_3$). Most of these compounds are attacked by OH radicals and ozone and subsequently oxidized to form $SO_2$. For example, methyl mercaptan is emitted into the atmosphere by industrial companies and is oxidized to form SO, $SO_2$, and $SO_3$, which are major pollution factors affecting the acidity of moisture and rain. By studying the collision-induced dissociation behavior of these selective organsulur

compounds, we hope to shed light on the fundamental properties of these pollutants and lead to the development of control methods for converting the pollution into harmless substances.

References

1. K. Levsen, and H. Schwaz, Mass Spectrom. Rev. 2, 77 (1983)
2. K. R. Jennings, Int. J. Mass Spectrom. Ion. Phys, 1, 227 (1968)
3. W. F. Haddon, and F. W. McLafferty, J. Am. Chem. Soc. 90,4745,(1968)
4. R. G. Cooks, L. Hendricks, and J. H. Beynon, Org. Mass Spectrom. 10, 625 (1975)
5. J. H. Baynon, R. M. Caprioli, and T. Ast, Int. J. Mass Spectrom. Ion. Phys. 7, 88 (1972)
6. K. C. Kim, M. Uckotter, J. H. Baynon, and R. G. Cooks, Int. J. Mass Spectrom. Ion. Phys. 15, 23 (1974)
7. R. W. Kondrat, and R. G. Cooks, Anal. Chem. 50, A81 (1978)
8. R. G. Cooks, Tandom Mass Spectrometry, Wiley, New York
9. C. L. Lifshitz, Adv. Mass Spectrom., 7a, 3 (1976)
10. R. D. Levine, and R. B. Bernstein, Molecular Reaction Dynamics and Chemical Reactivity, Oxford.(1987)
11. J. M. Farrar, and W. H. Saunders, techniques for the Study of Ion-Molecule Reactions. Wiley, 1988
12. S. L. Anderson, F. A. Houle, D. Gerlich, and Y. T. Lee, J. Chem. Phys, 75, 2153 (1981)
13. J.-D. Shao, and C. Y. Ng, J. Chem. Phys, 84,4317 (1986)
14. J. R. Barker, Progress and Problems in Atmospheric Chemistry, World Scientific

# III. BOND SELECTIVE DISSOCIATION OF $CH_3SH^+$ AND $CH_3CH_2SH^+$ VIA COLLISIONAL ACTIVATION

A paper published in the Journal of Chemical Physics

Y. J. Chen, P. T. Fenn, S. Stimson and C. Y. Ng

**Abstract**

Strong preference is observed for the C-S bond scission process, leading to the formation of $CH_3^+$ + SH ($CH_3CH_2^+$ + SH), in the collision induced dissociation (CID) reaction of $CH_3SH^+$ + Ar ($CH_3CH_2SH$+ + Ar). Since the dissociation energy of 81.4 kcal/mol (45.2 kcal/mol) for the $CH_3^+$-SH ($CH_3CH_2^+$ -SH) bond is significantly higher than that of 48 kcal/mol (33.9 kcal/mol) for the H-$CH_2SH^+$ [H-$CH(CH_3)SH^+$] bond, this observation indicates that the CID process is non-statistical. The high yield for the C-S bond breakage process is attributed to the more efficient translational to vibrational energy transfer for the C-S stretching mode than for C-H and S-H stretching modes via collisional activation, and to weak couplings between the low frequency C-S and high frequency C-H and S-H stretching vibrational modes of $CH_3SH^+$ and $CH_3CH_2SH^+$.

## Results and Discussion

A primary and long-standing motivation for detailed dissociation studies is to learn about the factors which control the outcome of a fragmentation process, such that bond selective dissociation pathways can be designed. A bond selective dissociation process is a process that violates the expectation of a statistical outcome. Most bond selective dissociation studies have been centered on dissociation processes activated by photoexcitation.[1-5] In a recent UV

photodissociation study, it was demonstrated that by selectively exciting a bonding electron localized on a specific bond to an anti-bonding orbital, prompt dissociation of the corresponding bond can be achieved. The short lived repulsive state does not allow energy randomization and results in selective bond-breaking. It has also been demonstrated that overtone excitation of the O-H (O-D) stretch of HOD, followed by photodissociation excitation, produces dominantly OD + H (OH + D) products.[2] The underlying principle of the overtone scheme is to shift the Franck-Condon excitation region such that the molecule is photoexcited to the repulsive part of an excited potential energy surface, favoring the formation of a specific product channel. The application of the principle of coherent control[3,4] is also potentially useful for controlling the branching ratio of photoproducts. An experimental demonstration of coherent control in the photoionization of HI has recently been made.[5] In this communication, we report the demonstration of bond selective dissociation of $CH_3SH^+$ and $CH_3CH_2SH^+$ via collisional activation. The dissociation of polyatomic ions are usually described using statistical models.[6,7] The selective C-S breakage process in the collisional activated dissociation of $CH_3SH^+$ and $CH_3CH_2SH^+$ is attributed to the more efficient translational to C-S vibrational energy transfer and inefficient energy flow between the C-S and X-H (X=C and S) vibrational modes.

The arrangement of the triple-quadrupole double-octopole (TQDO) photoionization ion-molecule reaction apparatus and procedures used to perform state-selected absolute total cross section measurements have been described in detail previously.[8-10] The reactant $CH_3SH^+$ ($CH_3CH_2SH^+$) is prepared by photoionization of $CH_3SH$ ($CH_3CH_2SH$) at its ionization threshold of 1311 Å (1334 Å).[11] By using a wavelength resolution of 6 Å (FWHM), $CH_3SH^+$

($CH_3CH_2SH^+$) is formed predominantly in its ground vibronic state. Furthermore, since the $CH_3SH$ ($CH_3CH_2SH$) sample is introduced into the photoionization ion source as a free jet, the $CH_3SH^+$ ($CH_3CH_2SH^+$) thus formed is also rotationally cold. For absolute total cross section measurements, the reactant $CH_3SH^+$ ions were extracted and selected by the reactant quadrupole mass spectrometer before entering the upper radio frequency octopole ion guide reaction gas cell, where collision activated dissociation occurred with Ar. The pressure of Ar in the gas cell was maintained at 2-3x$10^{-4}$ Torr. The reactant ions and the product ions formed in the upper reaction gas cell were then detected by the product quadrupole mass spectrometer. The center-of-mass kinetic energy ($E_{c.m.}$) resolution achieved in this experiment was ±0.2 eV.

Figures 1(a) and 1(b) show the absolute total cross sections for the collision-induced dissociation (CID) reactions of $CH_3SH^+$ + Ar [reactions (1) and (2)] at $E_{c.m.}$=2~30 eV and $CH_3CH_2SH^+$ + Ar [reactions (4) and (5)] at $E_{c.m.}$ = 1-30 eV, respectively.

$$CH_3SH^+ + Ar \rightarrow CH_2SH^+ + H + Ar \qquad \Delta H^0_0 = 2.09 \pm 0.09 \text{ eV} \qquad (1)$$

$$\rightarrow CH_3^+ + SH + Ar \qquad \Delta H^0_0 = 3.53 \pm 0.02 \text{eV} \qquad (2)$$

$$CH_3CH_2SH^+ + Ar \rightarrow CH_3CHSH^+ + H + Ar \qquad \Delta H^0_0 = 1.47 \text{ eV} \qquad (3)$$

$$\rightarrow CH_2SH^+ + CH_3 + Ar \qquad \Delta H^0_0 = 1.73 \text{ eV} \qquad (4)$$

$$\rightarrow CH_3CH_2^+ + SH + Ar \qquad \Delta H^0_0 = 1.96 \text{eV} \qquad (5)$$

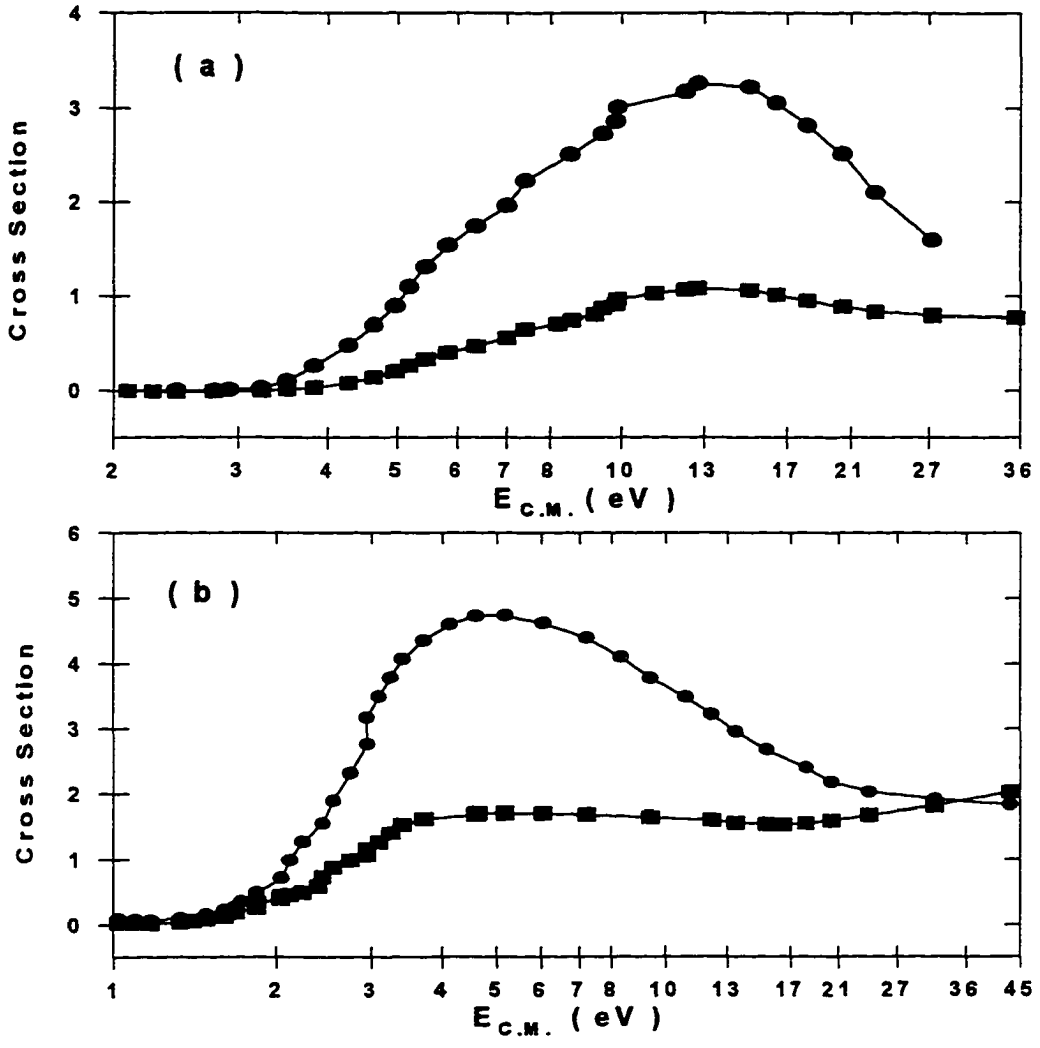


**Figure 1** (a)Absolute total cross sections for $CH_3^+$ (○) and $CH_2SH^+$ (●) formed in the CID reaction of $CH_3SH^+$ + Ar at E~rn. = 2-30 eV. (b) Absolute total cross sections for $CH_3CH_2^+$ (○) and $CH_2SH^+$ (●) formed in the CID reaction of $CH_3CH_2SH^+$ + Ar at $E_{c.m.}$ = 1-30 eV.

Using the currently available thermochemical data, we have calculated the heats of reaction at 0 K ($\Delta H^0_0$) for processes (1)-(5). Figures 2(a) and 2(b) depict the respective mass spectra observed for the CID reactions of $CH_3SH^+$ + Ar at $E_{c.m.}$ = 7.3 eV and $CH_3CH_2SH^+$ + Ar at $E_{c.m.}$ = 5.3 eV by scanning the product quadrupole mass spectrometer. These mass spectra illustrate that $CH_3^+$ and $CH_2SH^+$ (Ref. 14) are the major product ions from $CH_3SH^+$, while $CH_3CH_2^+$ and $CH_2SH^+$ are the dominant product ions from $CH_3CH_2SH^+$. Minor product ions, $CH_2S^+$, $HCS^+$, $HS^+$, and $CH_2^+$ from $CH_3SH^+$ and $C_2H_4^+$, $C_2H_3^+$, $CH_2S^+$, $HCS^+$, $H_2S^+$, and $CH_3^+$ from $CH_3CH_2SH^+$, have absolute total cross sections (not shown here) mostly <0.5 $Å^2$ in the $E_{c.m.}$ range of interest in this experiment.

As shown in Fig. 1(a), the maximum cross section of 3.4 $Å^2$ for $CH_3^+$ at $E_{c.m.}$ = 10-14 eV is 3 times higher than the maximum cross section of 1.2 $Å^2$ for $CH_2SH$ at the same $E_{c.m.}$. The appearance energy (AE) of 3.5 ± 0.2 eV observed for $CH_3^+$ is in excellent agreement with the $\Delta H^0_0$ value of 3.53 ± 0.02 eV for reaction (2). This observation is consistent with the expectation that the formation of $CH_3^+$ + SH involves a loose transition complex and the reverse activation barrier is zero.[15] The formation of $CH_2SH^+$ + H involves the H-elimination from the C atom of $CH_3SH^+$.[14] On the basis of *ab initio* calculations[14] and photoionization[16-18] AE measurements, the reverse activation for this process is also small (≤ 0.07 eV). The CID AE (≈3.9 eV) for $CH_2SH^+$ found here is significantly higher than the $\Delta H^0_0$ value of 2.09 ± 0.02 eV for reaction (1), indicating that the formation of $CH_2SH^+$ by reaction (1) is inefficient at $E_{c.m.}$ < 3.9eV.

The CID AEs for $CH_3CH_2^+$ (≈1.9 eV) and$CH_2SH^+$ (≈1.7 eV) from $CH_3CH_2SH^+$ [see Fig. 1(b)] are consistent with the $\Delta H^0_0$ values of 1.96 eV and 1.73 eV for reactions (4) and

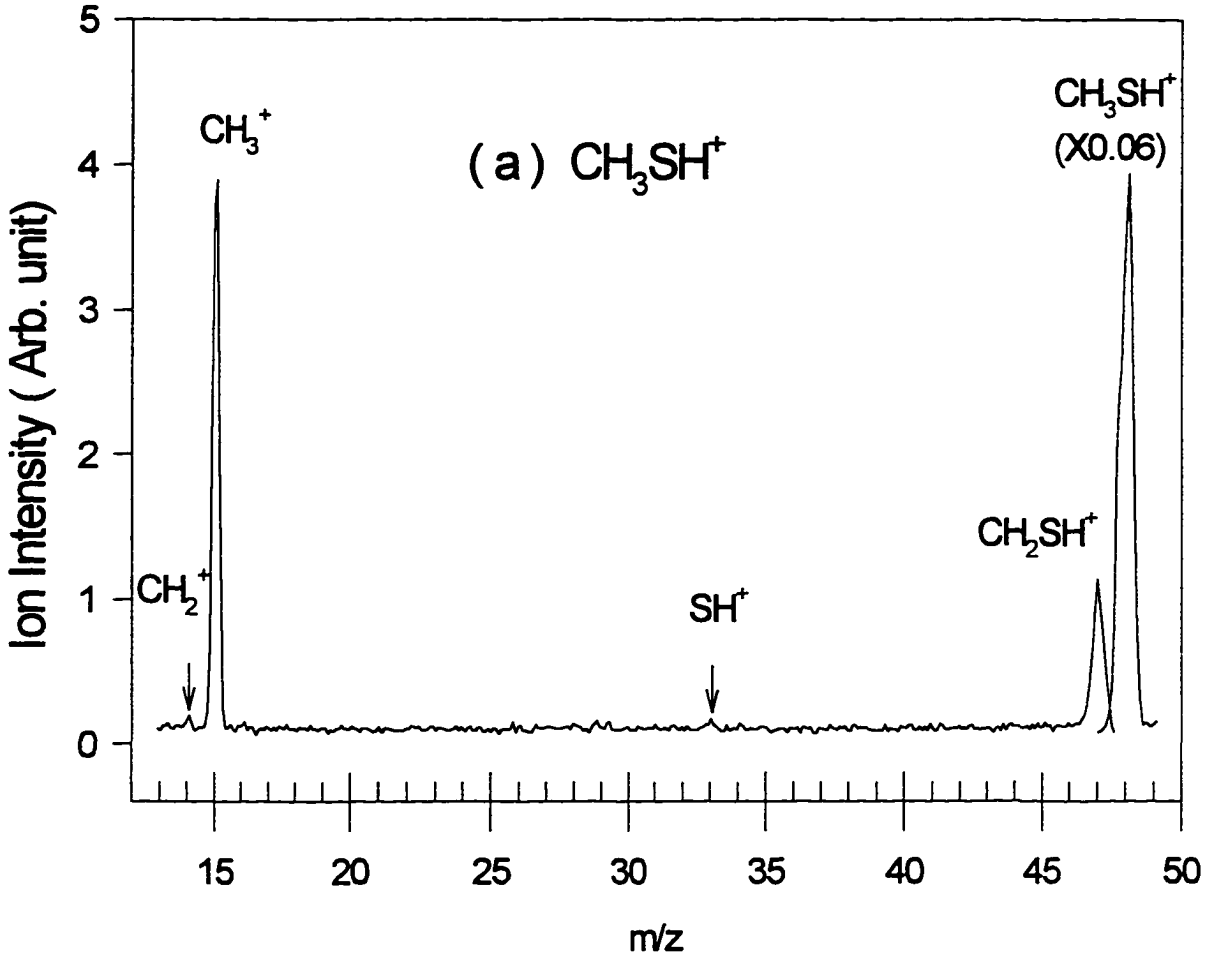


**Figure 2**(a)Mass spectrum in the mass range of m/e = 12-49 amu for the CID reaction of $CH_3SH^+$ + Ar obtained at $E_{c.m.}$ = 7.3 eV. The mass peak for m/e = 48 amu has been scaled by a factor of 0.06.

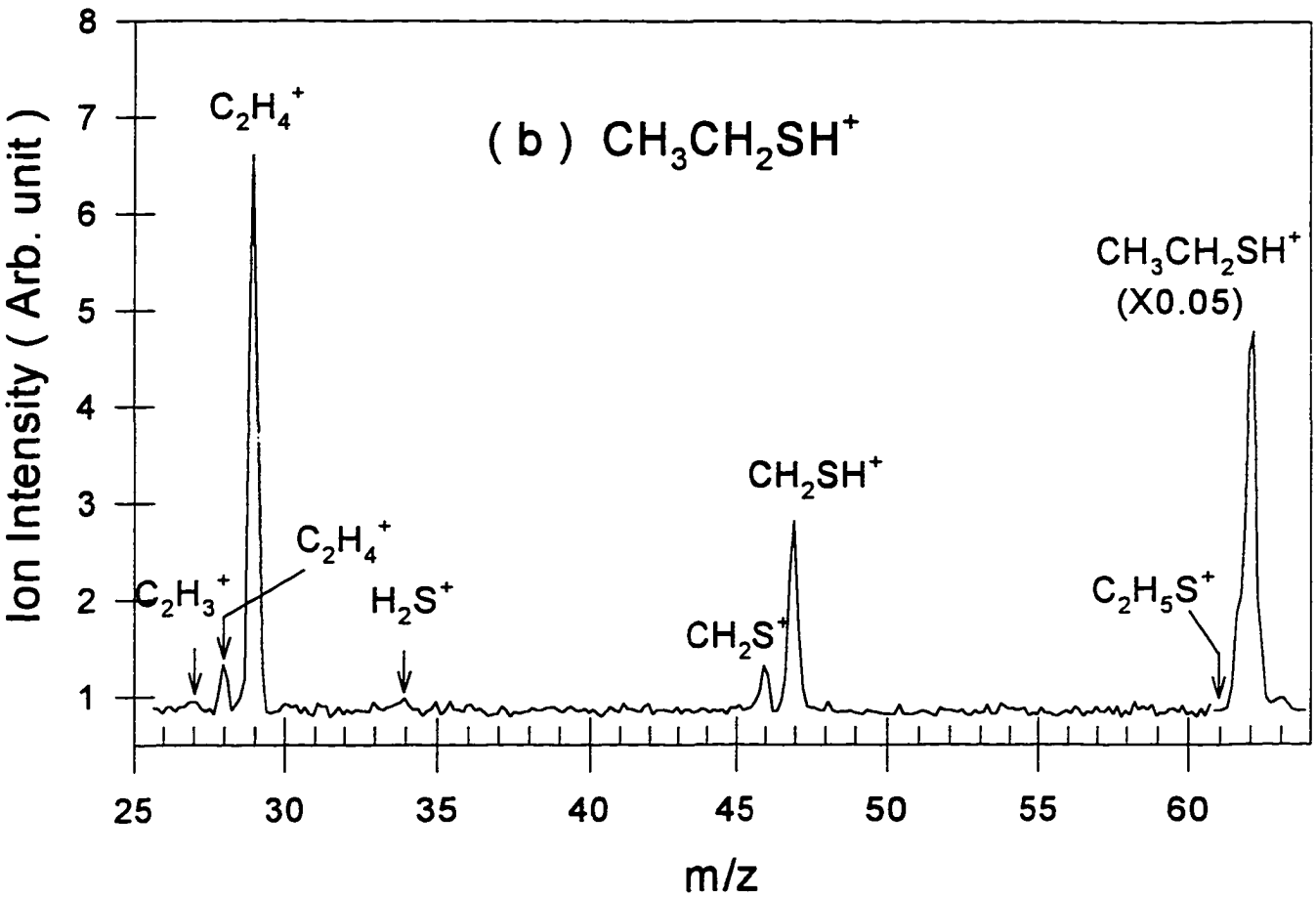


Fig. 2(b)Mass spectrum in the mass range of m/e = 36-64 amu for the CID of $CH_3CH_2SH^+$ + Ar reaction obtained at $E_{c.m.}$ = 5.3 eV. The mass peak for m/e = 62 amu has been scaled by a factor of 0.05. Note that the mass peak (m/e = 61 amu) corresponding to $CH_3CHSH^+$ formed by reaction (3) is absent in the spectrum.

(5), respectively. The maximum absolute total cross section for $CH_3CH_2^+$ is 5 $Å^2$ at $E_{c.m.}$ = 4-5 eV. The total cross sections for $CH_2SH^+$ at $E_{c.m.}$ = 3-30 eV are essentially constant with values of 1.6 $Å^2$.

The calculated $\Delta H^\circ_0$ values for reactions (1)-(5) indicate that the formation of $CH_2SH^+$ + H is significantly more stable than the formation of $CH_3^+$ + SH in the $CH_3SH^+$ + Ar reaction,[19] and that the formation of $CH_3CHSH^+$ + H channel is more stable than the $CH_3CH_2^+$ + SH and $CH_2SH^+$ + $CH_3$ channels for the reaction of $CH_3CH_2SH^+$ + Ar. The basic assumption of a statistical model is that the internal energy of the excited molecule is randomly distributed in the molecules active dissociating degrees of freedom, favoring the most stable product channel.[7] Hence, the result of the present CID experiment, which shows strong preference in the formation of the higher energy product channel, is clearly incompatible with the energy randomization assumption of a statistical model.

It is known that collisional activation at the $E_{c.m.}$ range of this experiment mainly involves translational to rotational and vibrational energy transfer. We expect that the low frequency vibrational modes of $CH_3SH^+$ are preferentially excited in such a process. The four highest vibrational frequencies[21] of $CH_3SH^+$ correspond to $CH_3$ and SH stretching modes, ranging from 2556 to 3035 $cm^{-1}$, while the C-S stretch[11,21] is the second lowest vibrational mode with a frequency of 687 $cm^{-1}$. Thus, the internal vibrational energy resulting from collisional activation is predominantly deposited in the C-S stretching mode instead of the C-H (S-H) stretching modes of $CH_3SH^+$. Owing to the large differences in vibrational frequencies between the C-S and C-H (S-H) stretching modes of $CH_3SH^+$, the C-S and C-H (S-H) stretching modes should only be weakly coupled, resulting in inefficient energy flow between

the C-S and $CH_3$ (SH) vibrational modes of $CH_3SH^+$. As a consequence, the product $CH_3^+$ ions resulting from the breakage of the C-S bond is favored over those due to the breakage of the C-H (S-H) bonds of $CH_3SH^+$.

The CID reaction of $CH_3CH_2SH^+$ + Ar can be considered as a test case for the physical picture gained in the analysis of the CID data for the $CH_3SH^+$ + Ar reaction. Since $CH_3CH_2SH^+$ contains a C-C bond as well as a C-S bond. Based on experimental[11] and *ab initio* investigations[22], the stretching frequencies associated with the C-H, S-H, and C-S bonds are similar to those of $CH_3SH^+$ . The frequency associated with the C-C bond is 1200 $cm^{-1}$ .[22] In addition to the more efficient excitation of the C-S and C-C stretching modes via collisional activation, the coupling between the C-S and C-C modes of $CH_3CH_2SH^+$ should also be more efficient. Hence, product channels [reactions (5) and (4)J arising from the breakage of the C-S and C-C bonds, respectively, should dominate in the CID of $CH_3CH_2SH^+$. This expectation is confirmed by the CID data presented in Figs. 1(b) and 2(b). As shown in Fig. 2(b), the mass peak at m/e = 61 amu corresponding to $CH_3CHSH^+$ formed by reaction (3), which is the most stable product channel, is not observed. Thus, we conclude that the CID reaction of $CH_3CH_2SH+$ + Ar is highly non-statistical.

A strong bond is usually associated with a high stretching vibrational frequency. The C-H stretching frequencies for $CH_3SH^+$ and $CH_3CH_2SH^+$ are typical of that expected for a single C-H bond. However, the dissociation energies for the H-$CH_2SH^+$ and H-$CH(CH_3)SH^+$ bonds are significantly lower than the expected energy for a single C-H bond because of the energy gained in the C=S double bond formation in $CH_2SH^+$ and $CH_3CHSH^+$.[23] We believe that the high vibrational frequency and weak bond dissociation energy combination

is a key feature for the bond selective dissociation of $CH_3SH$+ and $CH_3CH_2SH$ + observed in this collisional activation study.

We note that the relative abundances of product ions from the dissociation of $CH_3SH^+$ observed in previous photoionization and charge exchange studies are in qualitative agreement with predictions of the statistical quasiequilibrium theory, indicating that the energy randomization assumption is mostly valid when the internal energy of $CH_3SH^+$ is deposited by electronic excitation. The difference between the results of these experiments and those of the present study is in how the necessary internal energy for fragmentation is added to $CH_3\ SH^+$. It is known that collisional activation is highly inefficient for electronic excitation.[20]

**References**

1. S. L. Butler, E. J. Hintsa, S. F. Shane, Y. T. Lee, J. Chem. Phys. **86**, 2951 (1987).
2. R. L. Van der Wal, 1. L. Scot, F. F. Crim, K. Wiede, R. Schinke, J. Chem. Phys. **94**, 3548 (1991).
3. M. Shapiro and P. Brumer, J. Chem. Phys. **84**, 4103 (1986).
4. T. Nakajima and P. Lambropoulos, Phys. Rev. Lett. 70, 1081 (1993); Phys. Rev. A 50, 595 (1994).
5. L. Zhu, V. Kleiman, X. Li, S. P. Lu, K. Trentelman, R. J. Gordon, Science, **270**, 77 (1995).

6. T. Bear, in "The Structure, Energetics, and Dynamics of Organic Ions", edited by T. Baer, C. Y. Ng, and I. Powis, Wiley Series in Ion Chemistry and Physics (Wiley, Chichester, 1996), Chap. 3, p.125.

7. T. Baer and W. L. Hase, "Unimolecular Reaction Dynamics: Theory and Experiment (Oxford), New York, 1996.

8. J.-D. Shao and C. Y. Ng J. Chem. Phys. **84,** 4317 (1986); J.-D. Shao, Y. G. Li, G. J. Flesch, and C. Y. Ng, J. Chem. Phys. **86**, 170 (1987); G. D. Flesch and C. Y. Ng, J. Chem. Phys. **94,** 2372 (1991); J. D. Flesch, S. Nourbakhsh, and C. Y. Ng, 3. Chem. Phys. **92**, 3490 (1990); J. D. Flesch and C. Y. Ng, J. Chem. Phys. **92**, 3235 (1990).

9. C. Y. Ng in "State-Selected and State-to-State Ion-Molecule Reaction Dynamics: Experiment", edited by C. Y. Ng and M. Baer (Wiley, New York, 1992), Adv. Chem. Phys. 82, p.401-500.

10. X. Li, Y.-L. Huang, G. J. Flesch, and C. Y. Ng, Rev. Sci. Instrum. **65**, 3724 (1994); ibid. **66**, 871(1995).

11. The ionization energies for $CH_3SH$ and $CH_3CH_2SH$ have been determined to be 9.4553 ± 0.6 eV and 9.2927 ± 0.0006 eV, respectively. See Y.-S. Cheung, C.-W. Hsu, 1.-C. Huang, W.-K. Li, and S.-W. Chiu, Int. J. Mass Spectrom. Ion Proc. 159, 13 (1996).

12. C. Y. Ng, in "The Structure, Energetics, and Dynamics of Organic Ions", edited by T. Baer, C. Y. Ng, and I Powis, Wiley Series in Ion Chemistry and Physics (Wiley, Chichester, 1996), Chap. 2, p. 35; and references therein

13. S. G. Lias, 3. B. Bantmess, 1. L. Holmes, R. D. Levin, and W. G. Mallard, J. Phys. Chem. Ref. Data, 17, Suppl.1 (1988).

14. The im'e = 47 ion has two possible structures, $CH_2SH^+$ and $CH_3S^+$. The ground $CH_3S+(3A_1)$ state lies 1.45 eV (see Ref. 12) above the ground $CH_2SH^+$ ($^1A'$). Here, we assume that the mie = 47 amu ion is formed with the more stable $CH_2SH^+$ structure.

15. R. H. Nobes, W. 3. Bouma, L. Radom, J. Am. Chem. Soc. 106, 2774 (1984).

16. M. E. Akopyan, Y. L. Serhiev, and F. I. Vilesov, KIm. Vys. Energy 4, 305 (1970).

17. R. B. Kutina, A. K. Edwards, I. Berkowitz, J. Chem. Phys. 77, 5508 (1982).

18. S. Nourbash, K. Norwood, H.-M. Yin, C.-L. Liao, and C. Y. Ng, J. Chem. Phys. 95, 945 (1991).

19. The $\Delta H^0_0$ value for the formation of $CH_2S^+ + H_2$ from $CH_3SH^+$ is 1.28 ± 0.09 eV. Thus, $CH_2S^+ + H_2$ is the most stable dissociation product channel from $CH_3SH^+$. The previous photoionization AE measurements (see Refs. 16-18) indicate that the reverse activation for the formation of this product channel from $CH_3SH^+$ is zero.

20. R. D. Levine and R. B. Bernstein, "Molecular Reaction Dynamics and Chemical Reactivity" (Oxford, New York, 1987).

21. S.-W. Chiu, W.-K. Li, W.-B. Tzeng, and C. Y. Ng, J. Chem. Phys. 97, 6557 (1992).

22. Y.-S. Cheung and C. Y. Ng, unpublished results.

23. The dissociation energy for the C-C bond in $CH_3CH_2SH^+$ is lower than that expected for a C-C single bond. This is also due to the energy gained of forming the C=S double bond in $CH_2SH^+$.

24. B.-O. Jonsson and J. Lind, J. Chem. Soc. Faraday Trans. 2 70, 1399 (1974).

# IV:DIRECT IDENTIFICATION OF PRODUCT $CH_2SH^+/CH_3S^+$ STRUCTURES IN THE DISSOCIATION OF $CH_3CH_2SH^+$ AND $CH_3SCH_3^+$ VIA COLLISIONAL ACTIVATION

A paper submitted to the Journal of Chemical Physics

Y. J. Chen, P. T. Fenn, S. Stimson and C. Y. Ng

**Abstract**

We report an experiment on the structural identification of $CH_3S^+$ /$CH_2SH^+$ formed in the collision-induced dissociation (CID) reactions of $CH_3SCH_3^+$ ($CH_3CH_2SH^+$ ) + Ar. We found that $CH_2SH^+$ is the dominant ion formed in the CID of $CH_3CH_2SH^+$, while $CH_3S^+$ is produced in abundance along with $CH_2SH^+$ in the CID of $CH_3SCH_3^+$. The results are attributed to the nonstatistical nature of the dissociation processes.

**Results and Discussions**

In a recent study concerning the absolute total cross section measurements of the collision-induced dissociation (CID) reactions of $CH_3SH^+$ + Ar, strong preference for the C-S bond scission was found, yielding $CH_3^+$ + SH.[1,2] Since the dissociation energy ($D_0$) of 81.4 kcal/mol for the C-S bond in $CH_3SH$ + is significantly higher than the $D_0$ value of 48 kcal/mol for the H-$CH_2SH^+$ bond,[3] this observation indicates that the dissociation of $CH_3SH^+$ via collisional activation is non-statistical. In contrast, previous dissociation studies using photoionization[2,4-6] and charge transfer techniques found that the branching ratios of products ions are in qualitative agreement with the predictions of the quasi-equilibrium theory. The selective C-S bond breakage process in the CID of $CH_3SH^+$ is attributed to the more

efficient translational to C-S vibrational energy transfer and inefficient energy flow between the C-S and X-H (X=C or S) vibrational modes.[1,2] In accordance with this interpretation, the C-S and C-C bond cleavage channels (1) and (2) are strongly favored in the CID of $CH_3CH_2SH^+$, despite the fact that neither is the most stable product channel.[1,8]

$$CH_3CH_2SH^+ + Ar \rightarrow CH_3CH_2^+ + SH + Ar \qquad \Delta H^0_0 = 1.96 \text{ eV} \qquad (1)$$

$$\rightarrow CH_2SH^+ + CH_3 + Ar \qquad \Delta H^0_0 = 1.73 \text{ eV} \qquad (2)$$

$$\rightarrow CH_3S^+ + CH_3 + Ar \qquad \Delta H^0_0 = 3.18 \text{ eV} \qquad (3)$$

$$\rightarrow CH_3CHSH^+ + H + Ar \qquad \Delta H^0_0 = 1.47 \text{ eV} \qquad (4)$$

We note that the most stable channel (4), corresponding to the $H\text{-}CH(CH_3)SH^+$ bond breakage, was not observed, indicating that the CID of $CH_3CH_2SH^+$ is also non-statistical.[1,6] An interesting question is whether the non-statistical behavior also occurs in other CID reactions. In this communication, we present preliminary results of an experiment designed to identify the isomeric structures of the m/e = 47 amu (mass 47) ions observed in reactions (2) and/or (3) and in the CID of $CH_3SCH_3^+ + Ar$ [reactions (5) and/or (6)].

$$CH_3SCH_3^+ + Ar \rightarrow CH_3S^+ + CH_3 + Ar \qquad \Delta H^0_0 = 3.75 \text{ eV} \qquad (5)$$

$$\rightarrow CH_2SH^+ + CH_3 + Ar \qquad \Delta H^0_0 = 2.30 \text{ eV} \qquad (6)$$

Considering that $CH_3CH_2SH^+$ and $CH_3SCH_3^+$ are chemical isomers, a comparison of the branching ratios for product channels from the CID of these isomeric ions is expected to

shed light on their CID mechanisms. Using the charge exchange probing technique described here, we found that $CH_2SH^+$ is the dominant structure formed in the CID of $CH_3CH_2SH^+$, while $CH_3S^+$ is produced in abundance, together with $CH_2SH^+$, in the CID of $CH_3SCH_3^+$.

The arrangement of the triple-quadrupole double-octopole photoionization ion-molecule apparatus has been described in detail previously.[9,10] The reactant $CH_3CH_2SH^+$ ($CH_3SCH_3^+$) is prepared by photoionization of $CH_3CH_2SH$ ($CH_3SCH_3$) at its ionization threshold of 1334 Å (1425 Å).[11,12] By using a wavelength resolution of 6 A (FWHM), $CH_3CH_2SH^+$ ($CH_3SCH_3^+$) is formed predominately in its ground vibronic state. For absolute cross section measurements, the reactant ions were extracted and selected by the reactant quadrupole mass spectrometer (QMS) before entering the upper radio frequency octopole ion guide reaction gas cell (RFOIGGC), where CID occurred with Ar. The pressure of Ar in the gas cell was maintained at $2\text{-}3\text{x}10^{-4}$ Torr. The reactant ions and product ions thus formed were detected by the product QMS. The center-of-mass kinetic energy (Ecrn) resolution achieved was +0.2 eV.

As reported previously,' $CH_3CH_2^+$ and $CH_2SH^+$ ($CH_3S^+$) are the major product ions formed in the CID of $CH_3CH_2SH^+$ at $E_{c.m.} \leq 20$ eV, and have maximum total cross sections of 5 $Å^2$ and 1.6 $Å^2$, respectively. In the same $E_{c.m.}$ range, minor product ions observed in the CID of $CH_3CH_2SH^+$ include $C_2H_4^+$, $C_2H_3^+$, $CH_2S^+$, $HCS^+$, $H2S^+$, and $CH_3^+$, which have total cross sections mostly <0.5 $Å^2$.[1,2] In the $E_{c.m.}$ of 1-19 eV, the product ions observed here in the CID reaction of $CH_3SCH_3^+$ + Ar are $CH_2SH^+$ ($CH_3S^+$), $CH_2S^+$, $CHS^+$, and $CH_3^+$. When it is allowed energetically, the cross section for the mass 47 ion ($CH_2SH^+$ and/or CH3S+) formed by reactions (5) and (6) is significantly higher than those of the other product ions. As shown in Figure 1(a), the profile of the total absolute cross section curve for $CH_2SH^+$ (CH3S+) from

$CH_3SCH_3^+$, which exhibits a maximum of 3.8 Å$^2$, is quite different from that of reactions (2) and (3), which is essentially constant at 1.6 Å$^2$ in the $E_{c.m.}$ range of 3.5-20 eV. The appearance energy of the mass 47 ion from the CID of $CH_3SCH_3^+$ is found to be 2.6 ± 0.2 eV. Since this value is lower than the threshold of $\Delta H^0_0 = 3.75$ eV for reaction(5), we conclude that $CH_2SH^+$ is formed near its threshold.

To probe the structure of the mass 47 ions formed in the CID reactions (2), (3), (5), and (6), we used both the lower and upper RFOIGGCs. Reactant $CH_3CH_2SH^+$ ($CH_3SCH_3^+$) ions prepared by photoionization of $CH_3CH_2SH$ ($CH_3SCH_3$) were first selected by the reactant QMS to enter the lower RFOIGGC where the CID reaction of $CH_3CH_2SH^+$ ($CH_3SCH_3^+$) + Ar at a given $E_{c.m.}$ took place. The mass 47 product ions thus formed were selected by the middle QMS and guided into the upper RFOIGGC, in which the structure for the mass 47 ions was probed by the charge transfer reaction with benzene ($C_6H_6$) at $E_{c.m.} \approx$ 0.2 eV. The ionization energies (IEs) for $CH_3S$, $CH_2SH$, and $C_6H_6$ are known to be 9.2649±0.0010 eV (Refs. 13-15), 7.536±0.003 eV (Ref. 13), and 9.2438421±0.000006 eV (Ref. 16), respectively Using these IE values, we calculate that the charge transfer reaction (7) for $CH_3S^+$ is slightly exothermic by 0.0211eV, whereas the charge transfer reaction (8) for $CH_2SH^+$ is endothermic by more than 1.7 eV.

$$CH_3S^+ + C_6H_6 \rightarrow CH_3S + C_6H_6^+ \qquad \Delta H^0_0 = -0.0211 \text{ eV} \qquad (7)$$

$$CH_2SH^+ + C_6H_6 \rightarrow CH_2SH + C_6H_6^+ \qquad \Delta H^0_0 = 1.708 \text{ eV} \qquad (8)$$

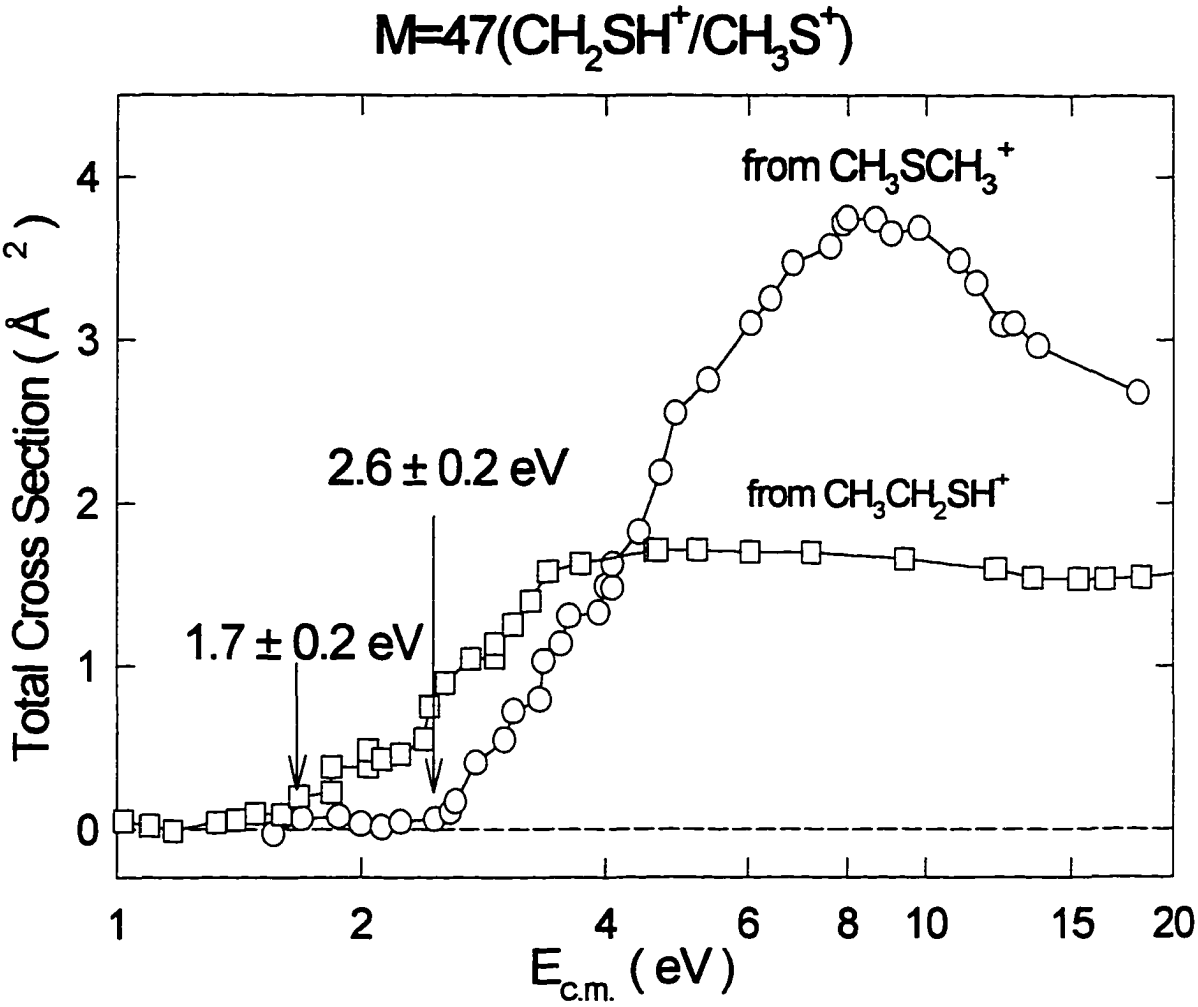


Figure 1(a) Absolute total cross section curves for mass 47 ions formed in the CID reactions of $CH_3SCH_3^+$ (o) and $CH_3CH_2SH^+$ (□) in the $E_{c.m.}$ range of 1-20 eV.

Any charge transfer product $C_6H_6^+$ ions formed were detected by the product QMS. The $C_6H_6$ pressure in the upper gas cell was $3x10^{-4}$ Torr. Because near-resonant charge transfer reactions usually have large cross sections, we should observe the formation of $C_6H_6^+$ if the mass 47 ions have the $CH_3S^+$ structure, while the charge transfer cross section should be negligibly small if $CH_2SH^+$ ions are produced by reactions (2) and (6).

Figure 1(b) depicts the cross sections for $C_6H_6^+$ resulting from the charge transfer reaction of benzene with the mass 47 ions which are formed in the CID reaction of $CH_3SCH_3^+$ + Ar in the $E_{c.m.}$ range probing reaction with benzene. Thus, we conclude that the cross section for process (3) is negligible, and the mass 47 ions resulting from the CID of $CH_3CH_2SH^+$ have mostly the $CH_2SH^+$ structure.

A recent experimental and *ab initio* study[1,2] shows that the C-S and C-H stretching frequencies for $CH_3SCH_3^+$ are in the ranges of 620-680 $cm^{-1}$ and 2880-3000 $cm^{-1}$, respectively. Although the $D_0[H\text{-}CH_2SCH_3^+]$ value of 2.28 eV is lower than that of 3.75 eV for $D_0(CH_3S^+\text{-}CH_3)$, the formation of $CH_3SCH_2^+$ + H from $CH_3SCH_3^+$ was not observed. The observation of reaction (5) can be attributed to the more efficient translational to vibrational energy transfer for the C-S stretching modes than the C-H stretching modes. The negligible yield of $CH_3SCH_2^+$ may be the result of the weak coupling between the low frequency C-S and high frequency C-H stretching modes of $CH_3SCH_3^+$. Thus, the results of this experiment are consistent with the physical picture gained in the previous total cross section measurements for the $CH_3SH^+$ ($CH_3CH_2SH^+$) + Ar reactions.[1,2,8] The difference in product ions and isomer structures for the mass 47 ions resulting from the CID of $CH_3CH_2SH^+$ and those of $CH_3SCH_3^+$ observed here strongly suggests that the CID processes for these ions are

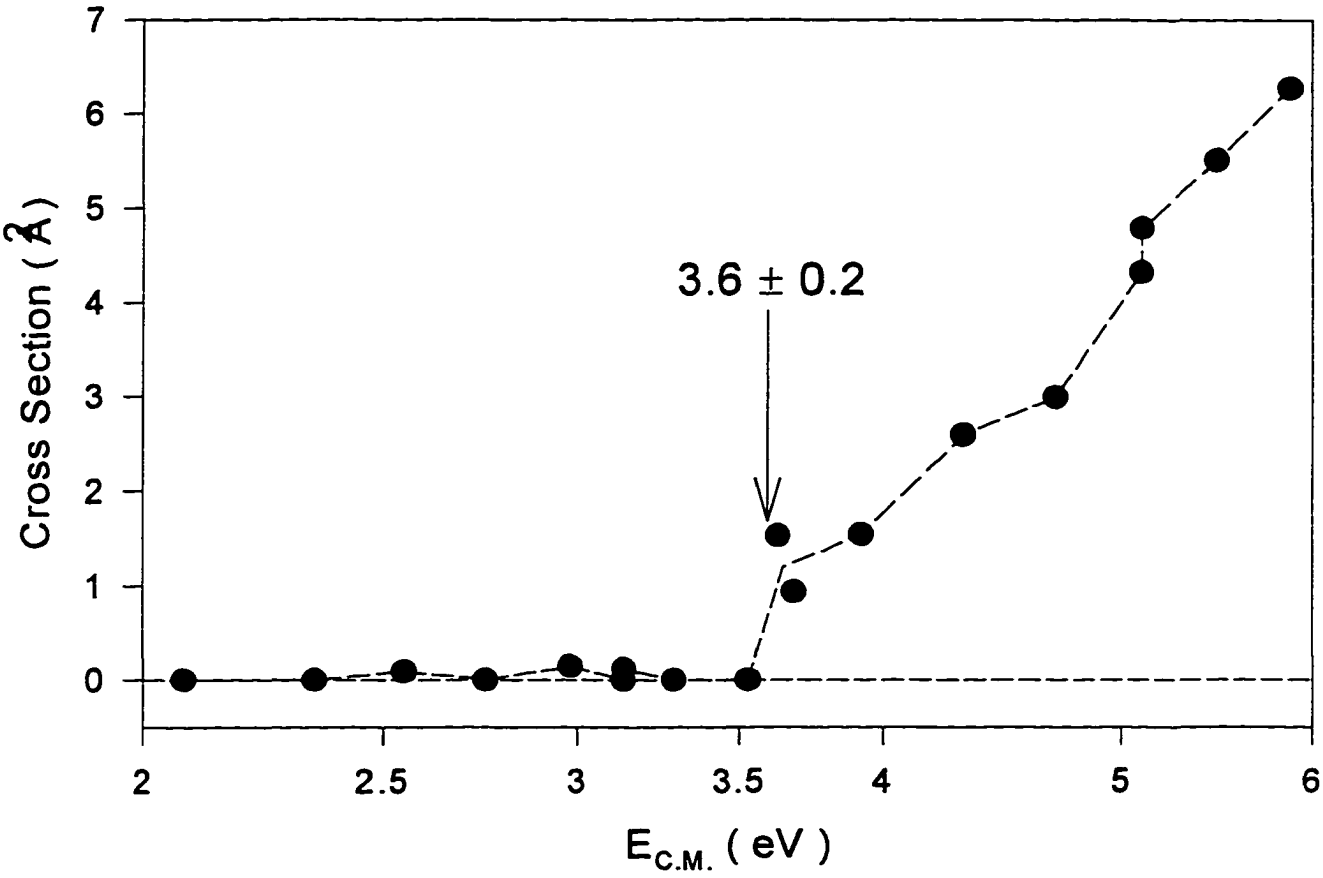


Fig.1(b) Absolute cross section for $C_6H_6^+$ (●) formed in the charge transfer reaction of benzene and the mass 47 ion at a fixed $E_{c.m.}$ of 0.2 eV. The mass 47 ions are formed in the CID reaction of $CH_3SCH_3^+$ + Ar in the $E_{c.m.}$ range of 2-6 eV. We note that the $E_{c.m.}$ onset at 3.6 ± 0.2 eV is in excellent agreement with the threshold of 3.75 eV for reaction(5).

non-statistical. Furthermore, this experiment demonstrates that the charge transfer probing technique is a promising method for the structural identification of isomeric ions formed in dissociation reactions induced by collisional activation or photoionization.

**References**


1. Y.-J. Chen, P. T. Fenn, S. Stimson, and C. Y. Ng, J. Chem. Phys., in press;
2. P. T. Fenn, S. Stimson, Y.-J. Chen, and C. Y. Ng, J. Phys. Chem., submitted.
3. C. Y. Ng, in "The Structure, Energetics, and Dynamics of Organic ions", edited by T. Baer, C. Y. Ng, and I. Powis, Wiley Series in Ion Chemistry and Physics (Wiley, Chichester, (1996), Chap. 2, p.35.
4. M. E. Akopyan, Y. L. Serhiev, and F. I. Vilesov, Klim. Vys. Energy 4, 305 (1970).
5. R. E. Kutina, A. K. Edwards, J. Berkowitz, J. Chem. Phys. 77, 5508 (1982).
6. S. Nourbakhsh, K. Norwood, H.-M. Yin, C.-L. Liao, and C. Y. Ng, J. Chem. Phys. 95, 945 (1991).

7 B.-O. Jonsson and J. Lind, J. Chem. Soc. Faraday Trans. 2 70, 1399 (1974).

8 Y.-J. Chen, P. T. Fenn, S. Stimson, C. Y. Ng, W.-K. Li, and N.-L. Ma, in preparation.

9 C. Y. Ng, in "State-Selected and State-to-State Ion-Molecule Reaction Dynamics: I. Experiment", edited by C. Y. Ng and M. Baer (Wiley, New York, 1992), Adv. Chem. Phys. 82, p.401-500.

10. X. Li, Y.-L. Huang, G. J. Flesch, and C. Y. Ng, Rev. Sci. Instrum. 65, 3724 (1994), ibid.66,2871(1995).
11. Y.-S. Cheung, C.-W. Hsu, J.-C. Huang, C. Y. Ng, W. K. Li, and S.-W. Chiu, Int. J.

Mass Spectrom. Ion Proc. 159, 13 (1996).

12 Y.-S. Cheung, J.-C. Huang, and C. Y. Ng, J. Chem. Phys., in preparation.

13. B. Ruscic and J. Berkowitz, J. Chem. Phys. 97, 1818 (1992)

14. S. Nourbakhsh, K. Norwood, G.-Z. He, and C. Y. Ng, J. Am. Chem. Soc. 113, 6311(199).

15. C.-W. Hsu and C. Y. Ng, J. Chem. Phys. 101, 5596 (1994).

16. R. G. Neuhauser, K. Siglow, and H. 3. Neusser, J. Chem. Phys. 106, 896 (1997).

# V: A STUDY OF THE DISSOCIATION OF $C_2H_5SH^+$ BY COLLISIONAL ACTIVATION: EVIDENCE OF NON-STATISTICAL BEHAVIOR

A manuscript prepared for submission to the Journal of Chemical Physics

Y. J. Chen, P. T. Fenn, S. Stimson, W. K. Li, S.-W Chiu and C. Y. Ng

**Abstract**

The absolute cross sections for $C_2H_5^+$, $C_2H_4^+$, $C_2H_3^+$, $CH_3^+$, $CH_2SH^+$, $CH_2S^+$ , $CHS^+$ and $H_2S^+$ produced by the collision-induced dissociation (CID) reaction of $CH_3CH_2SH^+$ + Ar have been measured in the center of mass collision energy range of 1-37 eV. The thresholds for the formation of $C_2H_5^+$, $C_2H_4^+$, $C_2H_3^+$, $CH_2SH^+$, and $H_2S^+$ are consistent with the corresponding thermochemical thresholds, while the thresholds for the formation of the other ion are higher than the thermochemical thresholds. The dominance of the $C_2H_5^+$ ion formed in the CID reaction shows that the dissociation of $CH_3CH_2SH^+$ strongly favors the C-S bond scission process, even though the formation of $C_2H_5^+$ + SH is not among the most stable product channels . This observation suggests that the collision-induced dissociation of $CH_3CH_2SH^+$ is contrary to a statistical model. The high yield of $C_2H_5^+$ + SH and $CH_2SH^+$ + $CH_3$ observed in CID can be attributed to the more efficient translational to vibrational energy transfer for the C-S stretch than for C-H stretches of $CH_3CH_2SH^+$ , weak couplings between the low frequency C-S and high frequency C-H stretching vibrational modes of $CH_3CH_2SH^+$ , and better coupling of C-C and C-S stretching vibrational modes of $CH_3CH_2SH^+$ . The different fragment ions and relative abundances observed in photoionization experiments are

attributed to the different excitation schemes used in photoionization and collision-induced dissociation.

**Introduction**

Industrial organosulfur pollutants are emitted into the atmosphere from the incomplete combustion of coal and oil.[1] These sulfur compounds are usually serving intermediate and then oxidized in the atmosphere. In order to study the energy transfer dynamics and to identify the major dissociation product channels of organsulfur compounds, we have previously carried out a collision-induced dissociation (CID) studies of $CH_3SH$. By comparing the results observed in CID reaction of $CH_3SH^+$ + Ar , photoionization, and charge exchange experiments, those differences in the dissociation product ions and product ion relative abundances reveal the fundamental aspects of the CID mechanism.[2] The breakdown diagrams of $CH_3SH^+$ obtained from photoionization[3] and charge exchange[4] agree qualitatively with the quasiquilibrium theory (QET). The reactant ion $CH_3SH^+$ can be readily formed in excited electronic state when prepared by photoionization or charge exchange, and the agreement between experiment and QET indicates that the couplings between the electronic excited states and the dissociating degrees of freedom of $CH_3SH^+$ are good, resulting in efficient energy flow between the electronic and vibrational modes of $CH_3SH^+$. On the other hand, low energy collisional activation mainly involves translational to rotational and vibrational energy transfer in the ground potential energy surface of $CH_3SH^+$. At very low collision energies, collisional activation should be equivalent to thermal excitation. Considering that translational to electronic energy transfer is inefficient at the energy range we are concerned with, it is

highly questionable whether collisional activation at low collision energies will access excited electronic states from the ground electronic energy surface of $CH_3SH^+$. If the region of phase space available to collisional activation is different from that available to charge exchange and photoionization, the branching ratios for the dissociation product channels observed in CID should be different from those formed in the other modes of excitation. In other words, the mechanism for CID of $CH_3SH^+$ may not be statistical in nature. Motivated by the striking results from our previous study of CID reaction of $CH_3SH^+$ + Ar, we further investigate a larger system with an extra C-C bond, the dissociation of $CH_3CH_2SH^+$ +by collision activation. Photoionization mass spectrometry has a well-known reputation of providing accurate thermochemical data for molecular and radical ions. In order to compare the differences of excitation scheme between the CID and photoionization, we also carried out the vacuum ultraviolet photodissociation mass spectrometric study of $CH_3CH_2SH$. In this article, we present the results and comparison on both experiments. The structure of mass 47 product ion formed in CID reaction and photoionization is also probed by using charge exchange probing method.

The reactant ion $CH_3CH_2SH^+$ in the present CID experiment is prepared by photoionization of $CH_3CH_2SH$ in the threshold region. By using a sufficiently high photon energy resolution, the reactant ion $CH_3CH_2SH^+$ is formed in its ground vibronic state. The $CH_3CH_2SH$ sample is introduced by supersonic expansion into the photoionization ion source, so the ion beam should be rotationally cold. The supersonic expansion and efficient rotational cooling can assure that there is no internal energy involved in the reactant ion prior to collisional activation.

On the basis of the self-consistent-field molecular orbital calculation using the 4-31G basis set,[5] the main electronic configuration for $CH_3CH_2SH$ is predicted to be

$$....(11a')^2(3a'')^2(12a')^2(13a')^2(4a'')^2.$$

The 4a″ orbital is a nonbonding orbital ($n_S$) localized at the S atom. The 13a′ and 12a′ orbitals are σ-bonding in character and are mainly localized along the C-S ($\sigma_{CS}$) and S-H ($\sigma_{HS}$), C-C ($\sigma_{CC}$) bonds, respectively. The first to fifth photoelectron bands observed in previous He I photoelectron spectroscopic studies[18] have been assigned to the removal an electron from the 4a″, 13a′, 12a′, 3a″, and 11a′ orbitals of $CH_3SH^+$. The vertical IEs for these corresponding states are 9.58, 11.87, 13.43, 14.62, and 16.82 eV.[18]

## Experiment

The arrangement of the triple-quadrupole double-octopole (TQDO) photoionization ion-molecule reaction apparatus (Fig. 1) and procedures used to perform state-selected absolute total cross section measurements have been described in detail previously.[6-9] The TQDO apparatus essentially consists of, in sequential order, a vacuum ultraviolet (VUV) photoionization ion source, an electron impact ion source (1), a reactant quadrupole mass spectrometer (QMS) (5), a lower radio frequency (RF) octopole ion guide reaction gas cell (RFOIGGC) [(6) + (7)], a middle QMS (10), an upper RFOIGGC [(11) + (14)], a product QMS (15), and a modified[10] Daly-type scintillation ion detector [(17) + (19) + (20)]. The electron impact ion source is not used in this experiment. The TQDO apparatus is partitioned into five chambers which are separately evacuated by liquid nitrogen- or freon-trapped diffusion pumps.

Figure 1 Schematic diagram of the TQDO apparatus. (1) Photoionization ion source, (2) atomic or molecular nozzle beam, (3) to freon-trapped 6" diffusion pump (DP), (4) to liquid-nitrogen ($LN_2$)-trapped 6" DP, (5) reactant QMS, (6) lower RF octopole ion guide, (7) lower RFOIGGC, (8) to $LN_2$-trapped 6" DP, (9) the lower RF octopole ion guide chamber, (10) middle QMS, (11) upper RF octopole ion guide, (12) to $LN_2$-trapped 4" DP, (13) upper RF octopole ion guide chamber, (14) upper RFOIGGC, (15) product QMS, (16) detector chamber, (17) plastic scintillator window, (18) to $LN_2$-trapped 2" DP, (19) photomultiplier tube, (20) aluminum ion target.

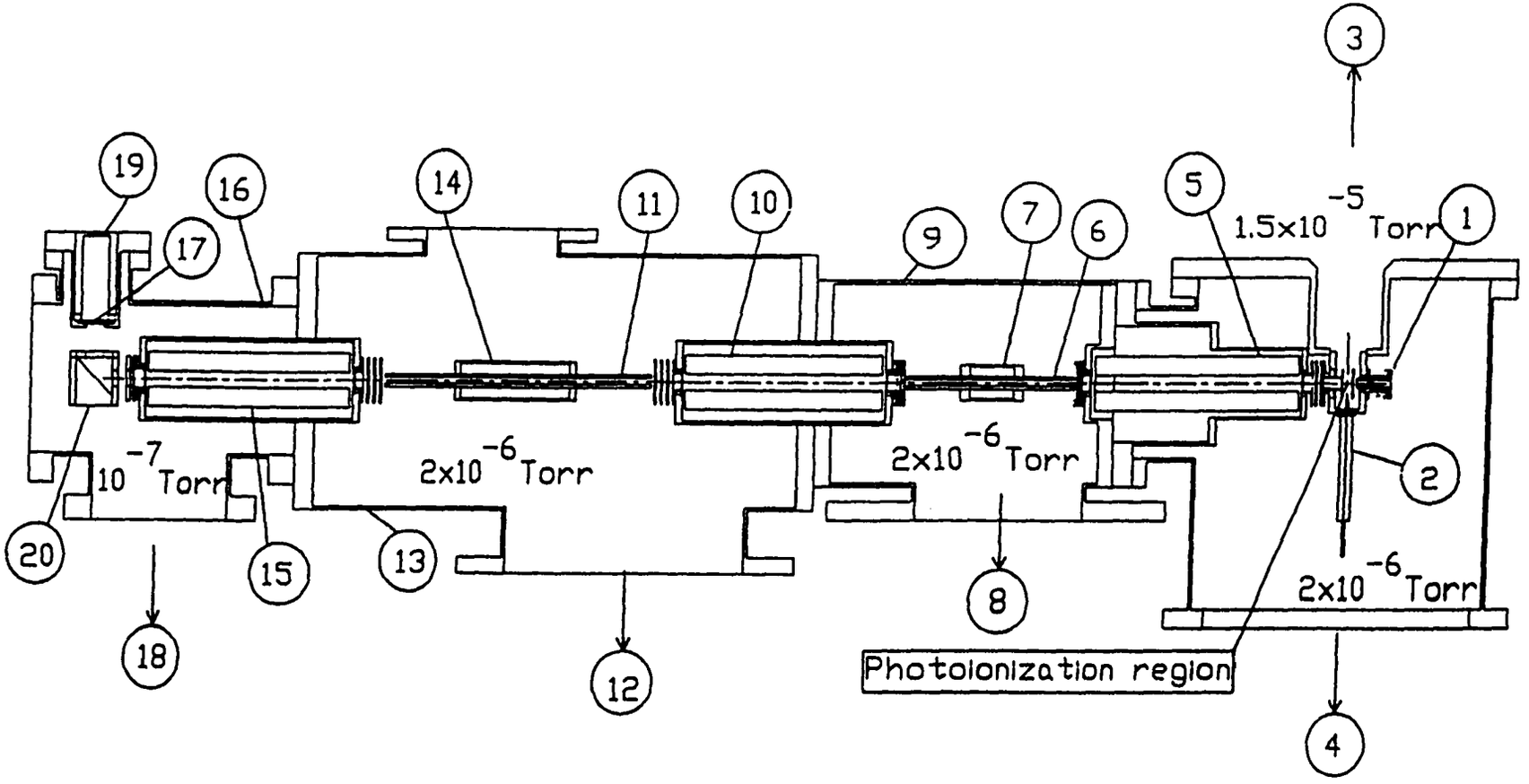
3
19
16
14
11
10
9
7
6
5
1.5x10 -5 Torr
1
17
10 -7 Torr
2x10 -6 Torr
2x10 -6 Torr
2
20
15
13
8
2x10 -6 Torr
18
12
Photoionization region
4

The photoionization ion source consists of a 0.2 m VUV monochromator (McPherson 234), a hydrogen discharge lamp and a photoelectric VUV light detector. The recent high resolution non-resonant two-photon pulsed field ionization photoelectron (N2P-PFI-PE) study of $CH_3CH_2SH$ near the ionization threshold yields a value of 9.2927±0.0006 eV (1334±0.08 Å) for the ionization energy (IE) of $CH_3CH_2SH$.[11] The N2P-PFI-PE spectrum also reveals a vibrational progression corresponding to excitation of the C-S stretching mode ($\nu_4^+$=628 $cm^{-1}$) of $CH_3CH_2SH^+$.[11] Ethanethiol is introduced into the photoionization source as a free jet formed by supersonic expansion through a nozzle with a diameter of 75 μm at a stagnation pressure of ≈120 Torr. By setting the photoionization wavelength at 1333 Å and a wavelength resolution of 6 Å [full-width-at-half-maximum (FWHM)], the $CH_3CH_2SH^+$ reactant ions were formed in their ground vibronic states. The rotational temperature of $CH_3CH_2SH^+$ thus formed is expected to be ≤150 K, characteristic of the neutral $CH_3CH_2SH$ jet.

For absolute total cross section measurements, the reactant $CH_3CH_2SH^+$ ions were extracted and guided by the lower QMS (operated in the RF only mode) and the lower RF octopole ion guide to the middle QMS. The middle QMS, functioning as a mass filter, passed only the desired $CH_3CH_2SH^+$ ions to the upper RFOIGGC, where collision-activated dissociation occurred with Ar. The pressure of Ar in the upper RFOIGGC was monitored with an MKS Baratron manometer, and maintained at 2-3x$10^{-4}$ Torr. In this pressure range, the CID product ion intensity was found to have a linear dependence on the Ar gas cell pressure. The reactant ions and the product ions formed in the upper RFOIGGC were then mass selected by the product QMS and detected with the modified Daly-type scintillation ion detector.

The reactant ion beam energies were determined by the retarding potential method, using the upper octopole ion guide to retard the reactant $CH_3CH_2SH^+$ ions. The retarding potential curve thus obtained was differentiated to yield the most probable laboratory kinetic energy ($E_{lab}$) of the reactant ions and the FWHM of the kinetic energy distribution. The $E_{lab}$ resolution for $CH_3CH_2SH^+$ achieved in this experiment was in the range of ±0.2 eV. The collection efficiencies for reactant and product ions were maximized at each center-of-mass collision energy ($E_{c.m.}$) by optimizing the DC voltage settings applied to the ion lenses, the octopole ion guides, and the QMS's.

To probe the structure of the mass 47 ions formed in the CID reaction of $CH_3CH_2SH^+$ + Ar, we used both the lower and upper RFOIGGCs. Reactant $CH_3CH_2SH^+$ ions prepared by photoionization of $CH_3CH_2SH$ were first selected by the reactant QMS to enter the lower RFOIGGC, where the CID reaction $CH_3CH_2SH^+$ + Ar took place. The Ar gas cell pressure used was $5x10^{-4}$ Torr. The mass 47 product ions thus formed in the $E_{c.m.}$ range of 4.5-6.5 eV were selected by the middle QMS and guided into the upper RFOIGGC, in which the structure for the mass 47 ions was probed by the charge transfer reaction with benzene ($C_6H_6$) at $E_{c.m.} \leq 2$ eV. Charge transfer product $C_6H_6^+$ ions, if formed, were detected by the product QMS. The $C_6H_6$ pressure used in the upper gas cell was $3x10^{-4}$ Torr. The IEs for $CH_3S$, $CH_2SH$, and $C_6H_6$ are known to be 9.2649±0.0010 eV[12], 7.536±0.003 eV[13], and 9.243842±0.000006 eV[14], respectively (see Table I). Using these IE values, we calculated that the charge transfer reaction (1) for $CH_3S^+$ is slightly exothermic by 0.0211eV, whereas the charge transfer reaction (2) for $CH_2SH^+$ is endothermic by more than 1.7 eV. The $\Delta H^\circ_0$ values given in reactions (1) and (2) are the corresponding heats of reaction at 0 K.

$$CH_3S^+ + C_6H_6 \rightarrow CH_3S + C_6H_6^+ \qquad \Delta H°_0 = -0.0211 \text{ eV} \qquad (1)$$

$$CH_2SH^+ + C_6H_6 \rightarrow CH_2SH + C_6H_6^+ \qquad \Delta H°_0 = 1.708 \text{ eV} \qquad (2)$$

Because near-resonant charge transfer reactions usually have large cross sections, we should observe the formation of $C_6H_6^+$ if the mass 47 ions have the $CH_3S^+$ structure, while the charge transfer cross section should be negligibly small if $CH_2SH^+$ ions are produced in the CID reaction of $CH_3CH_2SH^+ + Ar$.

It is known that $CH_2SH^+$ ions are produced at the onset by photoionization of $CH_3SH$.[4,15,16] This conclusion is based on the fact that the thermochemical threshold of $\Delta H°_0$ = 11.541 eV for process (3) is very close to the appearance energy (AE) of ≈11.55 eV for the mass 47 ion observed in the dissociative photoionization of $CH_3SH$.

$$CH_3SH + h\nu \rightarrow CH_2SH^+ + H + e^-, \qquad \Delta H°_0 = 11.541 \text{ eV} \qquad (3)$$

$CH_3CH_2SH^+$ is an analogous system of $CH_3SH^+$, and we expect the mass 47 ion might have the same $CH_2SH^+$ structure. To test the charge transfer detection scheme, we prepared $CH_2SH^+$ in the photoionization ion source by process (3) at $h\nu < 11.3$ eV, and measured the charge transfer cross section for reaction (2) using the upper RFOIGGC. No $C_6H_6^+$ ions were observed, indicating that $CH_2SH^+$ is indeed produced by process (3) at $h\nu < 11.3$ eV.

The data acquisition for the TQDO apparatus has recently been upgraded to be controlled by a Pentium PC system.[17] This improvement allows computer control of the QMS and monochromator scans, the voltage settings applied to individual components of the ion

optics system, the reactant ion kinetic energy determination, and the background corrections in absolute total cross section measurements. The procedures outlined above were conducted mostly in an automatic mode.

The Ethanethiol and benzene were obtained from Aldrich Chemical Co. and Fisher Scientific with purities of 99.5% and 99.9%, respectively. The Ar gas is from Air Products and has a purity of 99.998%.

## Results and Discussion

### A. Absolute total cross section and identification of CID product channels

Fig. 2 depicts the mass spectrum observed for the CID reaction of $C_2H_5SH^+$ + Ar at $E_{c.m.}$= 12 eV by scanning the product quadrupole mass spectrometer, showing that $C_2H_5^+$ and $CH_2SH^+(CH_3S^+)$ are the major product ions. The product ions observed in the CID reaction of $C_2H_5SH^+$ + Ar are $C_2H_5^+$, $C_2H_4^+$, $C_2H_3^+$, $CH_3^+$, $CH_2SH^+$, $CH_2S^+$ , $CHS^+$ and $H_2S^+$ . The absolute total cross section for these product ions in the $E_{c.m.}$ range of 1-37 eV are plotted in Fig. 3(a). The cross section curves for $CH_3^+$ and $CH_2SH^+$ have similar $E_{c.m.}$ dependence and exhibit a maximum at $E_{c.m.}$ = 3-5 eV. The maximum cross section for $C_2H_5^+$ is about 5 $Å^2$ , which is more than 3 times higher than the maximum cross section of 1.5 $Å^2$ for $CH_2SH^+(CH_3S^+)$. The cross section curve of $C_2H_3^+$ starts to compete with $C_2H_5^+$ and $CH_2SH^+(CH_3S^+)$ after $E_{c.m.}$ =8 eV, and these cross-sections curves are approaching the same magnitude at the highest energy we studied. A magnified view of the cross section curves for the minor product ions, all of which have cross section < 1 $Å^2$, are depicted in Fig. 3(b) and 3(c).

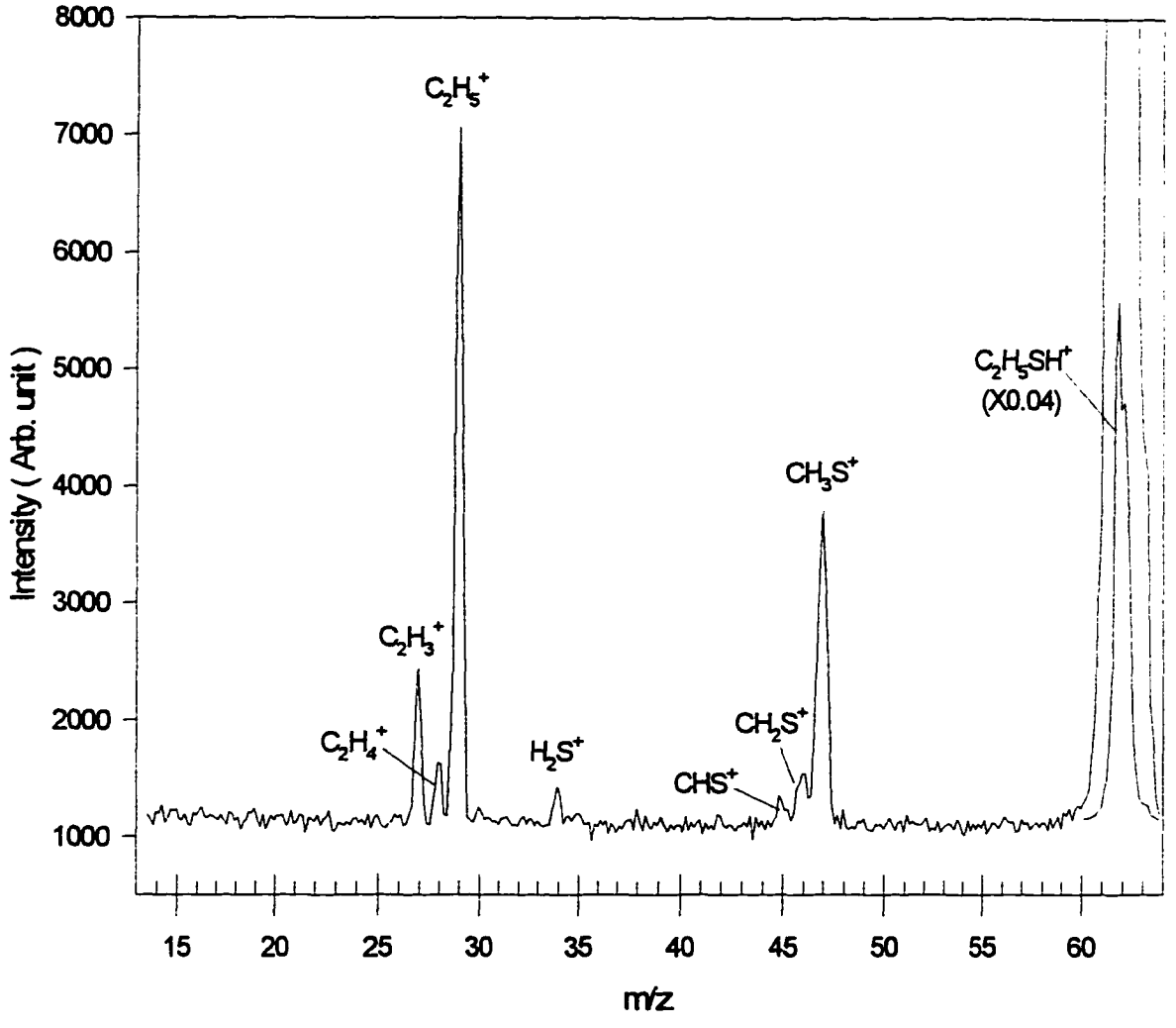


Fig.2 Mass Spectrum in the mass range of m/e = 13-63 amu for the CID reaction of $C_2H_5SH^+$ + Ar obtained at $E_{c.m.}$ = 12 eV. The mass peak of m/e = 62 amu has been scaled by a factor of 0.04. The mass peak (m/e = 61 amu) corresponding to $CH_3CHSH^+$ formed by reaction 1is absent in the spectrum

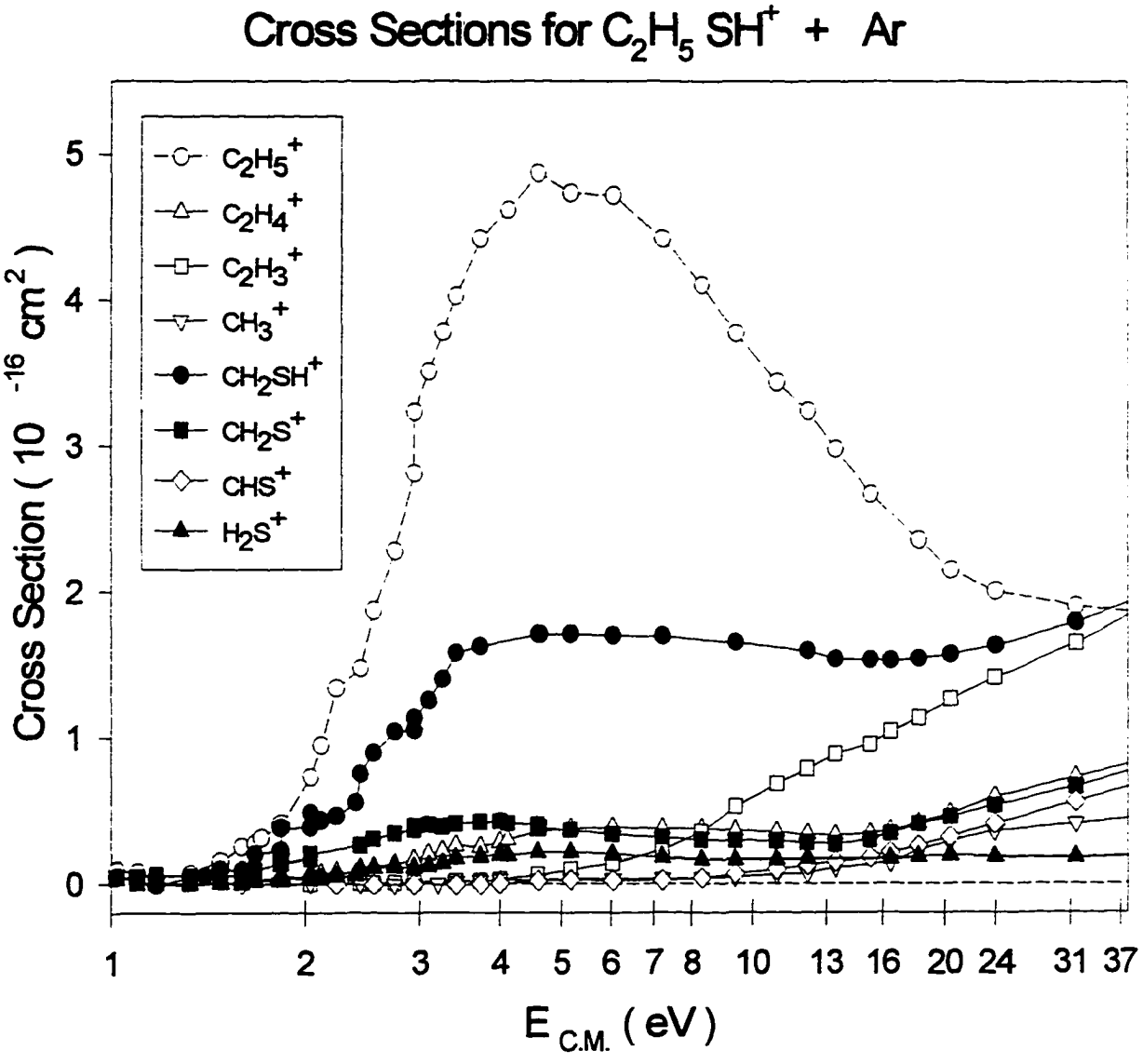


Fig. 3(a) Absolute total cross section curves for $C_2H_5^+$ (○), $C_2H_4^+$ (Δ), $C_2H_3^+$ (□), $CH_3^+$(▽), $CH_2SH^+$ (●), $CH_2S^+$ (■) , $CHS^+$ (◇) and $H_2S^+$ (▲) formed in the CID reaction of $C_2H_5SH^+$ + Ar

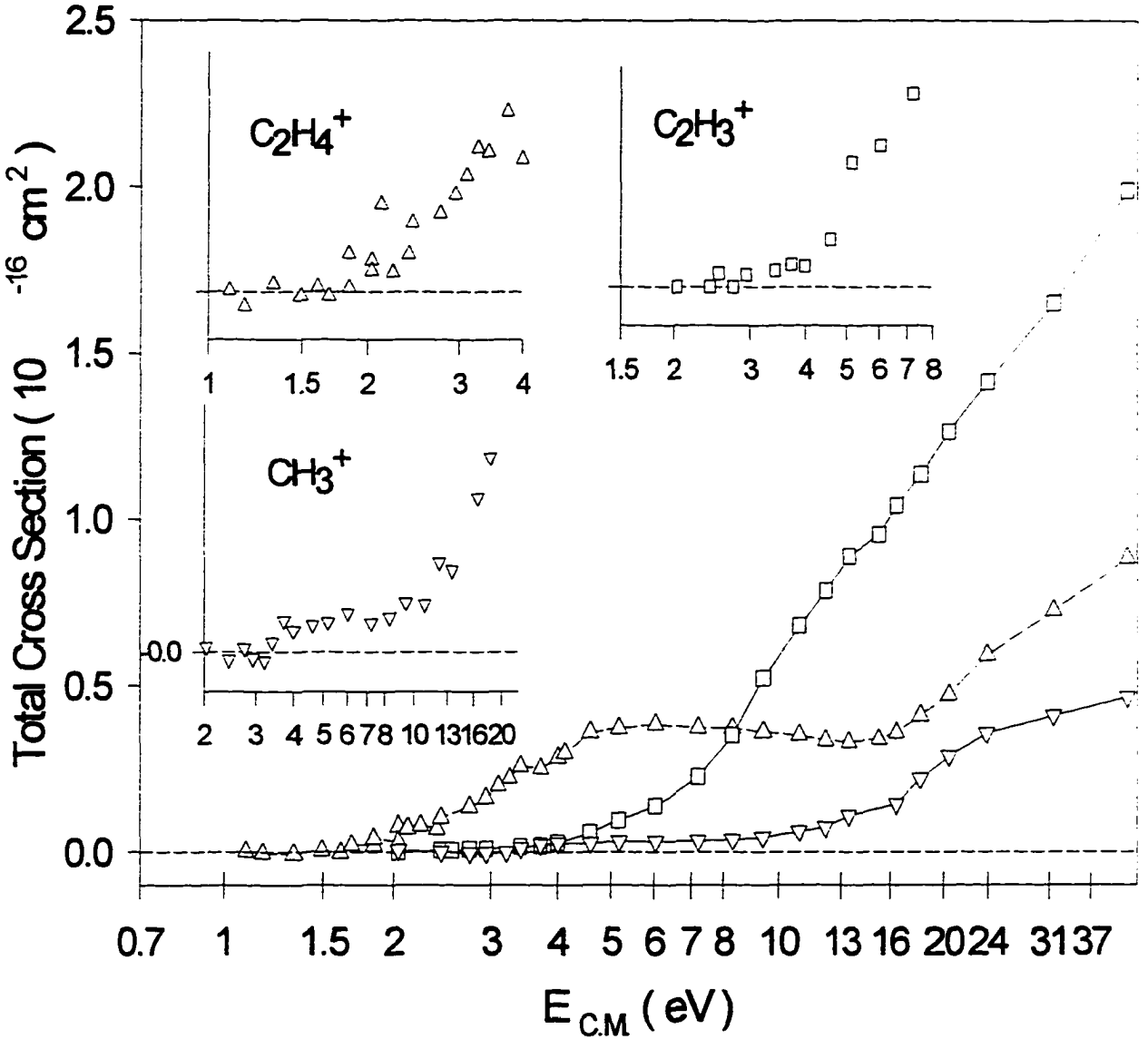


Fig. 3(b) Magnified total cross section curves of $C_2H_4^+$ (Δ), $C_2H_3^+$ (□), $CH_3^+$(∇)

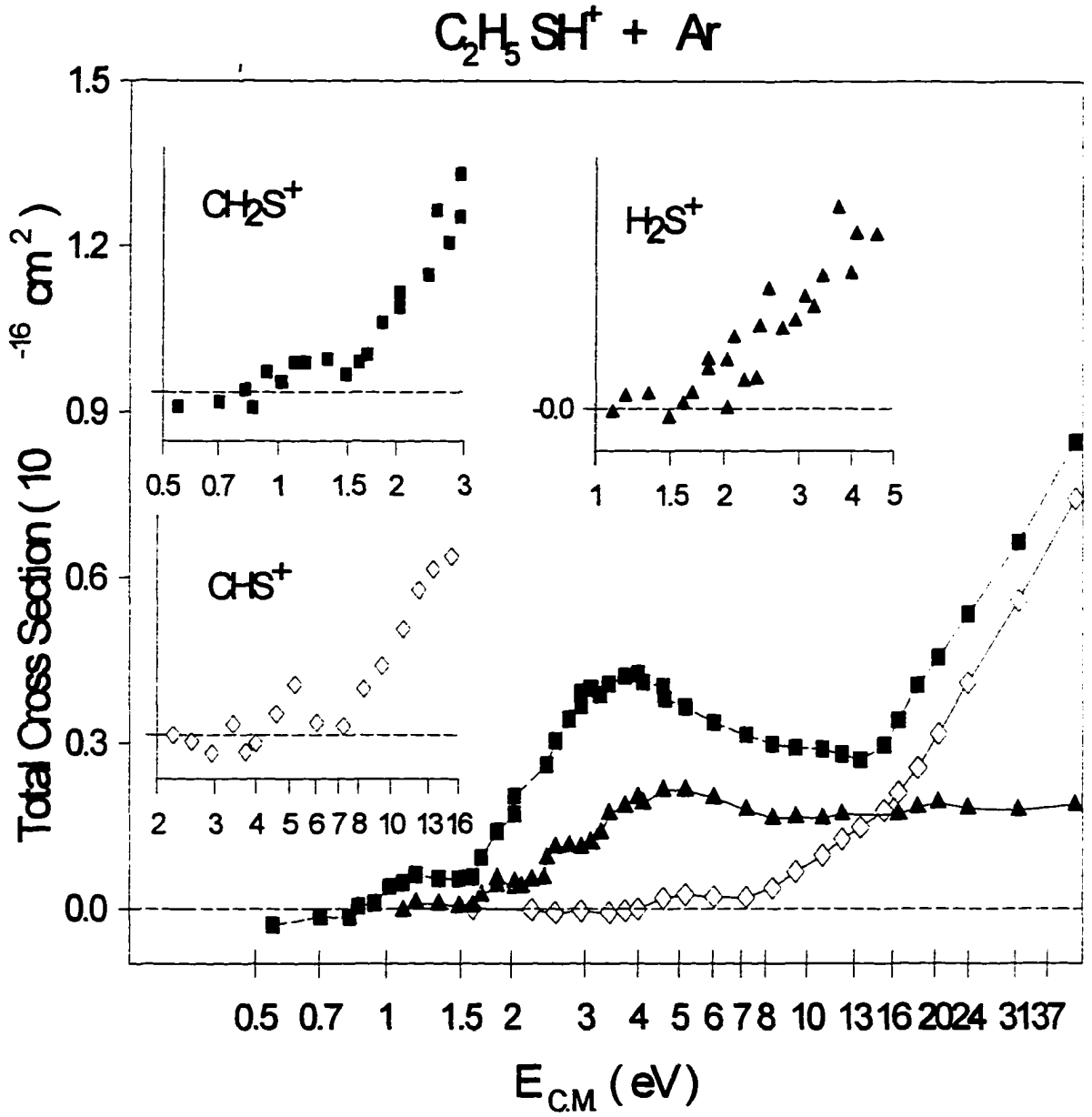


Fig. 3(c) Magnified total cross section curves of $CH_2S^+$ (■) , $CHS^+$ (◊) and $H_2S^+$ (▲)

All of the profiles for the cross section curves of these minor product ions are similar, i.e., they increase very slowly from their onset as $E_{c.m.}$ increases.Using the thermochemical data listed in Table 1, we have calculated the corresponding $\Delta H^{\circ}_0$ values for the reactions possibly responsible for the CID product ions. All atomic and molecular species in the following reactions are assumed to be in their ground states.

$CH_3CH_2SH^+ + Ar \rightarrow CH_3CHSH^+ + H + Ar$ $\Delta H^{\circ}_0 = 1.47$ eV 1

$\rightarrow CH_3CH_2^+ + SH + Ar$ $\Delta H^{\circ}_0 = 1.96$ eV 2

$\rightarrow CH_2CH_2^+ + H_2S + Ar$ $\Delta H^{\circ}_0 = 1.97$ eV 3(a)

$\rightarrow CH_2CH_2^+ + SH + H + Ar$ $\Delta H^{\circ}_0 = 5.87$ eV 3(b)

$\rightarrow CH_3CH^+ + H_2S + Ar$ $\Delta H^{\circ}_0 = 3.11$ eV 3(c)

$\rightarrow C_2H_3^+ + H_2 + SH + Ar$ $\Delta H^{\circ}_0 = 4.28$ eV 4(a)

$\rightarrow C_2H_3^+ + H_2S + H + Ar$ $\Delta H^{\circ}_0 = 4.87$ eV 4(b)

$\rightarrow CH_3^+ + CH_2SH + Ar$ $\Delta H^{\circ}_0 = 4.03$ eV 5(a)

$\rightarrow CH_3^+ + CH_3S + Ar$ $\Delta H^{\circ}_0 = 5.5$ eV 5(b)

$\rightarrow CH_3^+ + CH_2 + SH + Ar$ $\Delta H^{\circ}_0 = 7.91$ eV 5(c)

$\rightarrow CH_2SH^+ + CH_3 + Ar$ $\Delta H^{\circ}_0 = 1.73$ eV 6(a)

**Table I.** Current recommended experimental $\Delta_f H°_0$ and IE values for $CH_3CH_2SH$, $CH_3CH_2S$, $CH_2SH$, $CH_3S$, $CH_2S$, CHS, $CH_3$, $CH_2$, $CH_3CH_2$, $CH_2CH_2$, $C_2H_3$, $CH_3CH_2SH^+$, $CH_3CH_2S$, $CH_3CHSH^+$, $CH_3SH^+$, $CH_2SH_2^+$, $CH_2SH^+$, $CH3S^+$, $CH_2S^+$, $HCSH^+$, $CHS^+$, $CSH^+$, $CH_3^+$, and $CH_2^+$.[a]

| Species | $\Delta_f H°_0$ (Kcal/mol) | IE ( eV) |
|---|---|---|
| Neutrals | | |
| gauche-$C_2H_5SH$ | -7.1[a] | 9.2927±0.0006[a] |
| trans-$C_2H_5SH$ | -6.6[a] | --- |
| $CH_3SCH_3$ | 34±2.5[d] | 8.640±0.02[d] check |
| $CH_3CH_2S$ | 27.5[b] | 8.97±0.01[c] |
| $CH_2SH$ | 37.7±2.0[c] | 7.536±0.003[c] |
| $CH_3S$ | 31.4±0.5[c] | 9.2649±0.0010[c] |
| | | 9.2330±0.0010[c] |
| $CH_2S$ | 28.3±2.0[c] | 9.376±0.003[c] |
| HCS | 71.7±2.0[c] | 7.412±0.007[c] |
| CSH | ---- | ---- |
| $H_2S$ | -4.2±0.2 | 10.4682±0.0002[c] |
| SH | 34.0±0.6 | 10.4218±0.0004[c] |
| $CH_3CH_2$ | 28 | check |
| $CH_2CH_2$ | 14.5 | check |
| $CH_3$ | 35.6 ± 0.3 | 9.8380 ± 0.0004[l] |
| $CH_2$ | 93 | 10.396 ± 0.003 |
| H | 51.63 | 13.598 |
| | | |
| Cations | | |
| gauche-$C_2H_5SH^+$ | 207.3[a] | |
| trans-$C_2H_5SH^+$ | 207.4[a] | |
| $CH_3SCH_3^+$ | 194.1[d] | |
| $CH_3CHSH_2^+$ | 220.1[b] | |
| $CH_2CH_2SH_2^+$ | 220.0[b] | |
| $CH_3CH_2S^+$ | 236.5[d] | |
| $CH_2SH^+$ | 211.5±2.0[c] | |
| $CH_3S^+$ | 245.0±0.5[c] | |
| $CH_2S^+$ | 244.5±2.0[c] | |
| trans-$HCSH^+$ | 275[b] | |
| cis-$HCSH^+$ | 277[b] | |
| $HCS^+$ | 243.2±2.9[c] | |
| $CSH^+$ | 314.6[c] | |
| $H_2S^+$ | 237.2±0.2[c] | |

Table I (continued)

| | |
|---|---|
| $SH^+$ | 274.3±0.6[c] |
| $CH_3CH_2^+$ | 218.5±1 |
| $CH_3CH^+$ | 283.2[b] |
| $CH_2CH_2^+$ | 256.8 |
| bridged-$CH_2CH^+$ | 267.8[b] |
| nonbridged- $CH_2CH^+$ | 272.2[b] |
| $CH_3^+$ | 262.5 ± 0.3 |
| $CH_2^+$ | 332 |

References


a. Reference 11

b. G2 calculation

c. Reference 2

d. Reference 31

e. Reference 32


$$CH_3CH_2SH^+ + Ar \rightarrow CH_3S^+ + CH_3 + Ar \qquad \Delta H^\circ_0 = 3.18 \text{ eV} \qquad 6(b)$$

$$\rightarrow CH_2S^+ + CH_4 + Ar \qquad \Delta H^\circ_0 = 0.92 \text{ eV} \qquad 7(a)$$

$$\rightarrow CH_2S^+ + CH_3 + H + Ar \qquad \Delta H^\circ_0 = 5.40 \text{ eV} \qquad 7(b)$$

$$\rightarrow CHS^+ + CH_3 + H_2 + Ar \qquad \Delta H^\circ_0 = 3.1 \text{ eV} \qquad 8(a)$$

$$\rightarrow CHS^+ + CH_3 + 2H + Ar \qquad \Delta H^\circ_0 = 7.59 \text{ eV} \qquad 8(b)$$

$$\rightarrow CHS^+ + CH_4 + H + Ar \qquad \Delta H^\circ_0 = 4.57 \text{ eV} \qquad 8(c)$$

$$\rightarrow H_2S^+ + CH_2CH_2 + Ar \qquad \Delta H^\circ_0 = 1.93\ eV \qquad 9$$

One of the most important pieces of information obtained in a low energy CID study, such as this, is the AEs of the product ions, from which upper limits of the bond dissociation energies involved can be calculated. By comparison of the observed AE(CID) values for product ions with their corresponding thermochemical thresholds, the conclusion can be drawn about identifying the structure of product ions or the relative probability of a specific dissociation channels in a unimolecular dissociation of large polyatomic molecule. Table II lists the AE(CID) values for $C_2H_5^+$, $C_2H_4^+$, $C_2H_3^+$, $CH_3^+$, $CH_2SH^+$, $CH_2S^+$ , $CHS^+$ and $H_2S^+$ determined from the cross-section curves. Below these AE(CID) values, the intensities for the corresponding product ions are at the background level. These AE(CID) values represent upper limits for the true thermochemical thresholds of the processes involved. Using a semiempirical expression[18,19] for the cross-section ,

$$\sigma = \sigma_0 \frac{(E_{c.m.} - E_0)^n}{E_{c.m.}}$$

where $\sigma_0$ , $E_0$ and n are adjustable parameters, we have fitted the absolute cross-section data for the CID product ions near their onsets. This general form has been derived as a model for translationally driven reactions and has been applied to obtain accurate thermochemistry.[20] The best fit values for these parameters are also listed in Table II.

Figs. 3(a), 3(b) and 3(c) show the absolute total cross section curves of those product ion formed in CID reactions of $CH_3CH_2SH^+$ + Ar. The AE(CID) values for those product ions determined from the cross section curves are listed in Table II. In a photoionization (PI)

**Table II.** Appearance energies determined in CID and photoionization, and parameters [($E_0$, $\sigma_0$, and n, see Eq. (12)] for the fittings of the CID cross sections for $C_2H_5^+$, $C_2H_4^+$, $C_2H_3^+$, $CH_2SH^+$ ($CH_3S^+$), $CH_2S^+$, $CHS^+$, $CH_3^+$, and $H_2S^+$ near their onsets.

| Product Ions | AE(CID)[a] (eV) | $E_0$[b] (eV) | $\sigma_0$ ($Å^2$) | n | Δ (PI)[c] (eV) |
|---|---|---|---|---|---|
| $CH_3CHSH^+$ | ---- | ---- | ---- | ---- | 1.47 ± .06 |
| $C_2H_5^+$ | 1.9 ± 0.2 | 1.79 | 7.33 | 1.24 | 2.0 ± 0.06 |
| $C_2H_4^+$ | 1.9 ± 0.2 | 1.58 | 0.3 | 1.4 | 2.0 ± 0.06 |
| $C_2H_3^+$ | 4.0 - 4.6 | 5.88 | 1.2 | 1.0 | ---- |
| $CH_2SH^+/CH_3S^+$ | 1.7 ± 0.2 | 1.2 | 1.5 | 1.7 | 1.42 ± 0.06 |
| | | | | | 1.73 ± 0.06 |
| $CH_2S^+$ | 1.3 ± 0.2 | 1.36 | 0.58 | 1.21 | 1.42 ± 0.06 |
| $CHS^+$ | 7.2 - 8.3 | 6.96 | 0.23 | 1.13 | ---- |
| $CH_3^+$ | 3.8 ± 0.2 | 3.3 | | | ---- |
| | 8.4 - 9.4 | | | | |
| $H_2S^+$ | 1.8 ± 0.2 | 1.4 | 0.2 | 1.5 | 1.93 ± 0.06 |

a) This work. Appearance energy determined in the CID study of $CH_3SH^+(1^2A'') + Ar$. The uncertainties represent the precision of the measurements. The uncertainties for $CH_2S^+$, $HCS^+$, $HS^+$, $CH_2^+$ are shown by the energy ranges given in the table.

b) See Eq. (12). $E_0$ is the onset or AE of the process involved.

c) Appearance energy AE(PI) determined in photoionization mass spectrometric studies of $CH_3SH$. Δ (PI) = AE(PI) - IE($CH_3SH$).

d) Reference 20.

e) Reference 22.

Table II (continued)

f) Reference 19.

experiment, the product ions are produced by unimolecular dissociation from parent ions which have been prepared from excitation of neutral ground state to electronic excited states. In order to get insight into the consequences of the different excitation scheme, the photoionization threshold Δ(PI) values are also listed in table II for comparison with AE(CID) values. For the purpose of comparison, the Δ(PI) values are obtained by subtracting IE($CH_3CH_2SH$) from the appearance potential AP(PI) determined from the photoionization efficiency curves in Figs. 4(a) and 4(b). A detailed description of the photoionization spectra for individual fragment ions will be given in the next section.

As pointed out in the previous CID study of $CH_3SH^+$ + Ar, the threshold of the $CH_3^+$ ion, resulting from cleavage of C-S bond, has a very sharp onset, indicating formation by a direct dissociation from the $CH_3SH^+$. The $C_2H_5^+$ ion, formed in the CID reaction of $CH_3CH_2SH^+$ + Ar also has a relatively sharp threshold compared to the other minor product ions, implying that a similar direct breakage of the C-S bond is contributing to the production of $C_2H_5^+$. This conclusion is consistent with the observation that the AE(CID) value of 1.9 ± 0.2 eV is in excellent agreement with the thermochemical threshold of $\Delta H^\circ_0$ = 1.96 eV for reaction (2).

The AE(CID) value of 1.9 ± 0.2 eV for $C_2H_4^+$ is consistent with the thermochemical threshold $\Delta H^\circ_0$ = 1.97 eV in reaction 3(a) and is significantly lower than that of $\Delta H^\circ_0$ = 3.11 eV from reaction 3(c). So we might conclude that $CH_2CH_2^+$ is the structure accompanied by the formation of $H_2S$. If it is so, the very gradual rising at the threshold region might be due to

the tight cyclic transition state involved in the $H_2S$ elimination process. The possibility of secondary dissociation from $C_2H_5^+$ near the threshold region can be excluded because the thermochemical threshold of $\Delta H^\circ_0$ = 5.87 eV is apparently too high. At high collision energies, the formation of both $CH_2CH_2^+$ and $CH_3CH^+$ are possible and the H-elimination from $C_2H_5^+$ may also contribute to the production of $C_2H_4^+$ ions.

The AE(CID) value determined for the formation of $C_2H_3^+$ is 4.6 ± 0.2 eV, which is slightly higher than the thermochemical threshold of $\Delta H^\circ_0$ = 4.28 eV for reaction 4(a). This observation indicates that $C_2H_3^+ + SH + H_2$ are formed in the $C_2H_3^+$ CID threshold. The thermochemical threshold $\Delta H^\circ_0$ = 4.87 eV for the dissociation channel $C_2H_3^+ + H_2S + H$ is too high to be responsible for the $C_2H_3^+$ threshold. At high $E_{c.m.}$, both $C_2H_5^+$ and $C_2H_4^+$ might be the precursors for $C_2H_3^+$ and the corresponding products formed are from reaction 4(a) and 4(b) respectively. Since the intensity of $C_2H_4^+$ is lower than $C_2H_3^+$ when the collision energy is well above their thresholds, secondary dissociation from $C_2H_4^+$ is unlikely to be a significant route for the formation of $C_2H_3^+$. Another indication that $C_2H_5^+$ may be the precursor of $C_2H_3^+$ is the rapid growth of $C_2H_3^+$ at about $E_{c.m.}$= 7 eV where intensity of $C_2H_5^+$ start to drop.

The AE(CID) value of 1.7 ± 0.2 eV for the mass 47 ion is in excellent agreement with the thermochemical threshold $\Delta H^\circ_0$ = 1.73 eV for reaction 6(a), which indicates that $CH_2SH^+$ is formed near the CID onset for the mass 47 ion. The earlier study[2] suggested a substantial activation energy for the rearrangement of $CH_2SH^+$ to $CH_3S^+$. To ensure the unambiguity about the structure of the mass 47 ion, we have carried out the charge transfer probing experiment using the double RFOIGGC scheme described in the experimental section. On the

basis of the energetics of reaction (1) and (2), we expect to observe $C_6H_6^+$ if mass 47 ion has the $CH_3S^+$ structure, whereas no $C_6H_6^+$ ions should be formed if the mass 47 ion possesses the $CH_2SH^+$ structure. Since no charge transfer product $C_6H_6^+$ ions were observed, we conclude that the mass 47 ions formed in the CID reaction of $C_2H_5SH^+$ + Ar at $E_{c.m.}$ = 1.7 - 5 eV have mostly the $CH_2SH^+$ structure. This observation is analogous to the CID reaction of $CH_3SH^+$ + Ar, where $CH_2SH^+$ is the structure of mass 47 ion near the threshold. These observations are consistent with the *ab initio* prediction that $CH_2SH^+$ isomer is more stable than $CH_3S^+$.[2,21,22]

A very weak onset is observed at AE(CID) = 1.3 ± 0.2 eV for the $CH_2S^+$ ion. Although this value is slightly higher than the thermochemical threshold of $\Delta H^\circ_0$ = 0.92 eV for reaction 7(a), we still conclude that $CH_2S^+ + CH_4$ is formed at the AE(CID) for $CH_2S^+$. The thermochemical threshold of $\Delta H^\circ_0$ = 5.40 eV for reaction 7(b) is significantly too high, indicating that a hydrogen loss from the second most abundant ion $CH_2SH^+$ is not responsible for the formation of $CH_2S^+$ in the threshold region. The formation of other isomers, such as cis-$HCSH^+$, trans-$HCSH^+$ or $CSH_2^+$ , which are estimated[26] to be 1.1, 1.1, and 8.? eV respectively, could be possible at high $E_{c.m.}$ range.

The low intensity and slowly rising threshold, which might be due to the fact that the intermediates are formed in a range of internal energies during sequential decomposition, pose difficulty in determining the AE(CID) for $HCS^+$ ($CSH^+$) ion. The AE(CID) value is determined to be 7.0 ± 0.2 eV by extrapolating the increasing cross section curve to the background level. The formation of $HCS^+$ or $CSH^+$ might be from several different precursors, such as $CH_2SH^+$ or $CH_2S^+$. According to the CID study of $CH_3SH^+$ + Ar, $HCS^+$

is most likely produced by further dissociation of excited $CH_2SH^+$ via $H_2$ elimination. If the formation of $HCS^+$ from the CID reaction of $CH_3CH_2SH^+$ + Ar is analogous to that system, we expect to observed $HCS^+$ in the vicinity of the thermochemical threshold $\Delta H^\circ_0 = 3.1$ eV for reaction 8(a). The AE(CID) for $CHS^+/CSH^+$ value of 7 ± 0.2 eV is apparently much higher than that value. If we assumed that $CH_2S^+$ is the precursor, then the corresponding thermochemical threshold of 4.57 eV for reaction 8(c) to form $CHS^+ + H + CH_4$ is closer to the AE(CID) value of $CHS^+$.

The formation of $CH_3^+$ ion is the weakest channel among all of the products. There is a weak onset or tailing at 3.8 ± 0.2 eV , after which it levels off for several eV above the onset. Near 8 eV, the cross-section curve begins to gradually rise with increasing collision energy. The second rise extrapolates to the level at 9.0 ± 0.2 eV. Based on the thermochemical threshold $\Delta H^\circ_0 = 4.03$ eV for reaction 5(a), we attribute the weak onset to the direct dissociation of $CH_3$-$CH_2SH^+$ into $CH_3^+$ and $CH_2SH$ in the threshold region. Although the charge of $CH_3CH_2SH^+$ is originally located at the S atom, the charge may hop to the β-carbon or even the α-carbon, resulting in the formation of $CH_3CH_2^+$ and $CH_3^+$. Compared to the IE of $CH_3CH_2$ (8.13 + ? eV) and the IE of $CH_2SH^+$ (7.536 ± 0.003eV), the IE of $CH_3$ (9.838 ± 0.004eV) is the highest and therefore we expect that the formation of $CH_3^+ + CH_2SH$ is least favorable. A larger contribution to the formation of $CH_3^+$ may be from the further dissociation of $CH_3CH_2^+$, the most abundant product ion in the CID of $CH_3CH_2SH^+$ + Ar. The second onset AE(CID) at 9.0 ± 0.2 eV is slightly higher than the thermochemical threshold $\Delta H^\circ_0 =$ 7.91 eV for the formation of $CH_3^+ + CH_2 + SH$.

The IE(CID) for $H_2S^+$ is determined to be 1.8 ± 0.2 eV, indicating that the product channel is reaction 9, which leads to the formation of $H_2S^+ + CH_2CH_2$. The breakage of the C-S bond resulting in $SH^+$ and $C_2H_5$ seems to be more straight forward, yet no trace of $SH^+$ was observed over the entire all $E_{c.m.}$ range. This can be easily explained because the IE of SH ( 10.4218 ± 0.0004 eV)[2] is significantly higher than the IE of $CH_3CH_2$ ( 8.13 ± ? eV)[23] and the charge will be preferentially located on the α-carbon. In order to form $H_2S^+$ and $CH_2CH_2$, there might be a cyclic transition complex which is formed by the weakly bonding the sulfur atom to a hydrogen atom on the β-carbon. Due to the similar IE for $H_2S$ (10.4682 ± 0.0002 eV)[2] and $CH_2CH_2$ ( 10.507 ± 0.004 eV)[23], the charge may be located on either the sulfur or the β-carbon during the breakage of the C-S bond. This is consistent with the observation that $H_2S^+$ and $CH_2CH_2^+$ have similar abundances and their cross-section curves resemble each other near their thresholds.

**B. Photoionization efficiency spectra for fragment ions of $C_2H_5SH^+$**

The photoionization mass spectrum for $C_2H_5SH^+$ measured at 950 Å is depicted in Fig. 4. The major photoionization ions observed are $C_2H_5^+$ and $CH_2SH^+(CH_3S^+)$, which are also the major product ions in CID. The mass 61 ion, resulting from one hydrogen loss of the $C_2H_5SH^+$, shows small abundence while the CID experiment shows no evidence of its existence. Fig. 5(a), 5(b), 5(c), 5(d), 5(e), 5(f) and 5(g) show the PIE spectra of $C_2H_5S^+$ ($CH_3CHSH^+$), $C_2H_5^+$, $C_2H_4^+$, $CH_2SH^+$ ($CH_3S^+$) , $CH_2S^+$, and $H_2S^+$ in the region of 950 - 1400 Å.

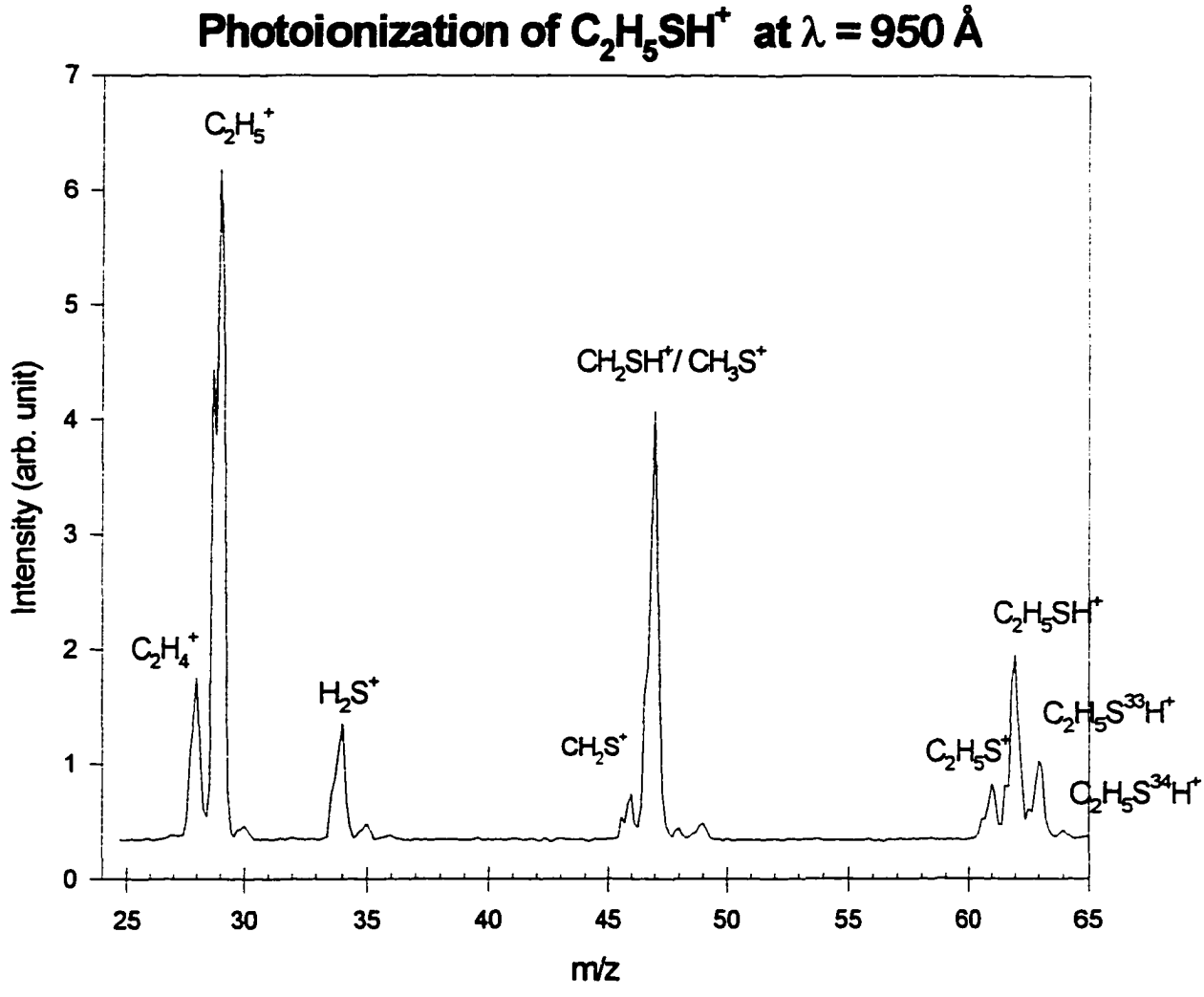


Fig.4 Mass Spectrum in the mass range of m/e = 24-65 amu for the photoionization of $C_2H_5SH$ at λ = 950 Å ( $E_{ex.}$ = 3.76 eV. Note the mass peak (m/e = 61 amu) corresponding to $CH_3CHSH^+$ formed by reaction 1 is present in the spectrum

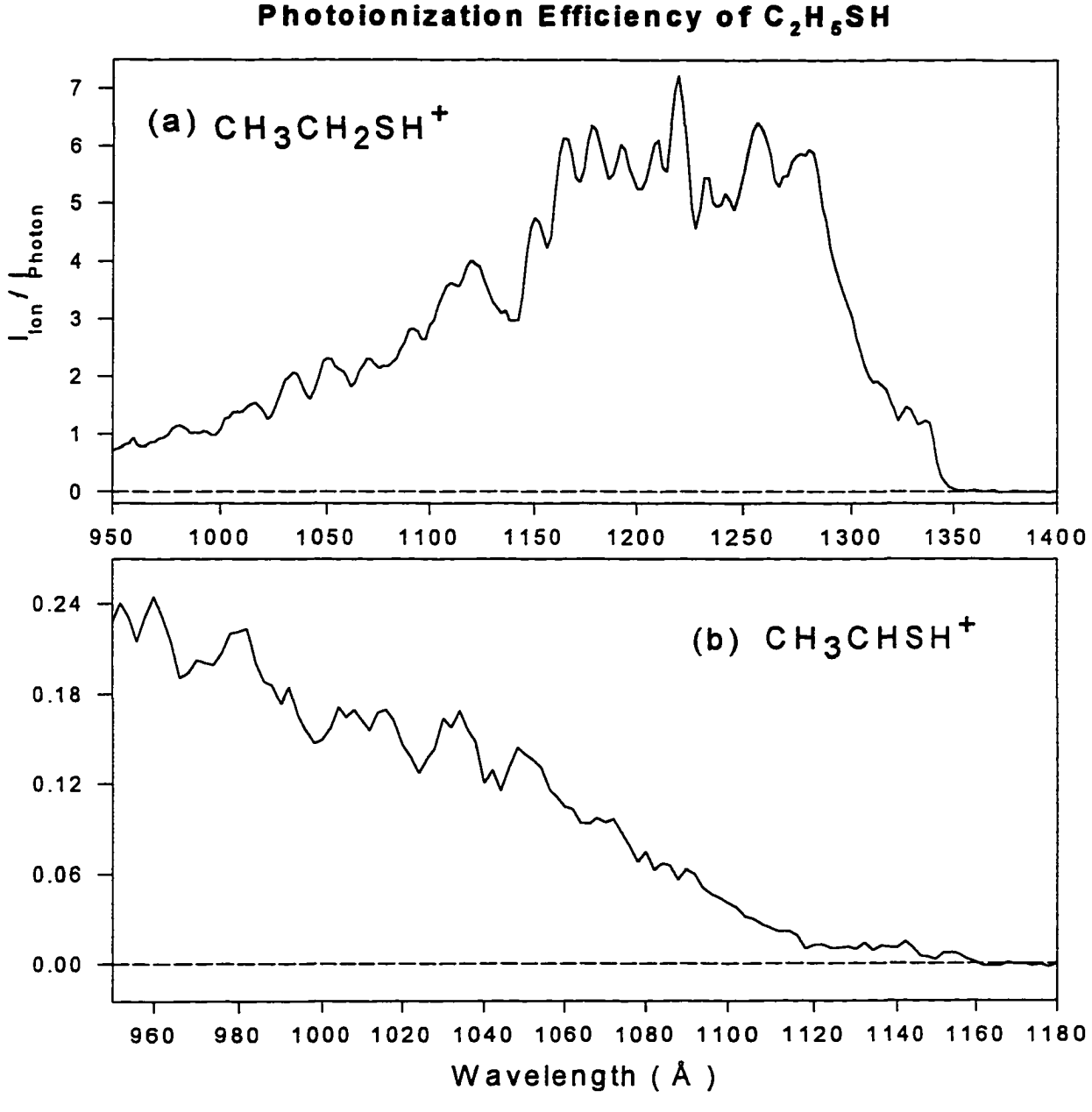


Fig.5(a) Photoionization efficiency curve for $CH_3CH_2SH^+$ from photoionization of $CH_3CH_2SH$ from 950 -1400 Å

5(b) Photoionization efficiency curve for $CH_3CHSH^+$ from photoionization of $CH_3CH_2SH$ from 950 -1180 Å

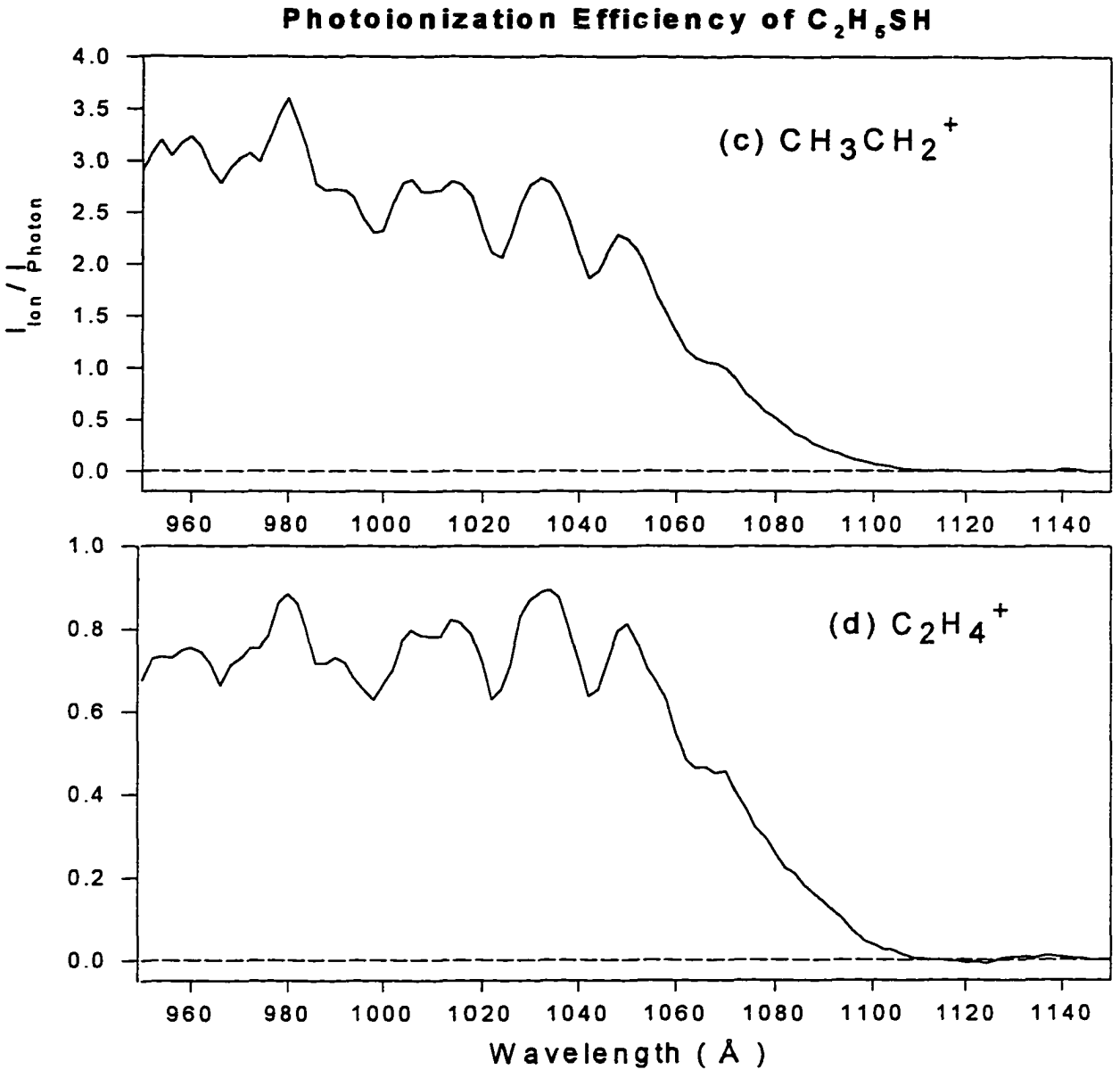


Fig.5(c) Photoionization efficiency curve for $C_2H_5^+$ from photoionization of $CH_3CH_2SH$ from 950 -1150 Å

5(d) Photoionization efficiency curve for $C_2H_4^+$ from photoionization of $CH_3CH_2SH$ from 950 -1150 Å

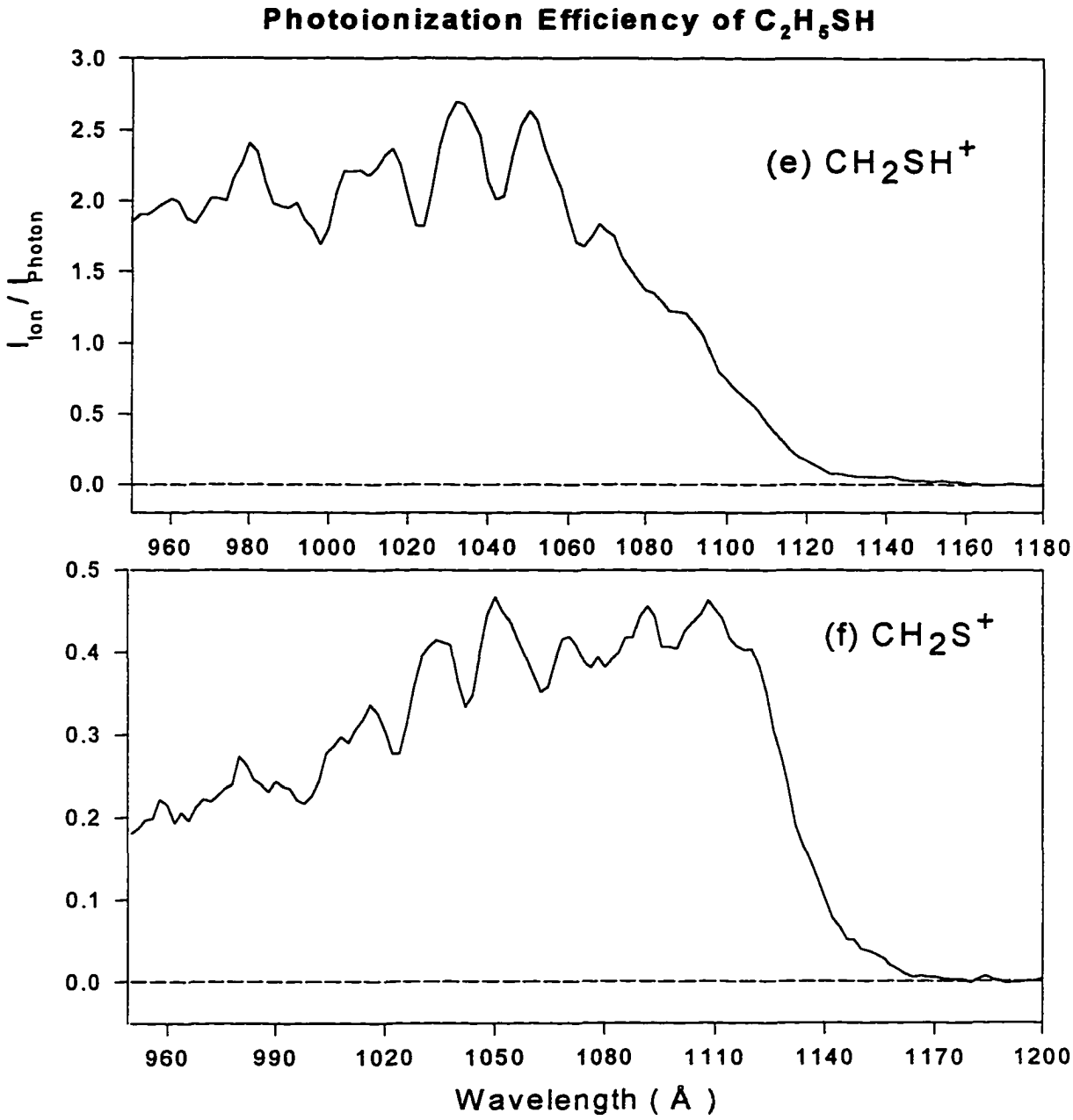


Fig.5(e) Photoionization efficiency curve for $CH_2SH^+$ from photoionization of $CH_3CH_2SH$ from 950 -1180 Å

5(f) Photoionization efficiency curve for $CH_2S^+$ from photoionization of $CH_3CH_2SH$ from 950 -1200 Å

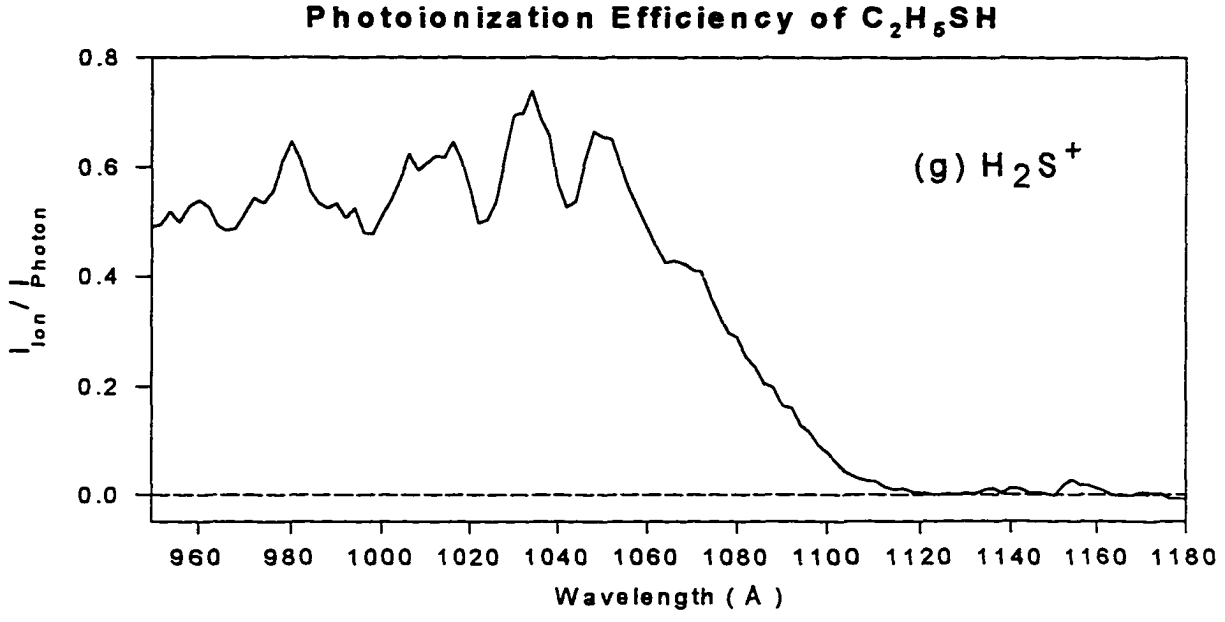


Fig.5(g) Photoionization efficiency curve for $H_2S^+$ from photoionization of $CH_3CH_2SH$ from 950 -1180 Å

The IE of 9.22 ± 0.06 eV for $C_2H_5SH^+$ is in reasonable agreement with a previous measurement[11] obtained in a high resolution nonresonant two-photon pulsed field ionization The AE value 10.99 ± 0.06 of the second onset agrees well with the thermochemical value of 11.03 eV within the uncertainty of measurement. Despite the efficient rotational cooling for $C_2H_5SH^+$ by supersonic expansion in the current experiment, the magnified view of the PIE spectrum for $CH_2SH^+$ ( $CH_3S^+$ ) in Fig. near the threshold region reveals a long tail extending to 1180 Å. The AE for $CH_2S^+$ is determined to be 10.71 ± 0.06 eV. No tailing is observed near the threshold region. The profile of the PIE curve for $H_2S^+$ behaves very similarly to that of $C_2H_4^+$ and the relative intensity is only slightly lower than $C_2H_4^+$. The expanded form of the threshold region shows a sharp onset at 1112 Å, yielding the AE of 11.15 ± 0.06 eV.

## C. Comparison of relative abundances for product ions observed in CID and photoionization

Fig. 6(a) shows the relative abundances in percentage for the observed CID product ions $C_2H_5^+$, $C_2H_4^+$, $C_2H_3^+$, $CH_3^+$, $CH_2SH^+$, $CH_2S^+$, $CHS^+$, and $H_2S^+$. The sum of the abundences for all product ions at a specific $E_{c.m.}$ is normalized to 100%. As shown in Figure 4(a), the relatively abundance of the most abundant ion, $C_2H_5^+$. reaches a plateau at 3 eV and decreases monotonically from 63% to 20% when $E_{c.m.}$ is increased from 6 eV to 40 eV. Over the same $E_{c.m.}$ range, the relative abundance of $CH_2SH^+$ remains at a constant 25 %. The relative abundance of $C_2H_3^+$ starts to increase rapidly after its AE(CID) onset at 7 eV, and competes with $C_2H_5^+$ and $CH_2SH^+$ at high collision energy. While the relative abundences for other minor product ions are < 10% over the entire $E_{c.m.}$ range, the $CH_2S^+$ decreases from 15% to 5% in the $E_{c.m.}$ of 2 eV to 14 eV, and starts to gradually increase as a function of $E_{c.m.}$ to < 10% at $E_{c.m.}$=40 eV.

Fig. 6(b) shows the relative intensities in percentages of the fragment ions $C_2H_5S^+$, $C_2H_5^+$, $C_2H_4^+$, $C_2H_3^+$, $CH_2SH^+$, $CH_2S^+$ and $H_2S^+$ observed in the photoionization of $C_2H_5SH^+$ in the wavelength range of 1270 - 950 Å. The sum of the abundances for all products except for $C_2H_5SH^+$ is normalized to 100% for the purpose of comparison with those in CID. In order to compare the product ions abundances observed in CID, the photon energies (PHE) in the photoionization experiment are converted to excitation energies ($E_{ex}$) with respect to the ground vibronic state of $C_2H_5SH^+$, where $E_{ex}$ = PHE - IE ($C_2H_5SH^+$). The collision energy at it center of mass $E_{c.m.}$ in CID will be equivalent to the difference between photon energy and IE

($C_2H_5SH^+$), i.e., $E_{c.m.} \equiv E_{ex}$. The relative abundances for fragment ions formed in the photoionization have been measured at 1200, 1150, 1100, 1050, 1010, and 950 Å, corresponding to $E_{ex}$ = 1.0, 1.5, 2.0, 2.5, 3.0, and 3.8 eV respectively.

As shown in 6(a), the relative abundences of $C_2H_5^+$ and $CH_2SH^+$ are the two most abundant ions in CID. In contrast, Fig. 6(b) shows that the relative ion abundances in PI are strongly dependent on $E_{ex}$ with several dramatic crossovers between the competition of different fragment ions over the small range of 1-4 eV. Considering that the endothermicity for the formation of $CH_2S^+ + CH_4$ is the lowest among all of the dissociation channels, we expect that the formation of $CH_2S^+$ should be the most favorable at low $E_{ex}$ which as seen in the Fig. 4(b). As the excitation energy increases, the lifetime of the tight transition complex prior 1,3 elimination from $C_2H_5SH^+$ might decrease and the other fragment ions formed by direct bond cleavage will compete in abundences. The formation of $CH_2SH^+ + CH_3$ , resulting from direct scission of the C-C bond during unimolecular dissociation of $C_2H_5SH^+$, has the second lowest thermochemical threshold $\Delta H^\circ_0$ = 1.73 eV and it starts to dominate $CH_2S^+$ abruptly right after its threshold. The relative abundance of $C_2H_5^+$, produced from the direct cleavage of the C-S bond in photoionization, has a similar thermochemical threshold $\Delta H^\circ_0$ = 1.96 eV, and it also shows a prominent abundance after $E_{ex}$ = 2.8 eV. We note that $C_2H_5^+$ , the most abundant product ion formed in the CID reaction of $C_2H_5SH^+ + Ar$ , remains 65% in CID in the $E_{c.m.}$ range of 2 - 4 eV while it reaches only 40% at $E_{ex}$ = 3.8 eV in photoionization. The relative abundances for other fragment ions are below 10% at $E_{ex}$ < 4 eV. $C_2H_5S^+$ was not observed in the CID reaction of $C_2H_5SH^+ + Ar$.

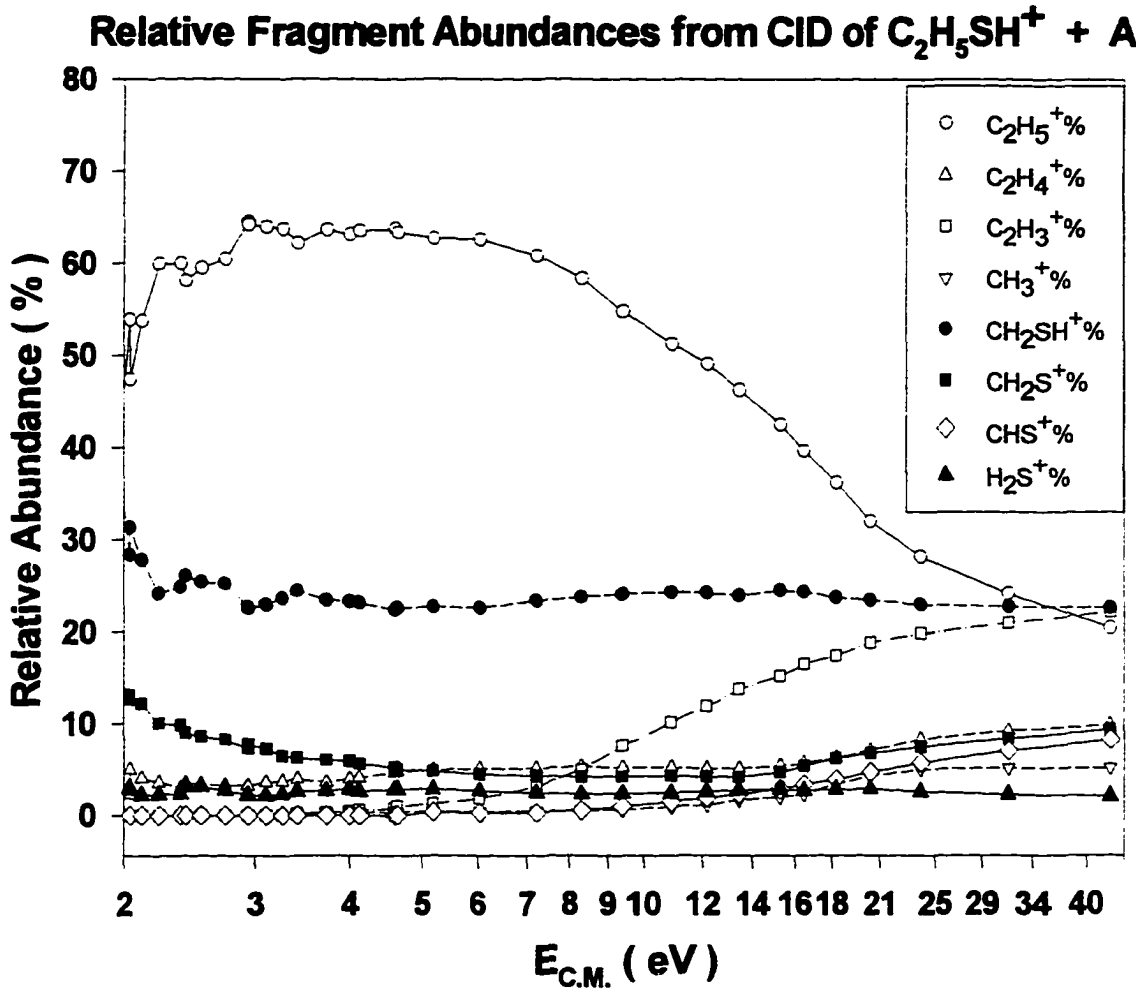


Fig. 6(a) Relative abundances in percentage for $C_2H_5^+$ (○), $C_2H_4^+$ (Δ), $C_2H_3^+$ (□), $CH_3^+$(▽), $CH_2SH^+$ (●), $CH_2S^+$ (■) , $CHS^+$ (◇) and $H_2S^+$ (▲) formed in the CID reaction of $C_2H_5SH^+$ + Ar. The sum of all the products are normalized to 100%

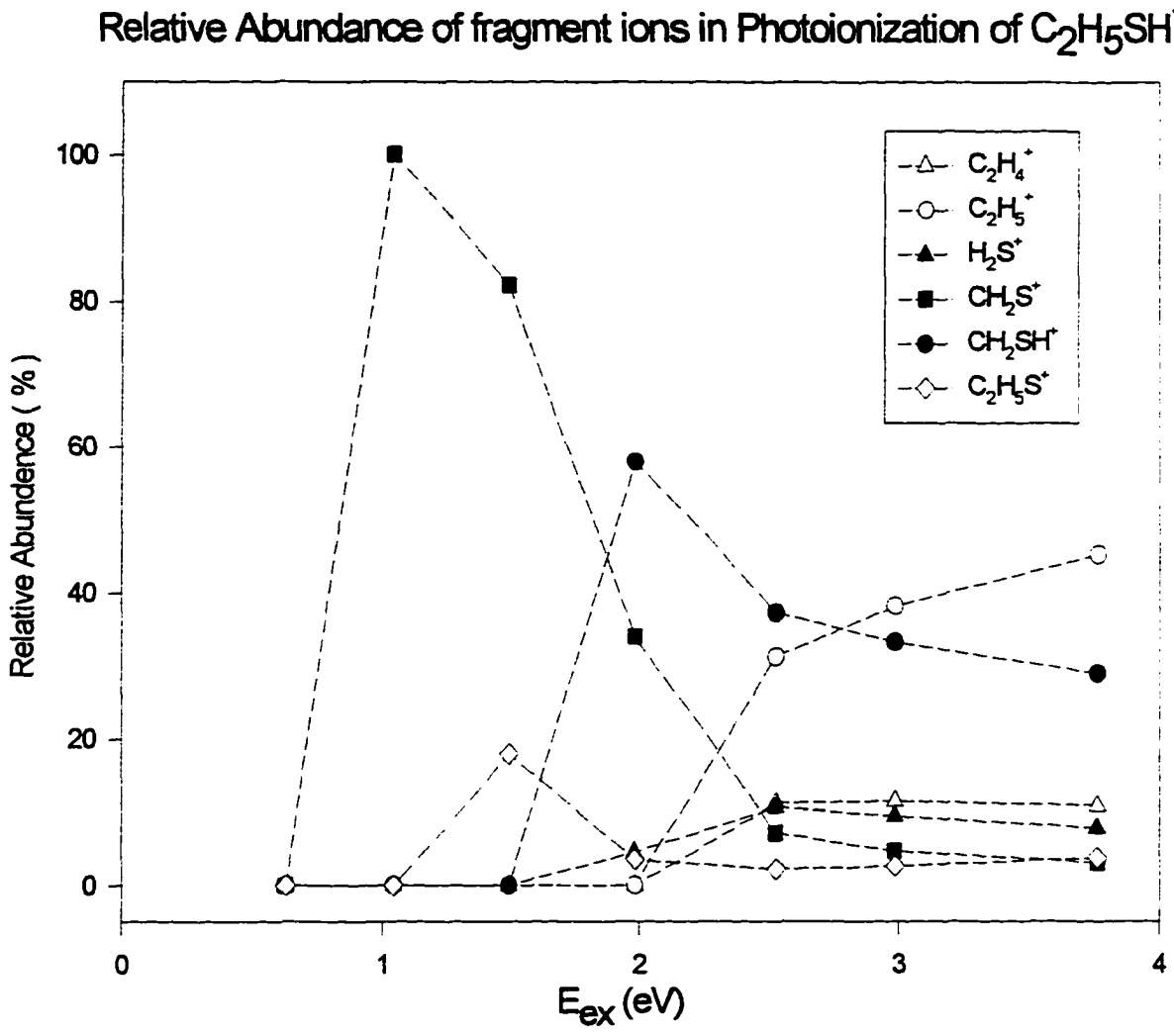


Fig. 6(b) Relative abundances in percentage for $C_2H_5^+$ (○), $C_2H_4^+$ (Δ),$CH_2SH^+$ (●), $CH_2S^+$ (■), $H_2S^+$ (▲) and $CH_3CHSH^+$ (◊) formed in the photoionization of $C_2H_5SH$ in the $E_{ex}$ =0.- 4 eV, where $E_{ex}$ = PHE (photon energy)- IE ($C_2H_5SH^+$). The sum of all the products are normalized to 100%

D. **Potential-energy profile for rearrangement and dissociation of $C_2H_5SH^+$**

The potential energy profile for the rearrangement and dissociation reactions of $C_2H_5SH^+$ were calculated[26] at G2 level of theory. The constructed rearrangement-dissociation pathways are shown in Fig. 7(a) and 7(b) and compared to the CID experiment results here.

The distonic ion , $CH_3CHSH_2^+$, is found to be a stable isomer on the potential energy surfaces and lies 0.55 eV above the conventional $CH_3CH_2SH^+$ ion. The transition structure which interconverts $CH_3CH_2SH^+$ and $CH_3CHSH_2^+$ by a 1,2-hydrogen shift is calculated to be 1.5 eV higher in energy respect to the $CH_3CH_2SH^+$ ion. Another isomeric ion, $CH_2CH_2SH_2^+$ , which is calculated to be almost equal in energy to $CH_3CHSH_2^+$ , lies 0.54 eV higher than $CH_3CH_2SH^+$ ion with a high activation barrier of 2.71 eV. Compared to the potential barrier of 1.5 eV for 1,2-hydrogen shift to form $CH_3CHSH_2^+$, the AE(CID) values for all of the product ions are higher and as a consequence it is very likely that $CH_3CH_2SH^+$ rearrange to $CH_3CHSH_2^+$ before unimolecular dissociation in the CID experiment. The rearrangement barrier of 2.71 eV to form $CH_2CH_2SH_2^+$ is higher than Some of the AE(CID) values, so the structure of $CH_2CH_2SH_2^+$ is only accessible in some dissociation channels whose AE(CID) is smaller than the value of 2.71 eV. As shown in Fig.5(a), the formation of $C_2H_5^+$ + SH from $C_2H_5SH^+$ involves a loose transition complex and the reverse activation energy for such a process is zero. The good agreement between the AE(CID) value of 1.9 ± 0.2 eV and the calculated dissociation energy threshold 1.95 eV supports the assumption of direct dissociation without a reverse activation energy. Similarly, the formation of $CH_2SH^+$ + $CH_3$ from $C_2H_5SH^+$ should also proceeds without a reverse activation energy.

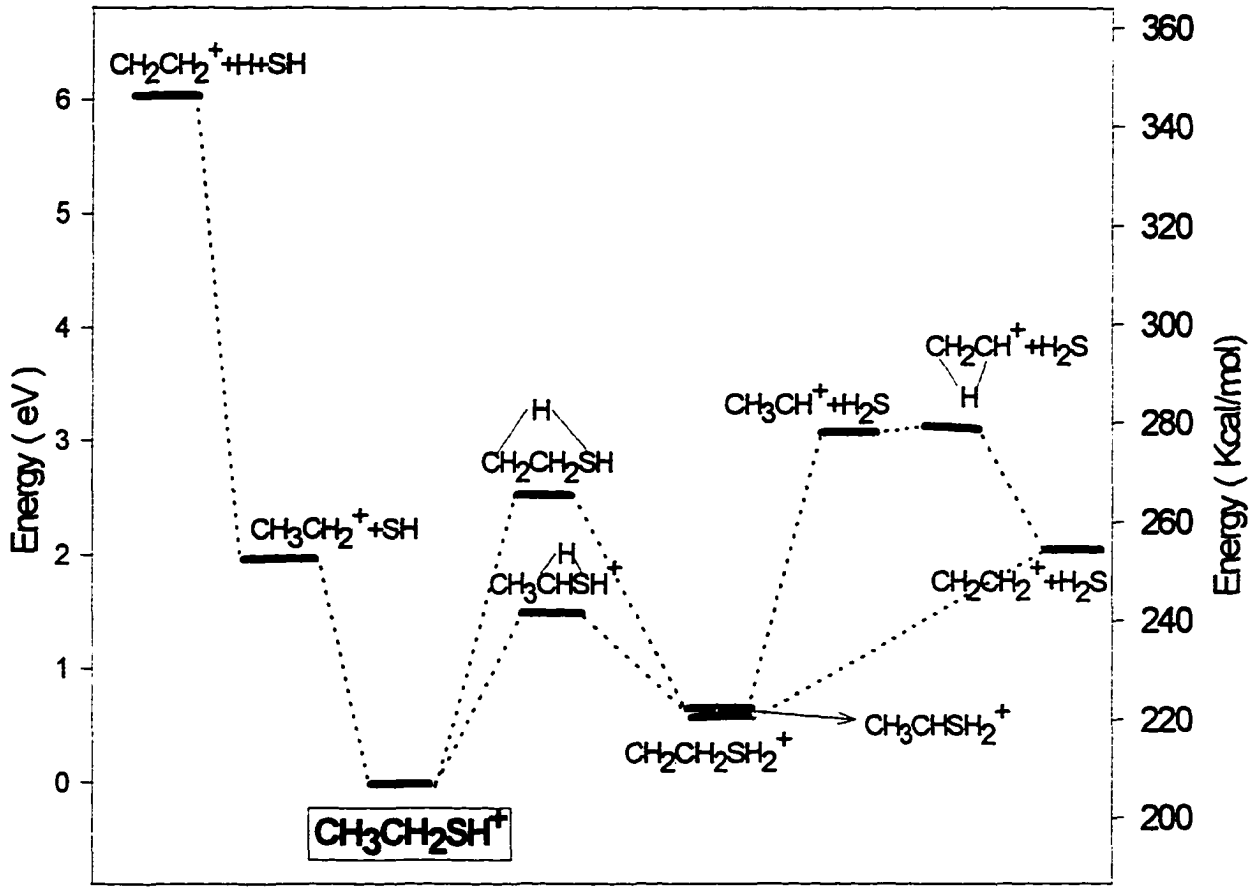


Fig. 7(a)Schematic of the potential-energy profile for the formation of $C_2H_5^+$, $C_2H_4$ from the rearrangement and dissociation reactions for $CH_3CH_2SH^+$

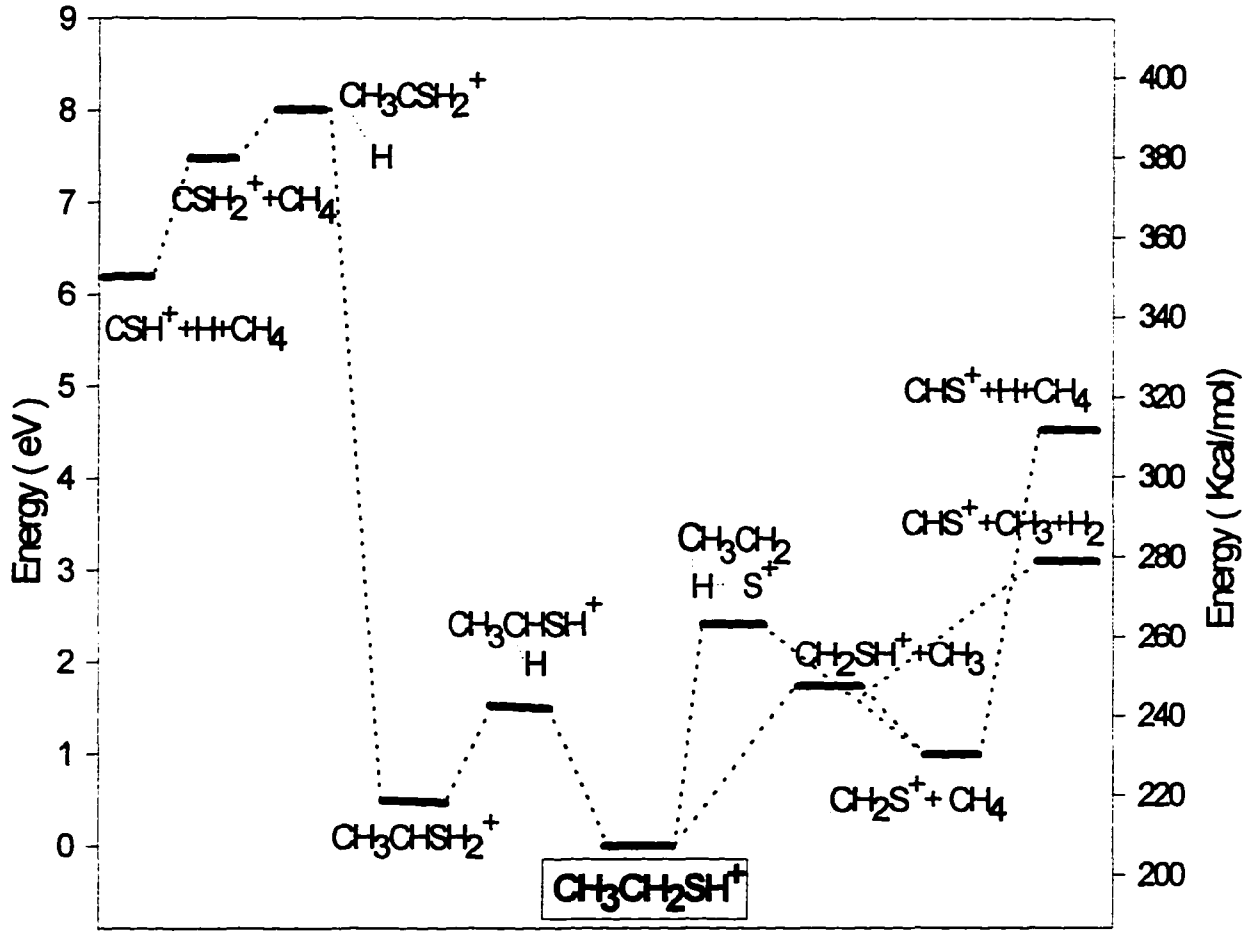


Fig. 7(b) Schematic of the potential-energy profile for the formation of $CH_2SH^+$, $CH_2S^+$ from the rearrangement and dissociation reactions for $CH_3CH_2SH^+$

The possibility of formation of $CH_2SH^+$ via 1,3-$H_2$ elimination from $CH_2CH_2SH_2^+$ is less likely because the AE(CID) value 1.7 ± 0.2 eV is significantly lower than the potential barrier($T_{sc}$) 2.71 eV interconverting the $CH_3CH_2SH^+$ and $CH_2CH_2SH_2^+$ . As mentioned previously, the $CH_3^+$ might be from further direct dissociation of $CH_3CH_2^+$ and there is no reverse activation barrier involved.

The AE(CID) value of 1.3 eV for $CH_2S^+$ observed in CID is higher than the thermochemical threshold $\Delta H^\circ_0$ = 0.92 eV for the formation of $CH_2S^+$ + $CH_4$ , indicating a potential energy barrier of at most 1.3 eV exists prior to dissociation. The Δ(PI) value 1.42 ± 0.06 eV for $CH_2S^+$ observed in photoionization experiment is close to the AE(CID) value , which suggest that a transition complex with similar barrier height is also present during the photofragmenation of $C_2H_5SH^+$ to form $CH_2S^+$ and $CH_4$. The transition structure $T_{sd}$ shown in fig.7(a) has a significantly higher barrier of 2.31 eV, which is significantly higher than the observed threshold, so the measured AE(CID) value seems not be able to overcome the activation barrier. The same situation also occurs to the formation of $C_2H_4^+$ + $H_2S$, its AE(CID) of 1.9 ± 0.2 eV is 0.81 eV lower than the transition state energy of 2.71 eV.

The AE(CID) value of 1.9 ± 0.2 eV for $CH_2CH_2^+$ is higher than the energy of $CH_2CH_2SH_2^+$, which is 0.55 eV above the conventional $CH_3CH_2SH^+$ ion. However, the transition structure ( Tsc) for the formation of the β-distonic ion $CH_2CH_2SH_2^+$ has a high barrier of 2.7 eV, which is significantly higher than the observed AE(CID). This means that dissociation should take place preferentially in the isolated conventional ion without rearrangement. If we neglect the possibility of the above two-step mechanism which involve the rearrangement from the conventional $CH_3CH_2SH^+$ to the β-distonic ion $CH_2CH_2SH_2^+$ and

consider the formation of $C_2H_4^+$ and $H_2S$ from direct dissociation of $CH_3CH_2SH^+$ , the direct fragmentation even has a higher barrier of ?( not done)eV. A recent study of the analogous system, conventional $CH_3CD_2OH^+$ showed that $CH_3CD_2OH^+$ will interconvert to distonic ion in the presence of polar neutral molecules.[26] In spite of the substantial energy barriers for the unassisted isomerization, the interaction between the reactant ion and the polar neutral molecule causes intramolecular hydrogen migration. A very recent high-level ab initio calculation[27] provides a rationalization for the experimental observations of this so-called "proton-transport catalysis"[28]. With the assistance of the bonding between the water molecule and the hydrogen atom on the carbon site, the barrier for the methanol radical $CH_3OH^+$ to methyleneoxonium $CH_2OH_2^+$ by water-catalyzed transformation is significantly lowered by about 100 kJ/mol ( 4eV). The neutral target , Ar atom, in the current CID experiment is not a polar molecule which has a high proton affinity. However, the van der weal interaction between the colliding Ar and the hydrogen atom on either the carbon or the oxygen site might facilitate the rearrangement of the reactant ion into the necessary transition state and consequently reduce the activation energy.

**E. Dissociation mechanism for collision activated $C_2H_5SH^+$**

The observation that $C_2H_5^+$ + SH [reaction (2)] is the dominant product channel over the full $E_{c.m.}$ range of 1 - 37 eV is most interesting. Such an observation is contrary to the prediction of QET calculations. The two basic assumptions of QET are that a critical configuration or transition state controls the reaction rate, and that the internal energy is randomly distributed in the molecule's active degrees of freedom. These assumptions lead to

the conclusion that the most favorable product will be the most stable channel with the lowest heat of formation when the transition state are similar. According to the calculated heat of formation at 0 K of the following reaction:

$$CH_3CH_2SH^+ + Ar \rightarrow CH_3CHSH^+ + H + Ar \qquad \Delta H^\circ_0 = 1.47\ eV \qquad 1$$

$$\rightarrow CH_2SH^+ + CH_3 + Ar \qquad \Delta H^\circ_0 = 1.73\ eV \qquad 6(a)$$

$$\rightarrow CH_3CH_2^+ + SH + Ar \qquad \Delta H^\circ_0 = 1.96\ eV \qquad 2$$

the formation of $CH_3CHSH^+ + H$ is least endothermic and should be expected to show a greater abundance than the formation of $CH_2SH^+ + CH_3$ or $CH_3CH_2^+ + SH$ channels in the CID experiments. However, no trace of $CH_3CHSH^+$ was observed and the formation of the higher energy products $CH_3CH_2^+$ and $CH_2SH^+$ are dominant. This indicates that the result of the CID dissociation of $CH_3CH_2SH^+$ is not compatible with the energy randomization assumption of a statistical QET model.

It is known that at collision energies in the $E_{c.m.}$ range of this experiment is mostly efficient for translational-vibrational[29] or translational-rotational energy transfer[30]. Electronic excitation is highly inefficient for the collision-induced dissociation in the low energy regime. The excitation energy is partitioned between the bent motion, the symmetric and antisymmetric stretches[6], and only the latter will result in dissociation provided that the available energy exceeds the thermochemical requirement. As a consequence, we expect that the low frequency vibrational modes of the $CH_3CH_2SH^+$ ions are preferentially excited in such a process. In the previous CID experiment on the $CH_3SH^+ + Ar$ system, the observation that

the formation of $CH_3^+$ + SH dominates the more stable product channel $CH_2SH^+$ + H is also contrary to the prediction of QET theory[1]. The four highest vibrational frequencies of $CH_3SH^+$ correspond to the $CH_3$ and SH stretching modes, which ranges from ≈ 2556-3035 $cm^{-1}$, while the C-S stretching is the second lowest vibrational mode with a frequency of 687 $cm^{-1}$. Thus, the internal vibrational energy resulting from collisional activation is predominantly deposited in the C-S stretch mode instead of the $CH_3$ stretching modes of $CH_3SH^+$. Owing to the large differences in vibrational frequencies between the C-S and $CH_3$ (S-H)stretching modes of $CH_3SH^+$, the C-S and C-H (or S-H) stretching modes are only weakly coupled, resulting in inefficient energy flow between the C-S and C-H (or S-H) vibrational modes of $CH_3SH^+$. As a consequence, the product $CH_3^+$ ion, which results from the breakage of the C-S bond, is favored over the product ions formed by the cleavage of the C-H (or S-H) bonds of $CH_3SH^+$.

The CID reaction of $CH_3CH_2SH^+$, which contains a C-C bond as well as a C-S bond, can be considered a further test for the physical picture gained in the above $CH_3SH^+$ + Ar system. Based on the recent experimental[6] and *ab initio* calculations, the stretching frequencies associated with the C-H, S-H, and C-S bonds are similar to those of $CH_3SH^+$. The additional C-C stretching mode is ≈1200 $cm^{-1}$, only slightly higher than the C-S stretching mode. So the excitation energy available for transfer will be favored to dump into the C-S and C-C bonds. In addition to the expected efficient excitation of the C-C and C-S stretching modes via collisional activation, the coupling between the C-C and C-S modes of $CH_3CH_2SH^+$ should be better because they possess vibrational frequencies of similar magnitude. On the other hand, the great differences in the vibrational frequencies between the C-S(C-C) and C-H(S-H)

stretching modes cause weak coupling between the C-S(C-C) and C-H(S-H) bonds, and the resulting inefficient energy flow will therefore confine the available excitation energy mostly in the C-S and C-C stretches on the time scale of unimolecular decomposition. Hence, product channels arising from the cleavage of the C-S and C-C bonds should dominate in the collision activated dissociation of $CH_3CH_2SH^+$. This expectation is confirmed by the dominant abundance of the $CH_3CH_2^+$ and $CH_2SH^+$ ions. The failure to observe $CH_3CHSH^+$ from H-elimination, which is the most stable product channel, is attributed to the high vibrational frequency of the C-H mode and the inefficient energy flow between the C-H and C-S(C-C) stretching modes. These results show that the CID reaction of $CH_3CH_2SH^+$ + Ar is not behaving statistically.

The mass spectrum shown in Fig. 4 from photoionization of $CH_3CH_2SH^+$, however, shows the existence of the formation of $CH_3CHSH^+$ + H , which is the most stable product channel, at $\lambda$=950 Å. This observation indicates the fair consistence of the photoionization experiment with the assumption of energy randomization predicted by QET, i.e, the internal energy of $CH_3CH_2SH^+$ by electronic excitation is somehow deposited into the C-H stretching and causes the antisymmetric stretching followed by dissociation to $CH_3CHSH^+$. The preparation of the precursor ion $CH_3CH_2SH^+$ in photoionization experiment near the onset of $CH_3CHSH^+$ is in the first photoelectronic band of $CH_3CH_2SH^+$.[14] This excited state mainly involves the ejection of a mostly nonbonding electron associated with the sulfur atom. According to a recent nonresonant two-photon pulsed field ionization photoelectron spectroscopic study, the main progression vibration peaks can be assigned to excitation of vibrational modes involving the low frequency C-S stretching as well as high frequency S-H torsional and S-H

bending.[6] The Franck-Condon factors for different vibrational excitation upon ionization favor $\nu_4$ mode, corresponding to the C-S stretching. The excitation of the C-S stretching mode will be more efficient compared to other higher vibrational modes. If several quanta of the C-S stretching modes are excited, the coupling between the C-S and C-H(S-H) stretching modes will improve and the energy randomization assumption should holds better compared to the poor coupling of the C-S and C-H(S-H) vibrational modes in the collisional activated dissociation of $CH_3CH_2SH^+$. As a consequence, the product $CH_3CHSH^+$ ion resulting from breakage of C-H bond of $CH_3CH_2SH^+$ should be more likely to be formed.

**Conclusion**

We have examined the CID reaction of $CH_3CH_2SH^+$ + Ar in the $E_{c.m.}$ range of 1-37 eV. The fragment ions observed are in general agreement with those observed in photoionization study. However, in the present CID study, $C_2H_5^+$ + SH is found to be the dominant product channel, which is contrary to the QET prediction and the results of the photoionization measurements. Stemming from the fact that the dissociation energy for the $CH_3CH_2^+$-SH bond is greater than that of the H-$CH_2CH_2SH^+$ bond, this observation suggests non-statistical behavior in the CID of $CH_3CH_2SH^+$. In effect, this system is an example of bond selective dissociation via collisional activation.

The dominant production of $CH_3CH_2^+$ + HS is attributed to the more efficient excitation of the C-S stretch compared to C-H stretches in the collisional activation of $CH_3CH_2SH^+$. The failure to observe product ions resulting from C-H bond cleavage is

rationalized by inefficient intramolecular energy flow due to weak couplings between the C-S and $CH_3$ stretching modes of $CH_3CH_2SH^+(1^2A'')$.

**References**


1. Benson, S. W. *Chem. Rev.*, *78*, 23 (1978)
2. Fenn, P. T, Stimson, S. S, Chen, Y. J, and Ng, C.Y, submitted to the Journal of Chemical Physics
3. Kutina, R. E.; Edwards, A. K.; Berkowitz, J. *J. Chem. Phys.*, *77*, 5508 (1974)
4. Jonsson, B.-Ö.; Lind,J. *J. Chem. Soc. Faraday Trans. 2*, **1974**, *70*, 1399.
5. *Handbook of Helium I Photoelectron Spectra of Fundamental Organic Molecules*, edited by Kimura, K; Katsumata, S.; Achiba, Y.; Yamazaki, T.; Iwata. S., Halsted: New York, 1981.
6. Shao, J.-D.; Ng, C. Y. *J. Chem. Phys.* **1986**, *84*, 4317; Shao, J.-D.; Li, Y. G.; Flesch, G. D.; Ng, C. Y. *J. Chem. Phys.* **1987**, *86*, 170; Flesch, G. D.; Ng, C. Y. *J. Chem. Phys.* **1991**, *94*, 2372; Flesch, G. D.; Nourbakhsh, S.; Ng, C. Y. *J. Chem. Phys.* **1990**, *92*, 3490; Flesch, G. D.; Ng, C. Y. *J. Chem. Phys.* **1990**, *92*, 3235.
7. Ng, C. Y. in *State-Selected and State-to-State Ion-Molecule Reaction Dynamics: I. Experiment*, edited by Ng, C. Y.; Baer, M.; Wiley: New York, 1992; *Adv. Chem. Phys.* **1992**, *82*, 401.
8. Li, X.; Huang, Y.-L.; Flesch, G. D.; Ng, C. Y. *Rev. Sci. Instrum.* **1994**, *65*, 3724; *ibid.* **1995**, *66*, 2871.
9. Li, X; Huang, Y.-L.; Flesch, G. D.; Ng, C. Y. *J. Chem. Phys.* **1997**, *106*, 564.
10. Gibbs, H. M.; Cummins, E. D. *Rev. Sci. Instrum.* **1966**, *37*, 1385.

11. Cheung, Y.-S.; Hsu, C.-W.; Huang, J.-C.; Li, W.-K.; Chiu, S.-W. *Int. J. Mass Spectrom. Ion Proc.* **1996**, *159*, 13.

12. Hsu, C.-W.; Ng, C. Y. *J. Chem. Phys.* **1994**, *101*, 5596.

13. Ruscic, B; Berkowitz, J. *J. Chem. Phys.* **1992**, *97*, 1818.

14. Linder, R.; Müller-Dethlefs, K.; Wedum, E.; Haber, K.; Grant, E. R. *Science* **1996**, *271*, 1698; Chewter, L. A.; Sander, M.; Müller-Dethlefs, K.; Schlag, E. W. *J. Chem. Phys.* **1987**, *86*, 4737; Linder, R.; Sekiya, H.; Beyl, B.; Müller Dethlefs, K. *Angew Chem., Int. Ed. Engl.* **1993**, *32*, 603; Neuhauser, R. G.; Siglow, K.; Neusser, H. J. *J. Chem. Phys.* **1997**, *106*, 896

15. Akopyan, M. E.; Serhiev, Y. L.; Vilesov, F. I. *Klim. Vys. Energy* **1970**, *4*, 305.

16. Kutina, R. E.; Edwards, A. K.; Berkowitz, J. *J. Chem. Phys.* **1974**, *77*, 5508

17. Li, X. *Ph.D. Thesis*, **1996**, Iowa State University.

18. Weber, M. E.; Elkind, J. L.; Armentrout, P. B. *J. Chem. Phys.* **1986**, *84*, 1521.

19. Rebick, C., and Levine, R. D., *J. Chem. Phys.* **1973**, *58*, 3942

20. Weber, M. E., Elkind. J. L., Armentrout, *J. Chem. Phys.* **1992**, 97, 4859.

21. Dill, J. D., Mclafferty. F. W., *J. Am. Chem. Soc.* **1979**, 101, 6526.

22. Chiu, S.-W., Li, W. K., Tzeng, W. B. Ng, C. Y., *J. Chem. Phys.* **1992**, 97, 6557.

23. G. Lias "Gas Phase Thermochemistry"

24. refer to Table I

25. Nourbakhsh, S., Norwood, K., Yin, H.-M., liao, C. L., Ng, C. Y. *J. Chem. Phys* **1991**, *92*, 946.

26. Audier, H. E., leblane, D., Mourgues, P., McMahon, Hammerum, S. 1994, *J. Chem. Soc., Chem. Commun.* **1994**, 2329

27. Gauld, J., Audier, H., Fossey, J., Radom, L., *J. Am. Chem. Soc.* **1996**, *118*, 6299.

28. Bohm, D. K., *int. J. mass spectrom. Ion proc.* **1992**, *115*, 95

29. Maham, B. H. *J. Chem. Phys* **1970**, 52, 5221.

30. de Sainte Claire, P.; Peslherbe, G. H.; Hase, W. L. *J. Phys. Chem.* **1955**, *99*, 8147; de Sainte Claire, P.; Hase, W. L. *J. Phys. Chem.* **1996**, *100*, 8190.

31. Nourbakhsh, S., Norwood, K., Yin, H.-M., liao, C. L., Ng, C. Y. *J. Chem. Phys* **1991**, *95*, 5014

Ma et al, C. L. Liao, H.-M. Yin, S.-W. Chiu, N. L. Ma, W. L Li, C. Y. Ng *Chem. Phys. Lett*, 213, 250 (1993)

## SUMMARY

In the molecular beam photoionization mass spectrometric study of metal carbonyls $M(CO)_6$, M= Cr, Mo, W, the PIE spectra have been measured over the photon energy range of 7.75 - 19.07 eV. The sequential bond energies $D_0$ for $M(CO)_6^+$ have been calculated using the experimental ionization energy (IE) of $M(CO)_6$ and the appearance energy (AE) values for $M(CO)_n^+$, n=0-6 and M=Cr, Mo, and W. By comparison to the well known heat of formation of $M^+$, CO and $M(CO)_6$ (M=Cr, Mo, W), we note that the AE values for the $M^+$ ion are upper limits and indicate that photoionization of $M(CO)_6$ produces $M^+$ ions in the excited state. The first bond energy ($D_0$) values of $M(CO)_6$ are found to be smaller compared to those of ions $M(CO)_6^+$, M=Cr, Mo, W, which strongly supports the importance of relativistic effects proposed by theorists. Those effects enhance π-back-donation (stabilization) by reducing the energy gap between the M(dπ) and CO($\pi^*$) orbitals for heavier transition metal elements. This observation also shows that π-back-donation plays a more important role than CO to M σ-donation in the first bond energy in metal carbonyl $M(CO)_6$, M=Cr, Mo, W.

The IE of $SF_6$ and the AE values for $SF_n^+$, n=1-6 were measured in the photon energy range of 8-17 eV. The related thermochemical data, including heat of formation ( $\Delta_f H^\circ_0$) and bond energies ($D^\circ_0$), were derived. Comparison of the experimental thermochemical data to the G2 calculation for those species allows us to recommend a set of self-consistent values and further confirms that the G2 method is a reliable procedure for obtaining thermochemical data accurate to 4-5 kcal/mol for complex sulfur-containing species. Alternating patterns were observed in the bond energies, ionization energies, and electron affinities for the $SF_n$, and

$SF_n^+$ systems (n=1-6), which can be well explained by transitions between the stable and unstable species in those hypervalent molecules. The VSEPR theory was used to rationalized the theoretical equilibrium structure for $SF_n$, $SF_n^+$, and $SF_n^-$ ( n=1-6).

With the triple-quadrupole double-octopole photoionization tandem mass spectrometer, the absolute total cross sections of collision-induced dissociation of $C_2H_5SH^+$ + Ar were measured in the $E_{c.m.}$ range of 1-37 eV. The observed thresholds for the formation of $C_2H_5^+$, $C_2H_4^+$, $C_2H_3^+$, $CH_2SH^+$, $CH_2S^+$, and $H_2S^+$ are consistent with the thermochemical threshold, while those for $CH_3^+$ and $CHS^+$ are upper bound for the corresponding dissociation channels. The dominance of the $C_2H_5^+$ and $CH_2SH^+$ ion formed in the CID reaction shows that the dissociation of $CH_3CH_2SH^+$ strongly favors the C-S and C-C bond scission process, even though the formation of $C_2H_5^+$ + SH and $CH_2SH^+$ + $CH_3$ are not the most stable channels. The observation suggests that the collision-induced dissociation is contrary to the quasiequilibrium theory (QET). Similar observation were found in the collision-induced dissociation studies of $CH_3SH^+$ and $CH_3SCH_3^+$ with Ar. The $CH_3^+$ and $CH_2SH^+$ ions are the most abundant in the CID reaction of $CH_3SH^+$ and $CH_3SCH_3^+$ , resulting from the cleavage of C-S bond, although they are not the most stable channels. This phenomenon can be attributed to the more efficient excitation of the C-S and C-C stretching mode compared to C-H stretches in the collisional activation of $CH_3SH^+$, $CH_3CH_2SH^+$ , and $CH_3SCH_3^+$ by Ar. By using a charge exchange probing technique, the $CH_2SH^+$ isomer is found to be the structure for the m/e = 47 ion formed near the threshold region for the CID reaction of $CH_3SH^+$, $CH_3CH_2SH^+$ , and $CH_3SCH_3^+$ with Ar, and the $CH_3S^+$ isomer is produced at higher $E_{c.m.}$ in the CID reaction of $CH_3SCH_3^+$ + Ar.